uOttawa

L'Université canadienne
Canada's university

FACULTÉ DES ÉTUDES SUPÉRIEURES ET POSTOCTORALES

uOttawa

L'Université canadienne
Canada's university

FACULTY OF GRADUATE AND POSDOCTORAL STUDIES

Altaf Khetani

AUTEUR DE LA THÈSE / AUTHOR OF THESIS

M.A.Sc. (Electrical Engineering)

GRADE / DEGREE

School of Information Technology and Engineering

FACULTÉ, ÉCOLE, DÉPARTEMENT / FACULTY, SCHOOL, DEPARTMENT

Photonic Crystal Fiber As a Biosensor

TITRE DE LA THÈSE / TITLE OF THESIS

Professor H. Anis

DIRECTEUR (DIRECTRICE) DE LA THÈSE / THESIS SUPERVISOR

CO-DIRECTEUR (CO-DIRECTRICE) DE LA THÈSE / THESIS CO-SUPERVISOR

EXAMINATEURS (EXAMINATRICES) DE LA THÈSE / THESIS EXAMINERS

Professor R. Gauthier

Professor K. Hinzer

Gary W. Slater

Le Doyen de la Faculté des études supérieures et postdoctorales / Dean of the Faculty of Graduate and Postdoctoral Studies

PHOTONIC CRYSTAL FIBER AS A BIOSENSOR

ALTAF KHETANI

A thesis submitted to
The Faculty of Graduate and Postdoctoral studies
in conformity with the requirements for the degree of
Master of Applied Science (M.A.Sc)
degree in Electrical Engineering

Ottawa-Carleton Institute for Electrical and Computer Engineering
School of Information Technology and Engineering
University of Ottawa
Ottawa, Ontario, Canada

Your file Votre référence
ISBN: 978-0-494-41671-6
Our file Notre référence
ISBN: 978-0-494-41671-6

Abstract

With the era of technological change at its all time high, advancements in the field of photonics offer us a wide range of innovative potential applications. Over the years photonics has played an important role in modern industries such as telecommunication, sensors and medical imaging. One of the fields which has received a lot of attention is Photonic Crystal Fibers (PCF) for biosensor application. Photonic crystal fiber is a unique type of optical fiber in which continuous channels of (typically) air run their entire length. These `holes' serve to both confine electromagnetic waves within the core of the fiber and to tailor its transmission properties. The classification of photonic crystal fiber can be solid core PCF where the light is guided by total internal reflection, and Hollow core photonic bandgap fibers (PBF) in which light is guided through the photonic bandgap effect. Simulation of PCF has been done through commercial software known as COMSOL which follows the finite element approach.

The focus of this thesis is on the application of PCF for different sensing applications. Traditionally, solid core PCF has been used for sensing purposes as the cladding channels can be filled with gas or liquid, thus serving as an efficient type of evanescent wave sensing. Hollow core PBF offers huge improvements as the interaction between light and matter is increased by the presence of sample in the core where most of the light is confined.

Conventionally, HC-PBF is used for sensor purposes by selectively filling the core. Here we have used a non-selective filling technique wherein all the channels of PCF are being filled with samples. When the fiber is empty it guides a particular band, and upon filling with other samples, the bandgap is shifted, and depending on this shift one can determine the refractive index of the sample. This type of sensor has been able to detect as low as 10^{-5} change in refractive index just by taking a few centimeters of HC-PBF.

Laser Flash Photolysis is one of the leading methods used in photochemistry to determine the transient species such as radicals, excited states or ions, in chemical and biological systems. By using HC-PBF we have replaced the conventional technique of LFP where in

a test-tube is used to hold the sample. The sample is excited through a laser and a monitoring beam is used to observe the amount of absorption. The sample required here is on the order of a milliliter which can be scaled down to pico liter by the use of PCF. The LFP results using PCF showed signal enhancement of at least an order of magnitude for samples like xanthone in toluene, xanthone in acetonitryl and water soluble benzoin in methyl viologen.

Raman Spectroscopy is yet another area which had a surge of growth for label free detection of samples. One of the reasons for its popularity is that it provides a unique optical fingerprint of chemicals and biomolecules. In this thesis we have focused on developing HC-PBF for enhancing the Raman signal from the sample. We have obtained an enhancement of over 40 times when using a HC-PBF with a length of 9.5cm. We have also used HC-PBF to study the enhancement of Raman signal from colloidal nanoparticles in an aqueous solution.

Supercontinuum generation is yet another area which has seen tremendous growth through the use of solid core PCF. Here we have covered the excitation of cladding and core mode in an endlessly single mode PCF which has the potential to be used as an effective type of biosensor as the penetration of light in the cladding channels is very strong compared to an evanescent wave field.

Acknowledgments

The author wishes to thank many individuals who during its concurrency offered me great support and guidance. The thesis has been a result of two years of research at the School of Information, Technology and Engineering (SITE) at University of Ottawa. Within this period I met many nice people and enjoyed many beneficial conversations.

First of all, I would like to express my sincere gratitude to Dr. Hanan Anis. As a supervisor, it was a rewarding experience to work under her supervision. She was always willing to stop her work and answer my queries and even accompany me to the lab if there were any problems. I have acquired a great deal of knowledge and attributes that will be a pillar of wisdom for my professional life. I would be grateful to her for allowing me to work in different labs.

I was also very fortunate to work in the Chemistry department at University of Ottawa under the able guidance of Dr. Tito Scaiano and in Electrical Engineering department at University of Toronto under Dr. Amr Helmy.

I have also benefited from the group discussion which was held biweekly. I would like to express my gratitude towards all the members of the group. Their valuable suggestions and discussions contributed to my research.

I would also like to thank Ontario Centre of Excellence for providing various courses which has allowed me to gain not only technical expertise but improve my business and managerial skills. I am thankful to Dr. Hanan Anis for giving me the opportunity to attend these courses.

My research work has been made possible by many blessings I receive in my personal life. I would like to praise and thank the Almighty God for His love, blessing, and guidance to my life; without which I am nothing. I would also like to thank my beloved parents, brother, sister-in-law and sister who have always trusted and showed unconditional love and support throughout my life.

Dedicated to

my beloved parents

Table of Contents

List of Figures

Number *Page*

List of Tables

Glossary

ACN: Acetonitrile

ARROW: Anti-Resonant reflecting optical waveguide

BPM: Beam Propagation Method

CARS: Coherent anti-strokes Raman spectroscopy

CCD: Charge coupled device

CRP: C-reactive protein (phase protein produced by the liver)

Cy5: Cyanine (reactive water-soluble fluorescent dyes)

DNA: Deoxyribonucleic acid

EM: Electromagnetic field

ESM: Endlessly Single Mode

FBG: Fiber Bragg Grating

FEM: Finite Element Method

GVD: Group Velocity Dispersion

HC-PCF: Hollow Core Photonic Crystal Fiber

HC-x: Hollow core PCF guiding at x wavelength

He-Ne: Helium Neon laser at 633nm

HF: Holey Fiber

LFP: Laser Flash Photolysis

LPG: Long Period Grating

MEB: Methyl Blue

MOF: Microstructure Optical fiber

mPOF: microstructured Polymer Optical Fiber

MV: Methyl viologen dichloride hydrate

NA: Numerical Aperture

Nd-YAG: Neodymium-doped yttrium aluminum garnet

NIR: Near Infra Red

NOA: Norland Optical Adhesive

PBF: Photonic bandgap Fiber

PBG: Photonic Bandgap

PCF: Photonic Crystal Fiber

PDE: Partial Differential Equations

PMT: Photo multiplier tube

R6G: Rhodamine 6G

RI: Refractive Index

SC: Supercontinuum

SC-PCF: Solid Core Photonic Crystal Fiber

SERS: Surface enhance Raman Spectroscopy

SiO2: Silica

SPM: Self Phase Modulation

SPR: Surface Plasmon Resonance

TIR: Total Internal Reflection

XPM: Cross Phase Modulation

ZDW: Zero Dispersion wavelength

Symbols

π : 3.14159265

A : Absorbance or optical density

$\mathbf{A_t}$: Absorbance at time t

$\mathbf{A_\infty}$: Absorbance of the products

α : Absorption coefficient

c : Concentration of the sample

θ : Contact angle

ρ : Density

μ : Dynamic viscosity

n : Frequency

L (t): Length of the fiber filled with sample

$\mathbf{A_{pk}}$: Maximum transient optical density

ε : Molar absorption coefficient

$I_{out}(t,\lambda)$: Monitoring light intensities after the sample

$I_{in}(\lambda)$: Monitoring light intensities before the sample

ΔP : Overhead pressure applied

h : Planck's constant

a : Radius of the capillary tube

k : Rate Constant

n_{air} : Refractive of air

n_{sil} : Refractive index of Silica

n_{liq} : Refractive index of the liquid or gas

σ : Surface tension

c : Velocity of light

λ^0 : Wavelength at which the bandgap originally occurs

λ' : Wavelength of the shifted bandgap

Chapter 1. Objectives and Contributions

This chapter presents objectives and contributions made to the thesis.

1.1 Background

The term biophotonics denotes a combination of biology and photonics, with photonics being the science and technology of generation, manipulation, and detection of photons. Biophotonics has therefore become the established general term for all techniques that deal with the interaction between biological items and photons. This refers to emission, detection, absorption, reflection, modification, and creation of radiation from bio-molecules, cells, tissues, organisms and biomaterials [1].

Use of light for detecting any samples is an attractive option for many reasons. Firstly, due to the very small size of biological species, this allows light to interact at a molecular level by focusing it onto small areas (micro-nano). Additionally, the molecules can also be engineered for light to interact in a specific way with them. Secondly, the photonic approach is non-invasive(in most cases), i.e., there is no direct contact with the material, thereby avoiding the risk of bio-fouling (undesirable accumulation of microorganisms), contamination, incompatibility and many other practical problems. Thirdly, most biological reactions take place in aqueous media which have wide wavelength windows that are transparent to visible and infrared light. The aqueous medium creates restrictions in electronic and mechanical systems due to damping, therefore switching to biophotonics would provide another alternative. Lastly, the development of optical telecommunication tools like fibers or photo detectors can be adapted to obtaining high sensitivity and sophisticated optics for use in biophotonics.

1.2 Thesis Objectives

According to a survey, optical sensors and biosensors are expected to register the fastest growth in the sensor market [2]. Very recently, a research group led by Gerald Loeb has reported that, a hair-like optical fiber monitors glucose level frequently by implanting it in the skin. The sensor demonstrated is very sensitive, affordable, and less invasive [3].

Photonic crystal fiber (PCF) is an interesting class of optical fiber where guiding of light is possible through either total internal reflection, similar to conventional fibers, or the

photonic bandgap effect, wherein a specific range of wavelengths is propagated while rejecting all other wavelengths. The novelty in the design of PCF is also due to the presence of channels, which has resulted in a novel range of applications. One such field where PCF has shown promise is biophotonics.

This brings us to the objective of this thesis, which focuses on using PCF for biosensing. We have experimentally demonstrated four novel and different techniques to sense various analytes for biosensing applications. These techniques are: bandgap shifting property in photonic bandgap fibers, excitation of cladding mode in PCF, Raman, and laser flash photolysis. The advantages of using PCF include:

- PCF uses samples in the nano to pico liter range, thereby significantly bringing down the sample consumption rate. Typically a sample under analysis uses at least a milliliter of volume when investigated using a "test tube" or a "cuvette".
- PCF can pave the way for non-invasive and label free detection of biomolecules.
- The small sample volume utilized and the large overlap of the propagating laser mode field with the sample in hollow core PCF provides the potential for devising simple, compact and sensitive biosensors.
- Hollow core PCF confines most of the signal in the core leading to a small effective area and large interaction length that can be exploited in Raman.

1.3 Thesis Contributions

We have demonstrated four novel techniques that enable using PCF as a biosensor:

- Bandgap shift: We have demonstrated a unique way to use the bandgap shift property of the fiber by non-selectively filling the fiber with a liquid and using it as a sensitive type of refractive index measurement biosensor. Although the non-selective approach has been already discussed in the literature, no one has reported using the bandgap shift property itself for biosensing. In non-selective filling approach, both the core and the cladding channels are filled with the sample. This results in a shift of the transmission wavelength of the fiber, depending on the

refractive index of the liquid in question. In the experiment, we have used a small piece of fiber HC-1060 which has 1060nm as its centre transmission wavelength. As the concentration of the analyte changes, the refractive index changes leading to a shift in the transmission wavelength. By monitoring the wavelength shift, one can find the concentration of the sample.

- Cladding mode excitation: Typically supercontinuum generation is achieved by exciting the core mode with an incident light in the anomalous dispersion range or very close to the normal dispersion range. We have for the very first time demonstrated the excitation of the cladding and the core mode for supercontinuum (SC) generation in a PCF. The advantage of using this method is that the strong penetration of light into the cladding channels can possibly be used for evanescent wave biosensor by having the sample in the cladding channels of the fiber.

- Laser flash photolysis (LFP): We have demonstrated this technique in PCF for the first time and used it to measure transients in chemical samples. The traditional approach is to use milliliter of samples in a test-tube or cuvette, which is excited with a laser and the transient's states such as a triple state of the sample is measured by monitoring a continuous wave source. The advantage of using a PCF is that it acts as a sample container, which can tremendously reduce the sample consumption, and interacts with the sample very efficiently. The results shows significant increase in the signal obtained compared to conventional techniques.

- Raman: PCF for measuring a Raman signal has been demonstrated in the literature using the selective filling technique. This approach is cumbersome and time-consuming. Moreover, the problem of liquid evaporation is unavoidable which requires a set of steps to be repeated to refill the fiber. To address this problem, we have proposed to use, for the first time, a non-selective filling technique that exploits the bandgap shift property of the fiber.

1.4 Thesis Outline

The rest of the thesis is organized as follows: Chapter 2 is an introduction to biosensors. In this chapter, we discuss light/matter interactions, photonic crystal and bandgap fibers, different filling methods for PCF, the bandgap shift property and simulation results. The study of far field patterns in PCF is also covered in this chapter. Chapter 3 discusses the literature review on photonic crystal fiber for different application presented in the literature. The experimental setup and results of bandgap shift property of the PBF when non-selectively filled with heavy water and different concentration of ethanol has been demonstrated. The results obtained detect solvents with refractive index change of up to 10^{-5}suggesting that PBF can be used as an effective and sensitive type of sensor.

Chapter 4 focuses on the excitation of the cladding and the core mode for generation of supercontinuum in a solid core PCF. The chapter covers a literature review on supercontinuum generation, PCF's dispersion characteristics followed by experimental setup and results. The PCF used is an endlessly single mode PCF which has a solid core surrounded by cladding channels. This technique proposes a possible use for biosensing as the cladding channels of the PCF can be filled with samples and the strong penetration through the cladding mode makes an interesting type of evanescent wave sensor. Chapter 5 discusses using laser flash photolysis and PCF for studying chemical reactions. In the experiment, we were successfully able to detect triplet state decay for samples like xanthone in toluene, in acetonitryl and benzoin soluble in water and in presence of methylviologen. This was done using solid core as well as hollow core fibers. This chapter also gives a brief introduction to history, traditional approach, interpretation of the data recorded.

Chapter 6 is Photonic Crystal Fiber as a Raman biosensor. The main purpose of this experiment was to observe enhancement in Raman signal by using a Photonic Bandgap Fiber. The chapter covers topics such as introduction and theory on the Raman Effect, instrumentation of Raman spectroscopy, followed by a literature review. In the experiment, we used ethanol as the solvent and observed a Raman signal enhancement of 40 times. For carrying out the experiments we used a small piece of fiber of different lengths: 3, 5, 7 and

9cm. The chapter also includes a section on the characterization of nanocrystal using a selective filling technique. Chapter 7 covers conclusion drawn from thesis and propose future research work.

List of Publications

1. **Altaf Khetani**, Marie Laferrière, Hanan Anis and J.C. Scaiano "Laser flash photolysis with subnanoliter samples. Photonic crystal fibers as ultra small smart test tubes", submitted to the Journal of Material Science (2008).
2. Majid Naji, **Altaf Khetani**, Neil Lagali, Rejean Munger, Hanan Anis, "A novel method of using hollow-core photonic crystal fiber as a Raman biosensor" Photonics West 2008(Paper 6865-19).
3. Yury logvin, **Altaf Khetani**, Hanan Anis, "Cladding mode assisted supercontinuum generation in solid core photonic crystal fiber for biosensor application", Photonics West 2008(Paper 6875-22)
4. J. Irizar, J. Dinglasan, J.B. Goh, **A. Khetani**, H. Anis, D. Anderson, C. Goh, A. S. Helmy "Raman Spectroscopy of Nanoparticles using Hollow-Core Photonic Crystal Fibers" CLEO 2008 (Paper 1539)
5. J. Irizar, J. Dinglasan, J.B. Goh, **A. Khetani**, H. Anis, D. Anderson, C. Goh, A. S. Helmy "Raman Spectroscopy of Nanoparticles using Hollow-Core Photonic Crystal Fibers" accepted in the Journal of Selected Topics in Quantum Electronics.

Bibliography

1. http://en.wikipedia.org/wiki/Biophotonics (accessed March 19, 2008)
2. http://answers.google.com/answers/threadview?id=460549 (accessed March 19, 2008)
3. Prachi Patel-Predd "New Optical Glucose Sensor: A hair-like optical fiber implanted in the skin could make frequent glucose measurements easier for diabetics," MIT Technology Review (Dec 28, 2006).

Chapter 2. Introduction to Biosensor and Photonic Crystal Fibers

This chapter demonstrates different filling techniques to fill a PCF. The selective filling technique followed in the literature is tedious and time-consuming which has led us to switch to the non-selective filling technique. This technique will shift the bandgap wavelength of the fiber, when filled with a sample. Far field patterns of photonic crystal fibers (Endlessly Single Mode–Photonic Crystal Fibers: ESM-PCF and Photonic Bandgap Fibers: PBF) empty and when filled with water is also demonstrated. The far field pattern in the case of ESM-PCF filled with water shows interesting results as the higher order harmonics and the spectral content of the peaks could lead to biosensing applications.

2.1 Introduction

In this chapter we start by presenting a brief overview on biosensor and the transconduction mechanism in Section 2.2. This is followed by optical biosensors discussed in Section 2.3. Section 2.4 covers photonic crystal fiber for biosensor which introduces photonic crystal fibers and theirs classification. Section 2.5 covers filing techniques such as selective and non-selective filling. The bandgap shift property of the fiber when filled with different refractive index is covered in Section 2.6. Modeling results of PBF when empty and filled are presented in Section 2.7. Finally, Section 2.8 covers far field patterns obtained from ESM-PCF, HC-PBF.

2.2 Introduction to Sensor

A sensor in a broad sense can be described as a complete device/system that receives a signal or physical stimulus such as heat, light, sound, pressure, magnetic or any particular motion and records, indicates or otherwise responds to it [1].

Sensors can be classified into three major categories:

1. Physical sensors – involve measurement of physical quantities such as length, weight, pressure, temperature, etc.
2. Chemical sensors - respond to a particular analyte in a selective way through a chemical reaction and can be used for the qualitative or quantitative determination of the analyte [2].
3. Biosensors - incorporate a biological sensing element connected to a transducer or a combination of a biological receptor compound and a physical or physiochemical transducer [3, 4]. Biosensors can detect chemical or inorganic analytes but their main purpose is to recognize the biological samples in nature.

Generally, all types of sensors contain two key components: the 'recognition element' and the 'transducer'. The sensor performance is judged by a few important factors such as, operation of the transducer, sensitivity range, accuracy, nature of the solution, response time, recovery time and selectivity which is principally a function of the selective recognition element.

An important role is played by the recognition element in governing the overall selectivity of the sensor system. This is because the key task of the recognition element is to respond only to particular species of interest in the sample and to avoid the interferences from other species present in the environment. The substances that are to be detected or measured by a sensor device are called analytes. Information obtained through a sensing mechanism is translated into a signal for further processing. The device that provides the conversion of information is called a 'transducer' [5]. A schematic of the sensor system is shown in Figure 2-1.

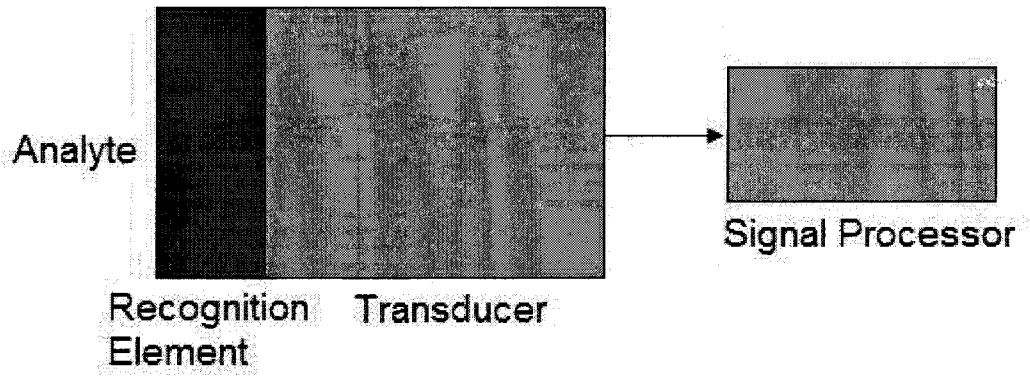

Figure 2-1 Schematic of a Sensor System

A variety of trans-conduction mechanisms used are: electrochemical, electrical, optical, thermal, and piezoelectric. Below is a table summarizing trans-conduction mechanisms used in sensors [6].

TRANSCODUCTION SYSTEMS	MEASUREMENT
Electrochemical	Amperometry Potentiometry
Electrical	Conductivity
Optical	Luminescence Fluorescence Refractive Index
Piezoeelctric	Mass-Quartz Crystal microbalances Surface acoustic waves
Thermal	Calorimetry

Table 2-1 Principal trans-conduction systems of different types of sensors

Rapid advancement in technology in recent times has led to optical transducers being preferred over other techniques. In the following section, we will be concentrating on the optical type of sensor. The advantage of using this type of sensor is that it allows light to interact directly with the sensing material thereby providing greater sensitivity, electrical passiveness, freedom from electromagnetic interference, wide dynamic range, and cost effectiveness. Moreover, it avoids conversion of electronics into photonics at each sensing site.

2.3 Optical Biosensor

In order to get a vivid analysis of methods mentioned above, a review of some basic concepts of the interaction of light with matter will be helpful. Optical sensors are based on the interaction of light with matter. When an electromagnetic radiation of frequency ν interacts with charged matter, it can cause a change in energy ($h\nu$) and linear momentum ($h\nu / c = h/\lambda$). This will in turn bring a change in the optical properties of the atoms and lead to stimulation of atomic electrons, thereby causing them to radiate. The optical changes that are produced as an outcome of these interactions contain information about the analyte [5].

There are several measurement techniques depending on the optical parameters being used. For example, absorbance, fluorescence, phosphorescence, evanescence, surface plasmon resonance, light scattering, and change in refractive index can be used as a measurement technique depending on the change in intensity, wavelength, and phase parameters [7] (summarized in Table 2-2).

MEASUREMENT TECHNIQUE	OPTICAL PARAMETER MEASURED
Absorption, Scattering, Reflectance, Fluorometry, Luminescence	Intensity
Evanescent Spectroscopy	Intensity ,wavelength
Surface Plasmon Resonance	Intensity ,wavelength
Interferometry	Intensity, phase
Refractometry	Intensity
Reflectrometry	Intensity, time
Lifetime based Fluorometry	Intensity, time, wavelength

Table 2-2 Measurement technique and corresponding optical parameter measured.

2.4 Photonic Crystal Fiber Biosensor

There are two different classification schemes for a fiber based biosensor. The first scheme classifies the sensors as being either extrinsic or intrinsic. In an extrinsic sensor the optical fiber is used to take the light to and from the sensing element, while in an intrinsic sensor the fiber itself acts as a sensing element. The optical transduction methods discussed earlier are used for measuring the target analyte. The second classification scheme is direct or indirect sensors. In a direct type of sensor, the intrinsic optical properties of the target analyte are measured, while in an indirect type of sensor, the absorbance or fluorescence of a fluorescent dye or tag is measured.

Development and availability of optical fiber has made fiber the front runner as a transducer. Although optical fiber has many important applications, particularly in

communication system, medical instrumentation, and many kinds of optical components, we will be using it for biosensing. In a fiber-optic based sensor, light is guided by total internal reflection at the core-cladding interface. This is illustrated in Figure 2-2 [8]. The optical signal obtained is either transferred back via the original sensing fiber, or through a separate reference fiber. Multiple fibers are often used to speed up the overall sensing process.

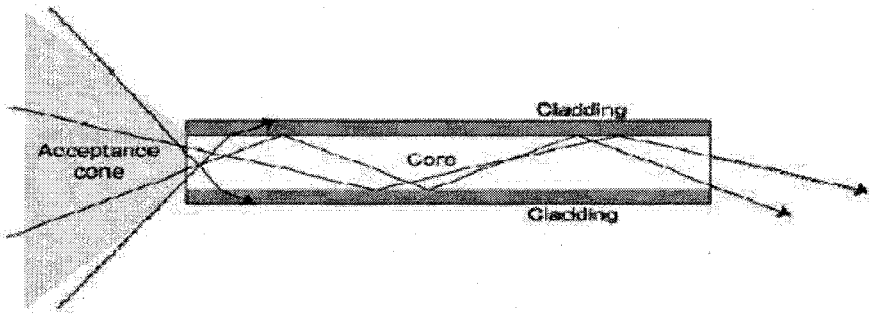

Figure 2-2 Diagram of a fiber based optical biosensor [8]

One class of optical fibers is photonic crystal fibers. It was demonstrated by Russell's group and has been applied to various fields [9]. We will concentrate on using Photonic Crystal Fiber as a biosensor which can serve as a sample container as well as a light guiding tool for optical sensing purpose. A brief introduction of PCF, filling techniques, simulation and far field patterns of the fiber will be helpful for demonstrating the use of PCF for biosensor applications.

2.4.1 Photonic Crystal Fiber

In the past three decades, a great deal of effort has been devoted to the development of new types of optical fibers to improve their performance and to reduce the cost of fibers. Photonic crystal fiber is one of the most recent advances in fiber-optic technology that has attracted considerable interest from many researchers around the world.

In 1991, J. Russell and his group invented microstructure optical fibers. The fibers were made from silica with a periodic arrangement (in the cross-section) of air-channels running

along the full length of the fiber. Philip Russell was awarded the Frauenhofer Award / Burley Prize of the Optical Society of America in 2000 for recognition of *"his invention of the photonic crystal fiber, an array of micron-spaced sub-micron holes allowing extremely large mode area single-mode fibers offering solid-core fibers with better power handling [9, 10]."*

The name photonic crystal fiber (PCF) is referred by other terms like holey fiber (HF), microstructured optical fibers (MOF), and microstructured fibers (MF).

A brief history of Photonic Crystal Fiber is given in the following table

YEAR	DEVELOPMENT	YEAR	DEVELOPMENT
1991	Photonic crystal fiber reported	2002	Ultra-flattened dispersion PCF
1996	PCF fabricated	2003	PCF with low loss (0.28dB/km) @ 1550nm
1997	Endlessly single mode PCF	2004	Solid PBF
1998	First PBF demonstration	2005	PBF with loss 1.2dB.km
1999	Hollow core Photonic bandgap fiber	2006	Hybrid PCF
2000	Highly non-linear PCF	2007	PCF with low loss(0.1dB/km) @1550nm
2001	High NA PCF		

Table 2-3 History of development of fibers and its applications [23]

2.4.1.1 Classification of Photonic Crystal Fiber

A broad classification of PCF is shown in Figure 2-3. The two main classification of PCF are index-guiding fibers and bandgap-guiding fibers. Throughout the thesis, we will denote the index-guiding photonic crystal fiber as PCF and bandgap-guiding fibers as PBF.

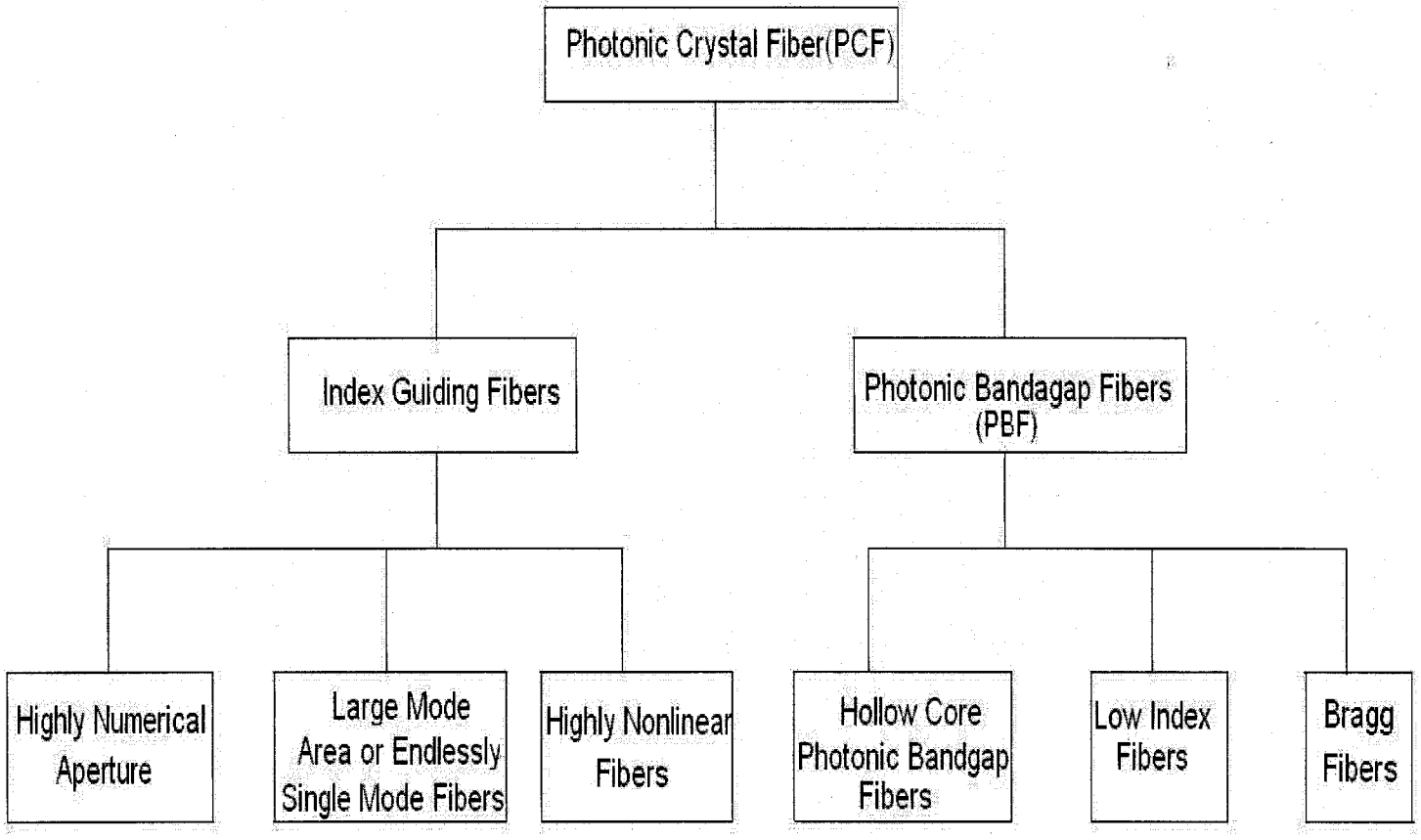

Figure 2-3 Classification of photonic crystal fiber types

a) Index-guiding fibers: The core of a microstructured fiber is made of fused silica and the cladding is formed by air holes running along the entire length of the fiber. In this class of fibers, decrease in the refractive index by air holes around the core, decreases the effective refractive index of the cladding and as a result light is guided inside the core by total internal reflection. Figure 2-4 shows one such example of a PCF known as endlessly single mode PCF [11].

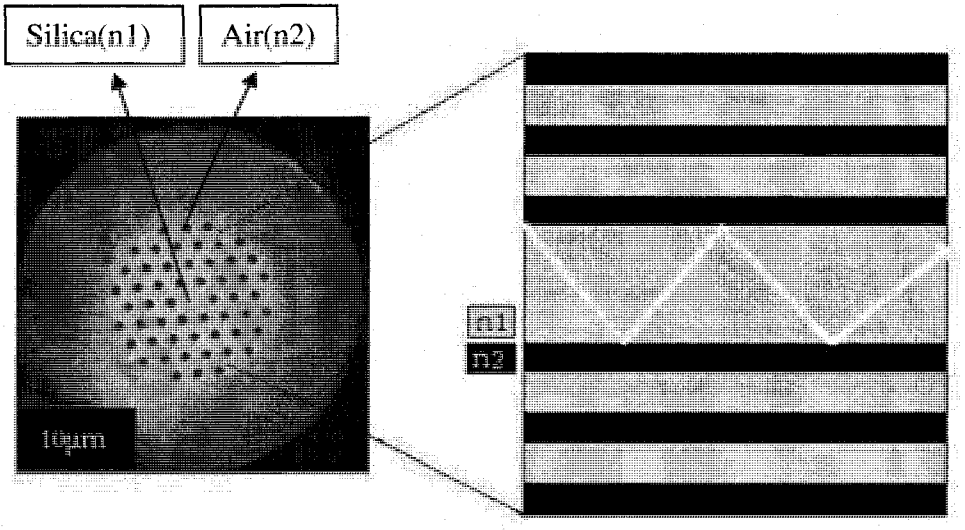

Figure 2-4 Guiding mechanism in Index Guiding PCF

b) Bandgap-guiding fibers: In this type of fibers, light is guided by a two-dimensional photonic bandgap in a hollow core or in a core made of a material with the refractive index lower than the effective index of the cladding. Due to the bandgap effect, certain light frequencies are not allowed to escape from the core, but will be reflected leading to wavelength dependent upon the light transmission.

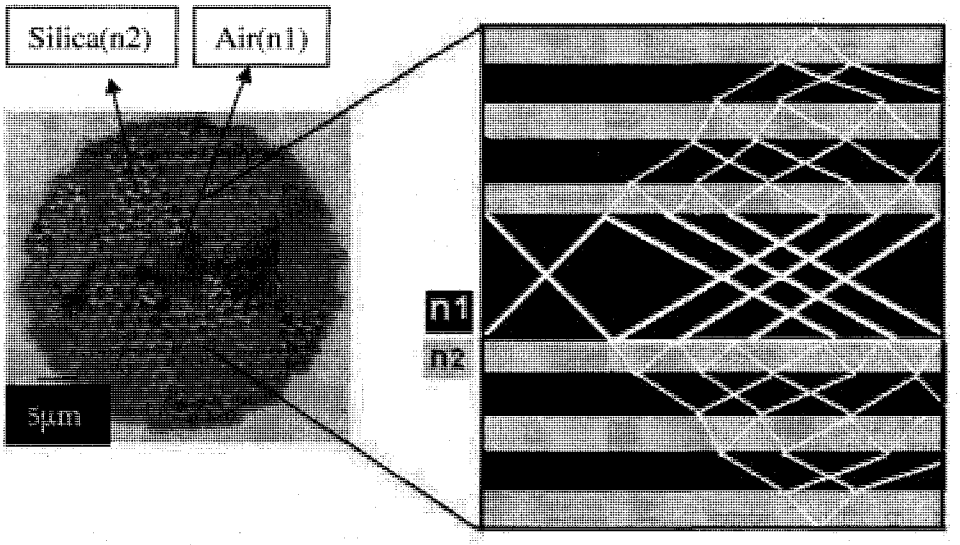

Figure 2-5 Guiding mechanism in Photonic Bandgap Fibers (PBF)

The guiding mechanism in bandgap-guiding fibers is unlike index guiding fiber due to lower refractive index of the core, and, therefore, the fiber guides the light by consecutive constructive interferences of reflections from several air-silica interfaces inside the core and destructively in the cladding. The guiding mechanism is as shown in Figure. 2-5. The type of periodic air-silica cladding exhibited by the fiber results in a bandgap for photons in the radial direction, forcing the photons to propagate inside the core [11, 12].

2.5 Filling a Photonic Crystal Fiber

PBF with its attractive design of hollow core has the potential to be used as an effective sensor. The guiding mechanism of PBF differs depending on the filling technique applied. For sensing applications, filling a PBF is a challenging and important step due to the core and cladding's micro size. There are two ways that PBF can be filled. Those are selective filling and non-selective filling. Both techniques will be discussed in the following subsections.

2.5.1 Selective filling core of PCF

The purpose of selective filling is to fill only the core of the PBF which is a more complex process because it has a core as well as cladding channels. At the end of the process, the core is readily accessible to be filled by a sample. The guiding occurs by total internal reflection (TIR) due to the sample's refractive index being lower than silica surrounded by claddings holes [13].

2.5.1.1 Selective filling by applying Overhead Pressure

The first possibility is to use overhead pressure to selectively fill the central core of the PBF. The basic principle is that the liquid/polymer travels at different speeds for different hole-size leading to variation in the distance travelled by the liquid depending on the size of the holes. The distance traversed in the holes is given by the equation [13]:

$$L(t)=\left(\frac{A}{B^2}\exp(-Bt)+\frac{At}{B}-\frac{A}{B^2}\right)^{1/2} \tag{2-1}$$

where $A=\frac{4\sigma\cos\theta+2\Delta Pa}{\rho a}$ and $B=\frac{8\mu}{\rho a^2}$, a is the radius of the capillary tube, σ is the surface tension, θ is the contact angle, ΔP is the overhead pressure applied, ρ is the density, and μ is the dynamic viscosity.

The principle behind selective filling is that, due to the core size being larger than the cladding holes, the liquid in the core transverses a considerably longer distance relative to the cladding holes. In the first step, PBF is filled with UV-polymer/adhesive under pressure and cured (hardened) with UV light source. The next step is to cleave the fiber at a point where the polymer seals only the center hole. As the center hole is now blocked, the next step is to fill the fiber's cladding holes with adhesive so that the polymer has resided further compared to the sealed center hole. Curing and cleaving at a point where the cladding holes are capped, this leaves the center hole accessible,

which now can be filled with the desired liquid. Figure 2-6 shows the steps performed. The last step is to fill the core with the desired liquid and cleaving out the polymer region in the cladding holes.

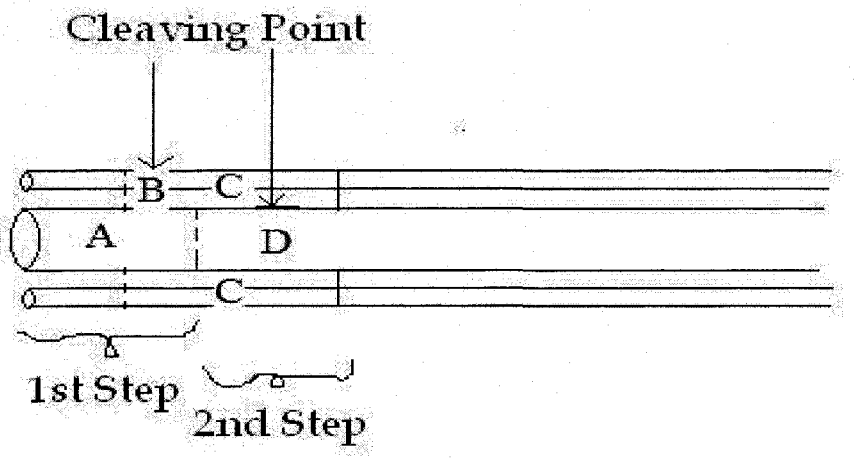

Figure 2-6 Steps involved in selective filling of a PBF showing sequence: A: shows the polymer travelling different distance for core and cladding channels; B: cleaving the fiber; C: filling only cladding channels as core is capped with the polymer; D: cleaving again will lead to capping only cladding channels

The selective filling technique is performed on a HC-633-01 fiber purchased from Thorlabs Inc. The adhesive used is Norland Optical Adhesive (NOA-73) purchased from Norland Products to which coumarin was added, just to know the position of the polymer in the fiber. As shown in Figure 2-6 in the first step the fiber is filled for 10 min under differential pressure of 2 bars. Due to difference in the size of the holes, polymer in the core has traveled to 1.8cm while in the cladding to 0.63cm. After curing the fiber with UV light, 1.5cm of the fiber is cleaved leaving the center hole capped with polymer. The next step is to fill the fiber again for 20 min under pressure, so that the polymer has traversed in the cladding holes to 1cm. This is followed by curing and finally cleaving around 0.6cm, leaving the center channel empty and now accessible for filling with the desired liquid. (Figure 2-7 e).

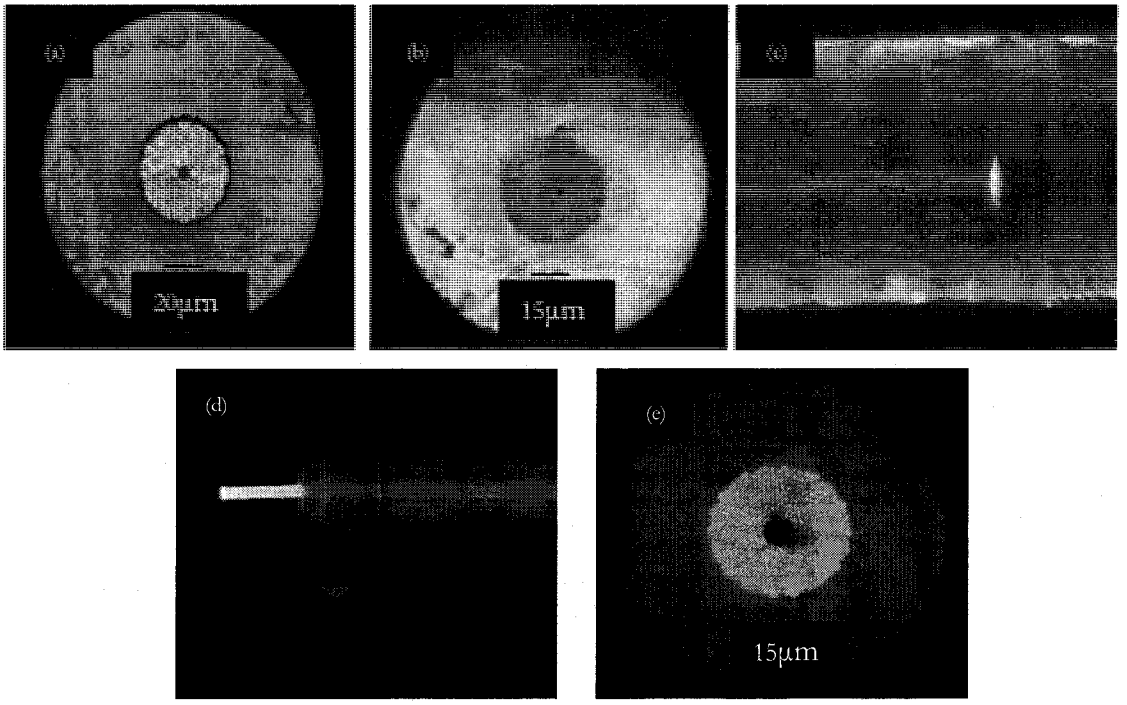

Figure 2-7 Various stages in selectively filling a PBF

(a) Cross sectional view of an Empty HC-633 (b) Cross sectional view of all channels of HC-633 filled with Norland Optical Adhesive (NOA). (c) Cross sectional view of NOA traveling in the central channel of HC-633 (d) Cross sectional view of HC-633 showing the central channel is filled with NOA. (e) Cross sectional view of HC-633 showing the central core empty to be filled with desired liquid.

In order to verify the selective filling, the fiber is filled with NOA and coumarin (as it fluoresces and helps in tracking liquid travelled in the micro channels) and later it is cleaved. The final result displays the core being selectively filled in Figure 2-8.

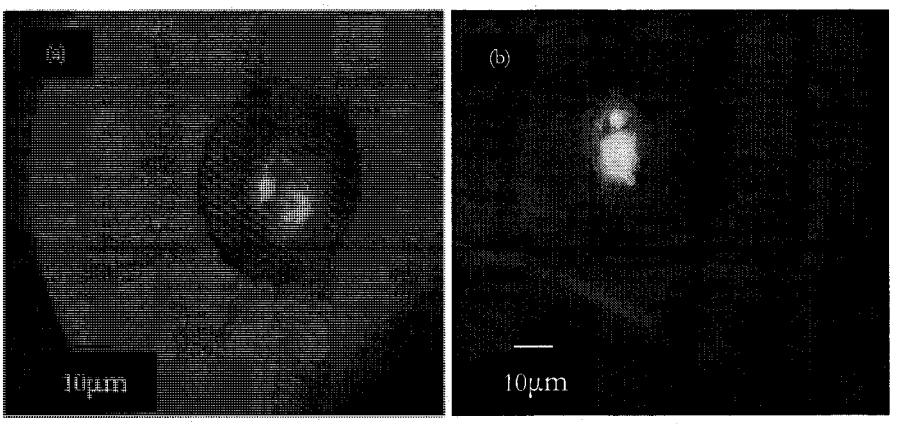

Figure 2-8 a) Image of HC-633 fiber after being selectively filled with NOA b) fiber under fluorescent lamp.

2.5.1.2 Selective filling by fusion splicer

Another way to achieve selective filling of the core of a PBF is by using a fusion splicer. In this method, the main principle is applying specific arc currents to the holes/channels of the PBF which leads in collapsing the cladding holes, leaving the core to be accessible and filled with a sample. [14]

In order to perform this experiment we have used an Ericsson FSU995 fusion splicer. The splicer's arc currents are varied depending on the size of holes of the fiber. A particular arc current will result in collapsing of cladding holes and not the core.

In this experiment we have used an HC 1550-01 fiber purchased from Thorlabs Inc. The specifications of the fiber are 10.9μm of core diameter with a pitch of 3.8μm.

The procedure is to use fusion parameter on the splicer, as this is important in carrying the selective filling technique by using fusion splicer. The fusion splicer's pre-fusion time was set to 8.0mA, the center position to 205um and fusion time one and three are set to zero. The next step is to strive and find out by varying fusion time two and fusion current two which will result in collapsing the cladding holes. After several attempts, the values generated are 14mA and 0.3sec for sealing the cladding holes. Figure 2-9 shows selective filling of HC-1550 central core.

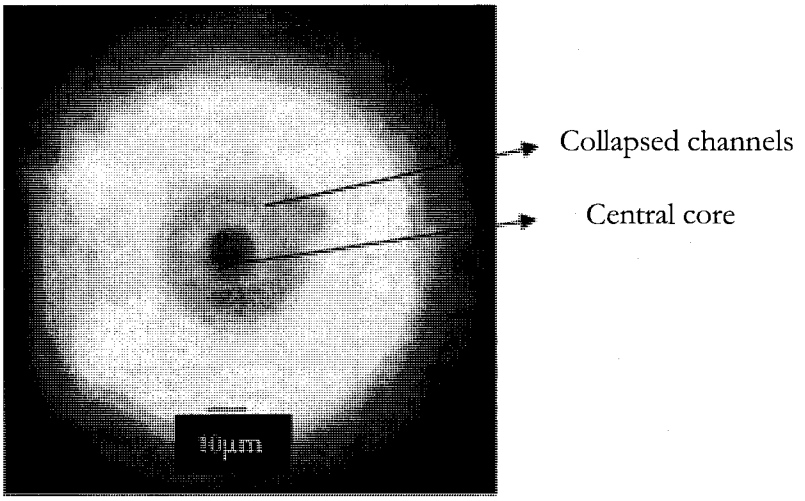

Figure 2-9 Image of HC-1550 fiber with cladding holes collapsed using fusion splicer

Thus, the selective filling process successfully allows filling just the center core hole, where the light is confined by total internal reflection which is similar to the index-guiding photonic crystal fiber. The disadvantage with this process is that it is tedious and time consuming as it involves several steps before the final stage is reached. In addition, the liquid which is filled tends to evaporate due to the heat generated from the optical intensity. This evaporation changes the mechanism of confinement of light in the core. Consequently, sensing can only be achieved using other selectivity mechanisms, such as Raman. This process is cumbersome and restricts the choice of liquid to avoid highly multimode behavior [15, 16].

2.5.2 Non selective filling technique for PBF

2.5.2.1 Non selective filling technique for PBF with lower refractive index than silica

In non-selective filling technique, core as well as cladding channels of PBF's are filled with the material for sensing purposes. The advantages of using this technique are that it is easy, much simpler to implement and even solves the problem of evaporation by inserting a reservoir of the liquid. The guiding mechanism for a filled fiber is through a bandgap effect, in which the center wavelength is shifted depending upon the refractive index of the filled sample [17-19]. The whole mechanism of bandgap shifting and guiding mechanism is explained in section 2.6.

2.5.2.2 Non selective filling technique for PBF with higher refractive index than silica

Another interesting phenomenon is to observe how the PBF behaves when filled with a liquid of higher refractive index than silica. It is now expected that PBF would behave as an "endlessly single mode" PCF. Simulation results were carried for HC-1060 fiber with solvent toluene (n=1.48661@633nm) and the results confirms that light would be guided in the tested wavelengths such as 400, 800, 1060 and 1550nm, confirming its endless single mode characteristics. The simulation results that confirm this is explained in section 2.6 (Figure 2-16, 2-17).

2.6 Band-gap shift property of the filled fiber

Non-selectively filling a PBF with different refractive index materials will result in its bandgap property being shifted [17]. Due to the shift in the bandgap, the center wavelength of the fiber shifted is given by the formula

$$\lambda' = \lambda^0 \left[\frac{1 - \left(\frac{n_{liq}}{n_{sil}} \right)^2}{1 - \left(\frac{n_{air}}{n_{sil}} \right)^2} \right]^{1/2} \tag{2-2}$$

where λ^0 is the wavelength at which the bandgap originally occurs, λ' is the wavelength of the shifted bandgap, n_{air} is the refractive index of air, n_{sil} is the refractive index of silica and n_{liq} is the refractive index of the liquid or gas.

In order to effectively use the bandgap shift property of the fiber, we need to choose the fiber which would guide the source wavelength when filled with liquid. For example, the experimental conditions are: the source wavelength is 633nm (λ') which corresponds to the wavelength shift and the liquid under examination is water (n_{liq}=1.33). By substituting the value λ', n_{liq}, n_{air}(=1) n_{sil}(1.46@633) in the above equation we can find λ^0, the wavelength of the fiber when empty to be 1060nm. This condition works with HC-1060 fiber.

We have investigated hollow core PBF's available from Crystal Fiber A/S. The center wavelength and the range of wavelength supported by the fiber when empty are obtained from the specifications provided by the manufacturer. Non-selective filling of the fiber will result in shifting up its center wavelength, as well as the wavelength supported which is calculated from formula (2-2). A list of the fibers and the wavelength supported when empty, filled with water, acetonitryl, and ethanol is shown in Table 2-4.

LIQUID	REFRACTIVE INDEX	HC-440 (410-470nm)	HC-580 (515-595 nm)	HC-633 (570-690 nm)	HC-800 (795-880 nm)	HC-1060 (990-1150 nm)	HC1550 (1450- 1650 nm)
Water	1.33	249(232-266)	328(291-336)	358(322-390)	452(450-498)	**600(560-651)**	877(820-934)
Acetonitryl	1.34	236(220-252)	311(276-319)	339(306-370)	429(426-472)	**569(531-617)**	832(778-886)
Ethanol	1.36	212(198-227)	280(248-287)	305(275-333)	386(384-425)	**512(478-555)**	748(700-797)

Table 2-4 List of different liquids and different fibers and their bandgap shift wavelength range in nanometer.

2.7 Modeling using COMSOL

Modeling a photonic bandgap fiber can be done in different ways: effective index method, plane wave expansion method, finite difference time domain method, multipole method, and finite element method (FEM) [11]. In this thesis, the modeling of PBF has been done using the commercial software by name COMSOL Multiphysics 3.3 which follows a finite element approach [22]. FEM was developed in the 1970s for aerospace structure design. Over the years it has become a convenient tool for wave guide design and offers a new dimension to the modeling process.

COMSOL is a FEM modeling software, which describes partial differential equations (PDE's) by simulating a structure. The software consists of unique modules, enabling users to solve a specific application or to study range of applications. Electromagnetic field simulation of photonic components can be solved through an electromagnetic module. We have presented steps for designing photonic bandgap fiber in particular the HC-633-01 fiber. In order to model other PBFs like HC-1060-01 fiber, the core diameter and pitch has been scaled according to the specification obtained from the manufacturer/supplier.

Step1: The geometry of the fiber HC-633-01 is defined in a Matlab program with a core diameter of 5.1μm and a pitch of 1.77μm. A separate code was written for defining a hexagonal cladding structure.

Step2: The geometry shown in Figure 2-10 is exported using COMSOL script.

Step 3: The COMSOL parameters are defined as follows: The application mode used is the partial differential equation (PDE) coefficient form, Constants k (propagation constant $2*\pi/\lambda$), n1 (RI of core), n2 (RI of silica), n3 (RI of cladding holes) are defined in this step.

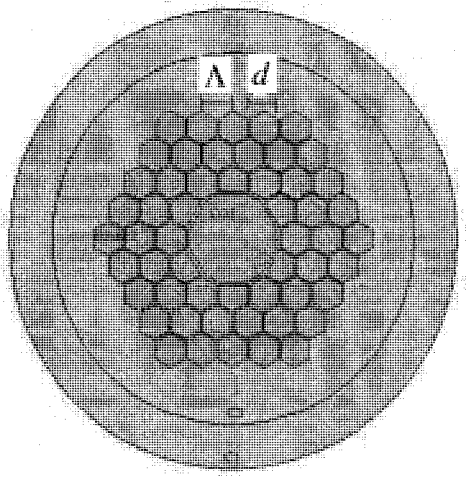

Figure 2-10 Geometry of the HC-633 fiber

Step 4: Initialize the mesh (Figure 2-11). The mesh consists of 23366 elements with 46793 degrees of freedom. This has been shown to accurately reproduce the results for modeling a fiber.

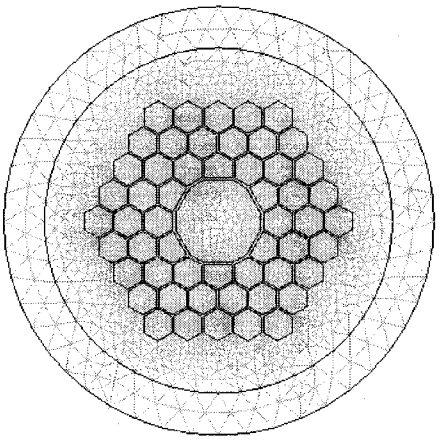

Figure 2-11 Mesh of the HC-633 fiber

Step5: Solving the fiber geometry with defined parameters leads to many eigen value modes supported by the fiber. For a particular eigen value, the fiber will support lowest mode operation as shown in Figure 2-12.

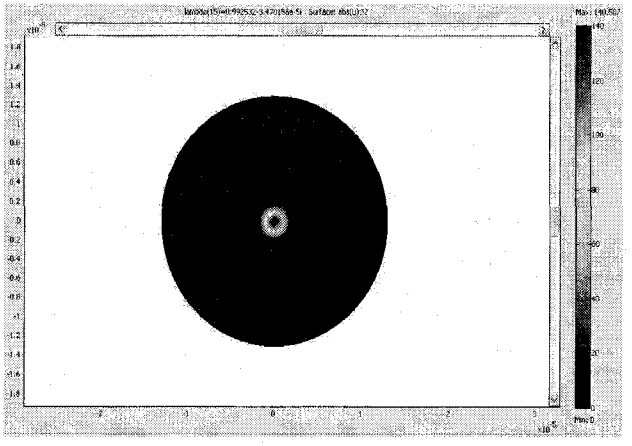

Figure 2-12 Lowest order mode operation of HC-633

We present simulation results for the HC-633-01 fiber which supports lowest order modes for two cases: a) selectively filled with water and b) non-selectively filled with water. In the case of selectively filled with water, the wavelength supported by the fiber is 633nm so the mode obtained is lowest order mode. In the later case, when the fiber is non-selectively filled with water, we were not able to obtain a lowest order mode at 633nm but when we changed λ value in propagation constant to 358nm(in accordance to Table 2-4) we did find a lowest order mode supported by the fiber. Figure 2-13 and Figure 2-14 display the simulation results for these two cases.

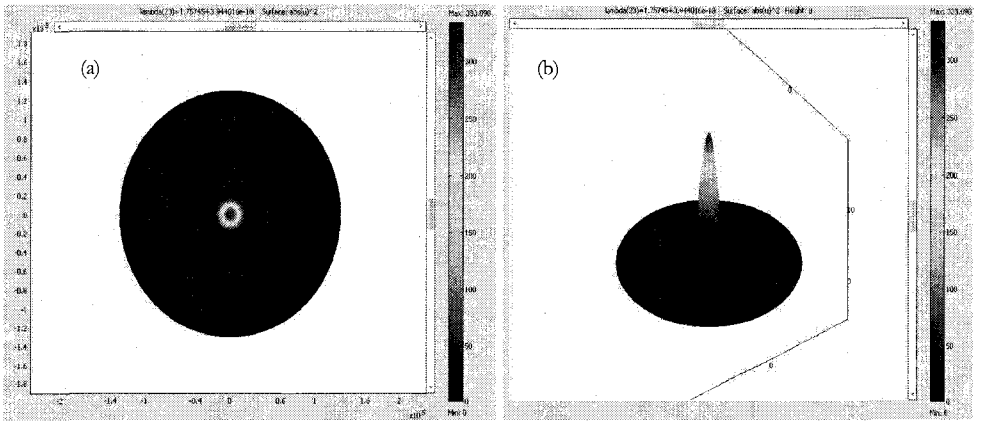

Figure 2-13 Simulation results for the HC-633 PCF when the core is selectively filled with water (n=1.33). a) 2-D view b) 3-D view

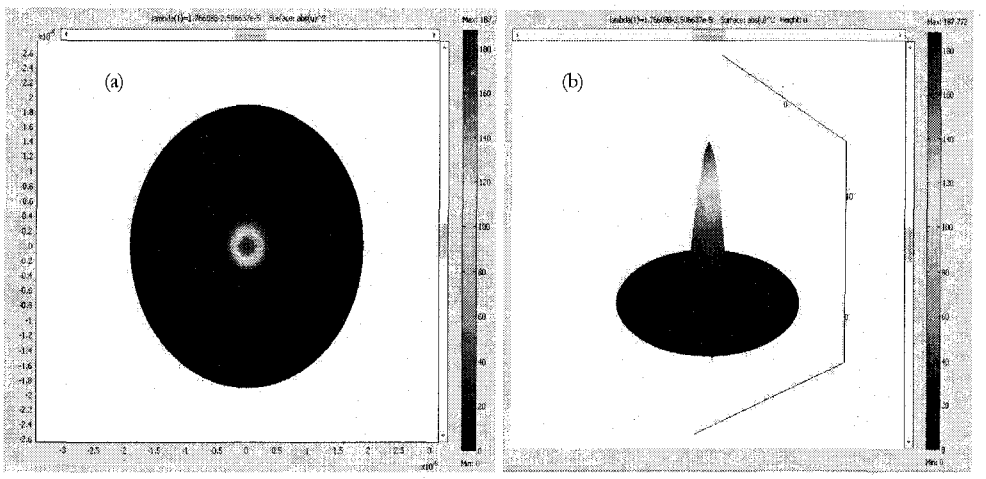

Figure 2-14 Simulation results for HC-633 fiber supporting 358nm when filled with water a) 2-D view b) 3-D view

We also present simulation result for the HC-1060-01 PBF for two scenarios: non-selectively filled with (a) lower refractive index liquid (water) (b) higher refractive index liquid (toluene). The simulation result of the HC-1060-01 fiber when filled with water is shown in Figure 2-15. The results obtained have been helpful in choosing the fiber to carry out experiments for various applications (Chapter 3, 5)

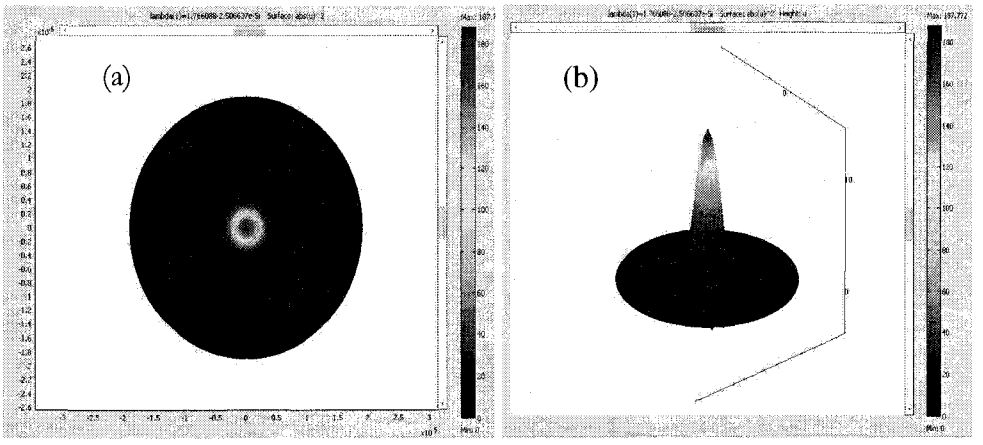

Figure 2-15 Simulation results for HC-1060-01 fiber when filled with water a) 2-D view b) 3-D view

The simulation results displayed in Figure 2-16 and 2-17 are for the case of the HC-1060-01 PBF non-selectively filled with toluene. The result shows an interesting property of the fiber supporting a very wide range of wavelength as discussed in section 2.5.2.2.

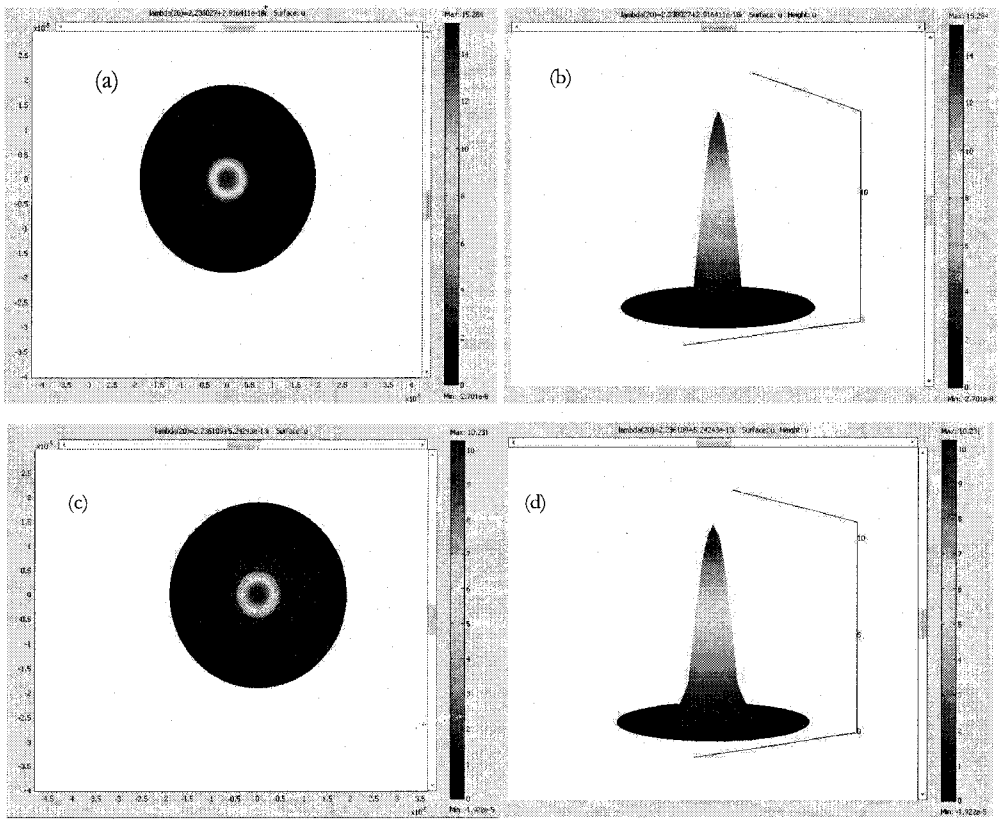

Figure 2-16 (a, b) Simulation results for HC-1060-01 fiber filled with toluene at wavelength= 400nm Figure (c, d) Simulation results for HC-1060 fiber filled with toluene at wavelength= 800nm

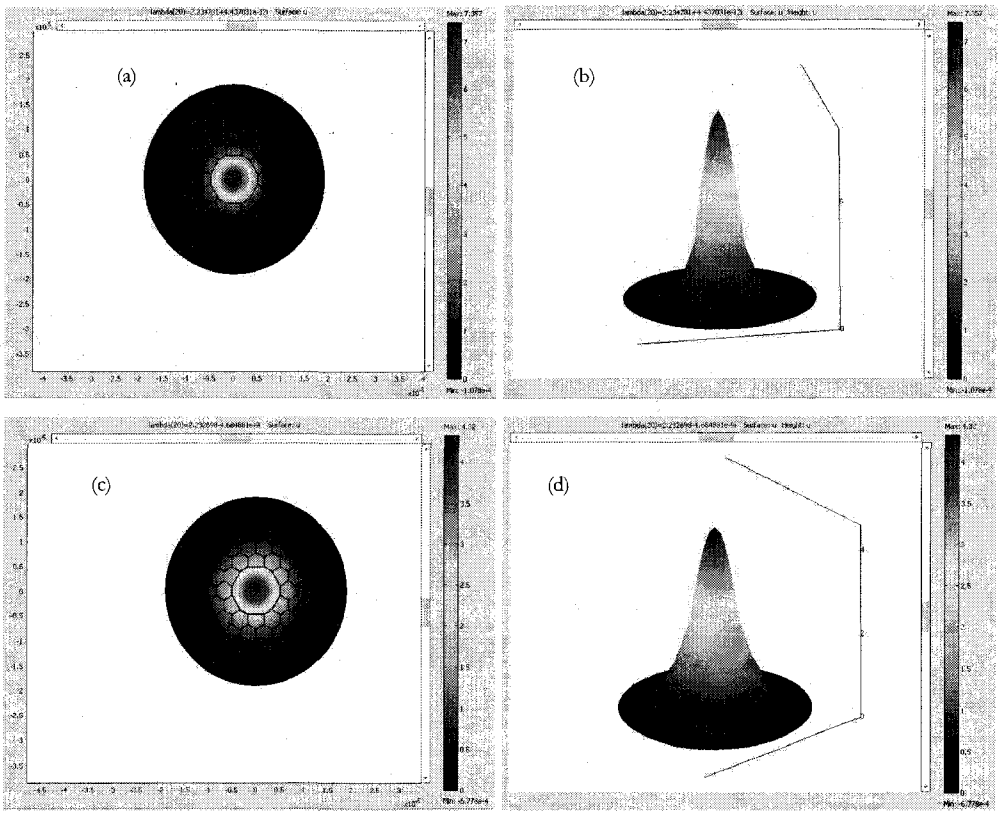

Figure 2-17 (a, b) Simulation results for HC-1060 fiber filled with toluene at wavelength= 1060nm Figure (c, d) Simulation results for HC-1060 fiber filled with toluene at wavelength= 1550nm

2.8 Far Field Patter of Photonic Crystal Fiber

The far field pattern from the PCF is obtained by launching a He-Ne at 633nm into the fiber. A 10cm long piece of PCF (ESM-12-01, or HC-633, or HC-1060 filled) was mounted on a 5-axis flexure stage (Thorlabs Inc.). Microscope objective lenses were chosen based on coupling factors such as spot size, wavelength of the beam and numerical aperture of the fiber. The coupling was done into different fibers and their far field pattern is discussed in the section following Figure 2-18 displaying the experimental setup. The far field pattern of the light emanating from the other end of the PCF was imaged using a CCD camera (Canon).

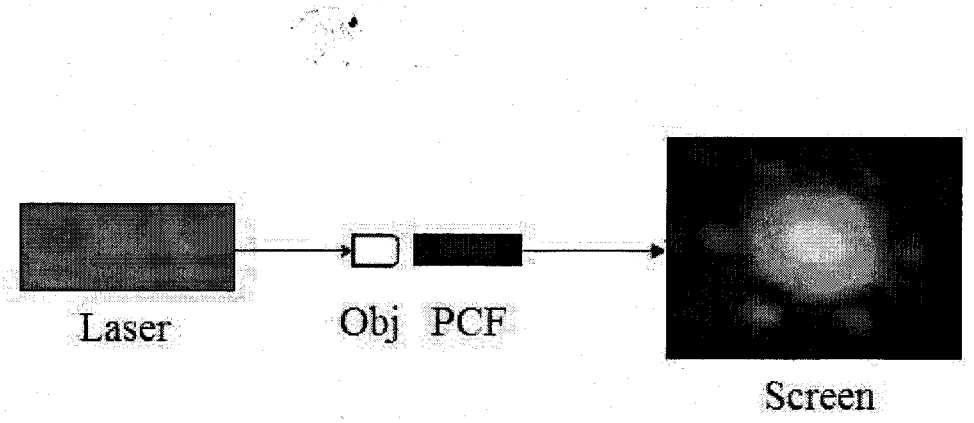

Figure 2-18 Experimental setup for the measurement of far field pattern: Laser: He-Ne light source; Obj: Objective; PCF: Photonic Crystal Fibers

2.8.1 Far field pattern from ESM-PCF

In the case of ESM-12-01, laser at 633nm is coupled with the help of a 6.3x, 0.2 NA microscope objectives (Melles Griot). The maximum coupling efficiency obtained is 80%. The various coupling conditions are shown in Figure 2-19. When a solid-core PCF with empty channels is properly aligned, far field patterns as displayed in Fig. 2-19(a and b) corresponds to the fundamental mode In accordance with reported data, we see a very pronounced central spot surrounded by six satellites of much less intensity. With some misalignment introduced, like in Fig. 2-19(c), we observe a decrease in the intensity of the central spot with six satellites becoming more pronounced and consisting of sub-peaks. At a relatively large misalignment (Fig. 2-19(d)), the central peak and satellites are comparable in intensity and the pattern has speckle-like structure, which can be explained by the interference of several modes and the statistical properties of light.

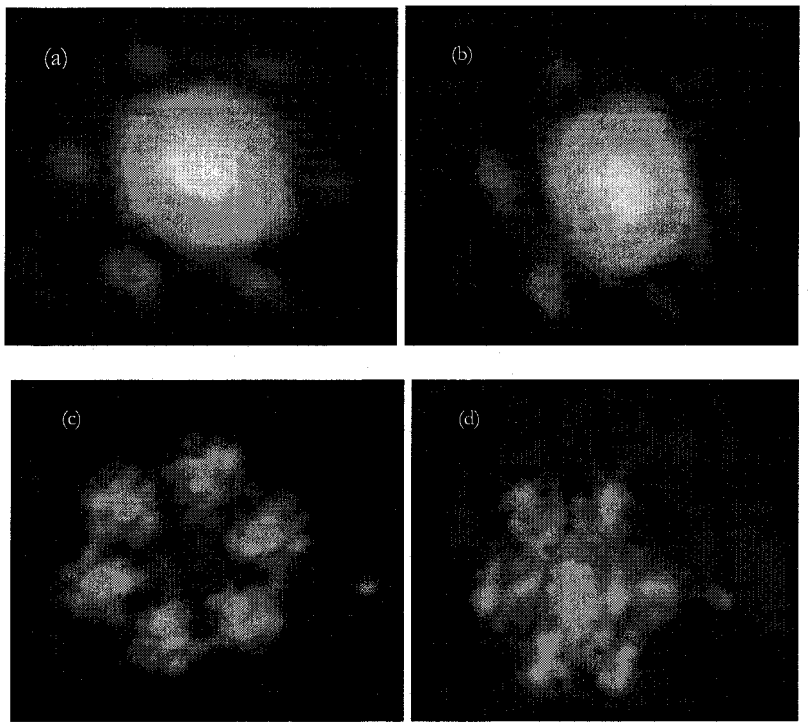

Figure 2-19 (a-d) Far field pattern for ESM-12-01 fiber showing different coupling condition

Under similar conditions when the fiber was filled with water, we find that the far field pattern changes. Fig. 2-20 shows far field pattern for PCF filled with water, in (a) a perfectly aligned situation and (b) at some misalignment. In contrast to the case when the holes are empty, we observe quite pronounced peaks corresponding to higher order spatial harmonics. These spatial harmonics are formed due to light propagation in the cladding mode and they contain distinctive spectroscopic information about light interaction with analytes dissolved in water. In turn, the central spot and first six satellites reflect optical properties of the PCF core. This observation may be especially important for biosensors in which the evanescent field interacts with biomolecules attached to the inner surface of the holes. The strength of the higher order harmonics or/and spectral content of the peaks could serve as a biosensing instrument.

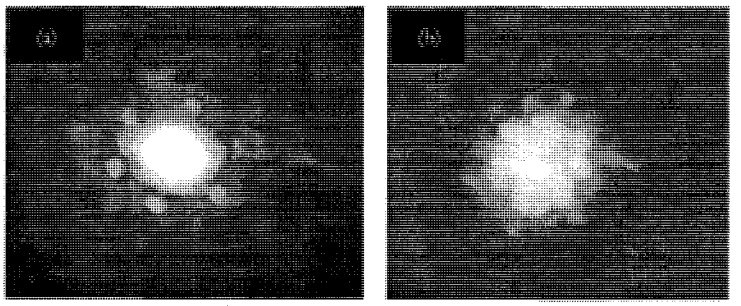

Figure 2-20 Far field pattern from the solid core PCF with water in the holes for different optical alignment parameters (a) 0 um, (b) 10 um with a 5-axis flexure stage.

2.8.2 Far field pattern from HC-PBF

The HC-633-01fiber, which is a hollow core surrounded by cladding channels, was coupled using a 10x, 0.25 NA microscope objectives (Melles Griot) by placing the fiber on 5-axis flexure stage (Thorlabs). The coupling efficiency of 90% is obtained by aligning the fiber with the focused incoming light. In the Figure 2-21(a-e), we see the central spot becoming more pronounced as the fiber matches the coupling conditions.

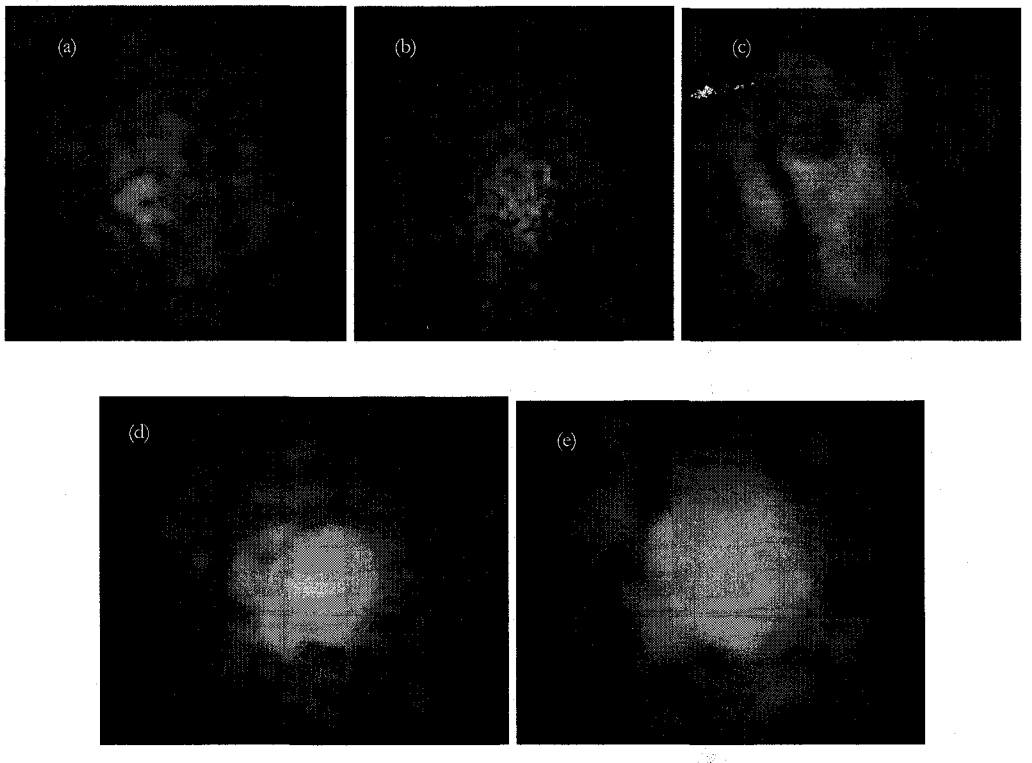

Figure 2-21 (a-e) Far field pattern of the HC-633-01 fiber showing different stages of optical alignment, while achieving a lowest order mode

Once the HC-633-01 PBF is non-selectively filled with water, the bandgap property is destroyed leading to a strange structure which shows interaction between many modes (similar to Figure 2-21 (a)). So the fiber which would guide 633nm when filled with water was found to be HC-1060-01 as discussed in section 2.6. When the filled fiber was launched with a He-Ne source, it demonstrates a lowest order mode operation as displayed in Figure 2-22(b).

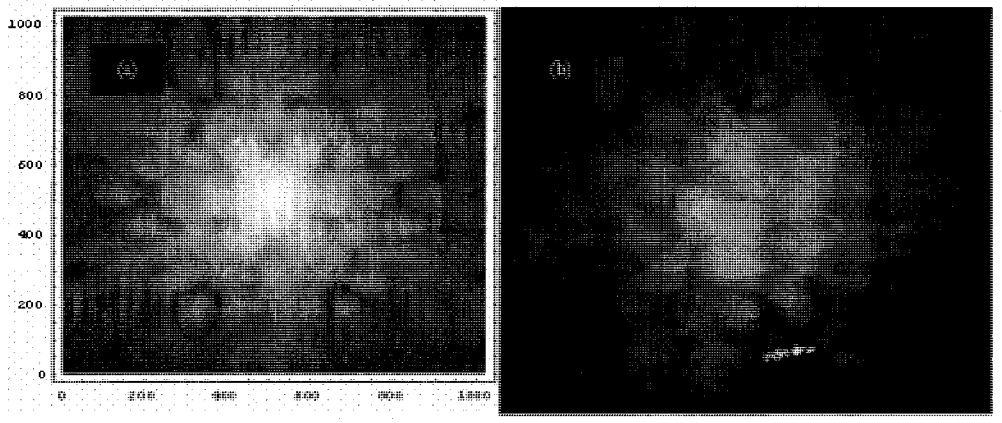

Figure 2-22 (a) Typical far field pattern from manufacturer Crystal Fiber for HC-1060 fiber (b) Experimental results of far field pattern when filled with water

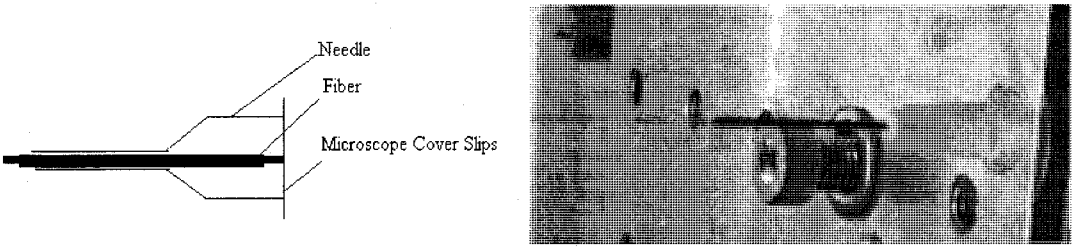

Figure 2-23 Schematic of a reservoir/cell with a fiber and sample and photograph of the prototype arrangement

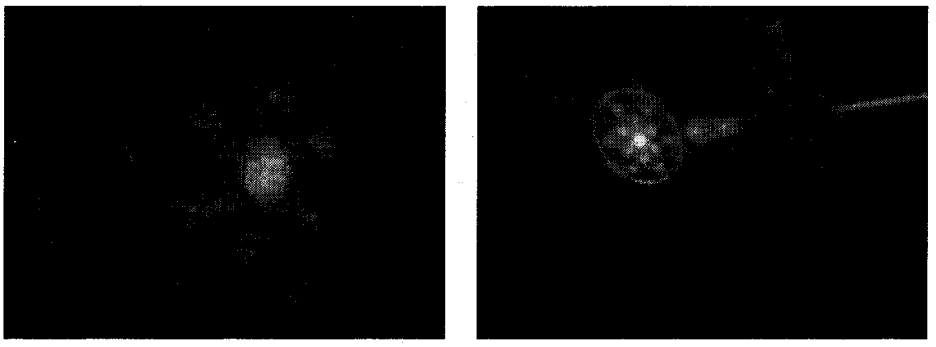

Figure 2-24 Far field pattern of a filled HC-1060 fiber with the fiber in the reservoir

The description of the reservoir is arranged using a needle, whose broader end is filled with liquid, glued with a cover slip, and the fiber is inserted from another end. The purpose of the reservoir is to make sure that the liquid is continuously supplied inside the channels of the fibers, thereby solving the problem of evaporation. Figure 2-23 shows a schematic and a prototype of a reservoir with the fiber inside it. Figure 2-24 shows the far field pattern obtained through a fiber inside a reservoir which shows the reservoir serves as holder for fiber without disturbing the pattern when filled as well as solves evaporation problem.

Bibliography

1. *WordNet® 3.0.* Dictionary.com website, retrieved March 20, 2007, http://dictionary.reference.com/browse/sensor
2. Catterall, "R.W. Chemical Sensors", Oxford University Press (1997).
3. A. Brecht, and G. Gauglitz, "Optical probes and transducers. Biosensors and Bioelectronics", pp. 923-936 (1995).
4. B.R. Eggins, "Chemical Sensors and Biosensors. Analytical Techniques in the Sciences", John Wiley & Sons, LTD. 273 (2002).
5. N. Paras Prasad "Introduction to Biophotonics", John Wiley & Son, Inc., 2003.
6. R. Lakowicz Joseph, "Topics in fluorescence spectroscopy", Probe Design and Chemical Sensing Series, Vol. 1- 4, pp. 524 (1994).
7. D. Diamond, "Principles of Chemical and Biological Sensors", John Wiley and Sons, New York (1998).
8. S. O. Wolfbeis "Fiber Optic Chemical Sensors and Biosensors Vol. 1" CRC Press, Inc. (1991)
9. J. C. Knight, T. A. Birks, P. St. J. Russell, and D. M. Atkin, "All-silica single mode optical fiber with photonic crystal cladding", Optics Letter 21, pp.1547 (1996).
10. "Frauenhofer Award / Burley Prize 2000" Optical Society of America, http://www.osa.org/aboutosa/awards/theawards/awardsdesc/award18.asp.
11. M. Lehtonen, "Application of Microstructured Fibers, supercontinua and novel components ", Helsinki University of Technology (2005)
12. J. C. Knight, J. Broeng, T. A. Birks, and P. St. J. Russell, "Photonic band-gap guidance in optical fibers", Science, 282, pp.1476-1478 (1998).
13. K. Nielsen, D. Noordegraaf, T. Sørensen, A. Bjarklev and T. P Hansen "Selective filling of Photonic Crystal Fibres" Journal of Optics. A: Pure and Applied Optics, 7, pp.L13-L20 (2005).
14. L. Xiao, W. Jin, M. Demokan, H. Ho, Y. Hoo, and C. Zhao, "Fabrication of selective injection microstructured optical fibers with a conventional fusion splicer," Optics Express 13, pp.9014-9022 (2005).

15. Y. Zhang, C. Shi, and C. Gu, L Seballos and J. Z. Zhang "Liquid core photonic crystal fiber sensor based on surface enhanced Raman scattering" Applied. Physics Letter 90, pp.193504 (2007).
16. S. Yiou, P. Delaye, A. Rouvie, J. Chinaud, R. Frey, G. Roosen, P. Viale, S. Février, Philippe Roy, J. Auguste, and J. Blondy, "Stimulated Raman scattering in an ethanol core microstructured optical fiber", Optics Express 13, pp.4786 (2005).
17. G. Antonopoulos, F. Benabid, T. A. Birks, D. M. Bird, J. C. Knight and P. St. J. Russell "Experimental demonstration of the frequency shift of bandgaps in photonic crystal fibers due to refractive index scaling", Optics Express, Vol 14 No.7, pp.3000-3006(2006).
18. T.A Birks, D.M Bird , T.D Hedley , J.M Pottage and P.J. Russell, "Scaling laws and vector effects in bandgap-guiding fibers" Optics Express 12, pp.69-74 (2004).
19. F. M. Cox, A. Argyros, and M. C. J. Large, "Liquid-filled hollow core microstructured polymer optical fiber," Optics Express 14, pp.4135-4140 (2006).
20. Crystal Fibre A/S http://www.crystal-fibre.com/About/profile.shtm (accessed March 20, 2008)
21. Thorlabs Inc http://www.thorlabs.com/ (accessed March 20, 2008)
22. COMSOL Multiphysics and Modeling http://www.comsol.com/ (accessed March 20, 2008)
23. Arismar S. Jr., "What are Photonic Crystal Fibers" Frontiers of Nanophotonics and Plasmonics.

Chapter 3. Bandgap shift property of Hollow Core PBF as a Biosensor

In this chapter, we experimentally demonstrated a simple and efficient method of using non-selectively filled Hollow Core PBF as a biosensor. Such a fiber transmits a particular wavelength band when empty and upon filling the wavelength band is shifted. This property enabled us to measure the wavelength shift and determine the refractive index of heavy water and ethanol. In addition, by monitoring the wavelength shift, we were able to determine the changes in ethanol concentration in water. The advantage of using this technique is that it can detect variations of refractive index as low as $1x10^{-5}$ by just taking a piece of Photonic Bandgap Fiber (PBF) and noting the shift in the wavelength using an optical spectrum analyzer. The small sample volume utilized and the large overlap of the propagating laser mode field with the sample provides the potential for devising simple, compact and sensitive biosensors.

3.1 Introduction

This Chapter focuses on the bandgap shifting property of HC-PBF and exploiting this property in biosensing. In Section 3.2, we discuss literature review on various applications and techniques in which photonic crystal fibers are used. The experimental approach to use bandgap shift property of photonic bandgap fibers will be presented in Section 3.3. We will verify the bandgap shift property of the fiber when filled with heavy water in Section 3.4. In the same section we present the experimental approach to use the bandgap shift property of the filled PBF as a sensitive biosensor. The approach demonstrated monitors the wavelength shift when filled with different concentration of ethanol in water thereby tracing the refractive indices of ethanol concentrations.

3.2 Literature Review

In recent years, photonic crystal fibers (PCF) have attracted researchers for their possible use in biosensing applications. Features which have encouraged PCF as a sensor are long interaction length, mode field overlap between the light and matter, and extremely small volumes of the sample required for sensing. One of the advantages of using PCFs for biosensing is that they are typically made from pure silica (SiO2), which is biocompatible and chemically inert. PCFs can also be made of polymer materials. Microstructured polymer optical fibers (mPOF) are well suited for biosensing, since polymers allow a wide range of surface chemistries to be used [1, 2]. In the following section, some of the ways in which PCF are used for biosensing are discussed.

Evanescent wave sensors can be defined as the sensor which utilizes evanescent wave i.e., the electromagnetic field that extends away from the surface of the light medium due to exponential decay of the field. This type of sensor relies on the light that is not confined within the waveguide itself, but penetrates into the surrounding medium of the cladding region. The index-guiding PCF, which has a solid core surrounded by cladding, forms a perfect evanescent wave based sensor because detecting the sample is possible when the

sample interacts with the light present in the cladding channels. Monro et al. were the first ones to demonstrate the application of holey fibers for evanescent field sensing [3].

The absorption spectra of acetylene when inserting one end of a 75-centimeter long PCF into a pressure chamber filled with 100% acetylene gas was measured by Hoo et al. The fiber was subsequently removed and the absorption spectrum was measured quickly in order to minimize out-diffusion of the gas. In this experiment, the fiber used had a relatively weak penetration of the optical field into the air holes, but long interaction length compensated efficiently for the weak overlap [4].

In another set of experiments performed by Jensen et al, the research group demonstrated evanescent wave biosensing using PCF. The presence of Cy5-labeled DNA was detected in less than 1pL sample volume. A fiber section of 10 centimeters was filled with the sample using capillary forces and the transmission spectrum of the fiber was measured. When the sample contains labeled DNA, the transmission spectrum shows a dip at a wavelength corresponding to the absorption bands of the Cy5 molecule [5]. By designing 6 holes of 60μm around the core of the mPOF of 20cm fiber length, Jensen et al. have shown the selective detection of fluorescent labeled antibodies, α-streptavidin-Cy3 and α-CRP-Cy3, which can be used as a reliable and a sensitive biosensor [6].

Evanescent wave sensing for biochip application has been demonstrated by Rindorf et al. The experiment was carried out by taking a 16mm piece of PCF incorporated into an optic-fluidic coupler chip. While integrated in the chip, the PCF captures a specific single-stranded DNA string by immobilizing a sensing layer on the microstructured internal surface. The above method is demonstrated by labeling a biomolecules [7].

Cordeiro et al. have demonstrated a very unique structure, which has microstructures both in the core and the cladding for evanescent field sensing. In the experiment, PCF of length 18cm was filled with Methyl Blue (MeB) and diluted in water, and absorption coefficient at different concentrations were measured by coupling SC generated source. The spectrum of the water filled PCF was taken first and was compared with PCF filled with MEB solution

at different concentrations. The PCF was selectively filled with a sample, either in the tiny core microstructure or the external cladding microstructure [8].

One of the disadvantages of evanescent wave sensing is that the mode-field overlap is just 1%. In order to obtain more than 98% mode field overlap, hollow core PBF was preferred, where the sample can be present in the core or both the core and the cladding channels. Below are some of the methods where PBF is being used for biosensing purposes.

Although selective filling techniques were discussed in Chapter 2, we will provide a short review of selective filling technique proposed by various research groups. Selectively filling a PBF is an interesting process where one can selectively fill the core of the fiber. This can be done in different ways. One of the earliest methods demonstrated by Huang et al was to fill the fiber with Norland Optical Adhesive in multiple steps using a syringe [9]. This method allows the core to be filled with the desired liquid in which guiding is through total internal reflection.

In another method demonstrated by Kristian et al., an overhead pressure was applied to fill the core of the fiber selectively. This method gives a very detailed approach to fill a fiber and explains the steps involved in this complex process. The approach gives a model for calculating the time necessary to fill one or more specific holes with a polymer as well as water in a photonic crystal fiber [10].

The selective filling method with fusion splicer was demonstrated by L. Xiao et al. The method is based on a conventional fusion splicer which causes the cladding holes to collapse, leaving the central hollow core open. It shows theoretical and experimental investigations of the hole-collapse property of PCF which depends on the fusion current, the fusion duration and the fusion offset position [11].

The above selective filling method has some drawbacks; by applying pressure the chances are that the fiber structure might be damaged and using a fusion splicer will result in the reduction of the core size. Moreover, the fiber is filled through the tip, which is optically accessible for coupling and collecting the output signal. In order to overcome the drawbacks, a different approach is mentioned by Cordeiro et al. In this method, increase in

gas pressure inside the holes and by heating a section of the fiber will result in melting, expanding and laterally tearing of the side channels. This allows fiber to be filled laterally (side channels) than the tip or end of the fiber. In order to prove the experimental feasibility of the procedure, rhodamine in ethylene-glycol was inserted through the side channels of a solid and hollow core PCF for measuring fluorescence spectrum [12].

A special type of fiber known as ARROW PCF has also been reported by Sun et al. for biosensing application with very high sensitivity, apt for refractive index measurement [13]. It was found that refractive index variation of 0.035 could induce resonant wavelength shifts of 450 and 110nm when liquid has refractive index of 1.5 and 1.7, respectively. This method was capable of measure a change of refractive index as low as $8x10^{-7}$ and $3.2x10^{-6}$ for a liquid of concentration $2x10^{-7}cm^3$. Theory and experimental results of bandgap shift has been reported by Antonopoulos et al. [14].

Hollow-core PCF is adapted to transmit high-energy laser pulse for laser-induced ablation on solid surfaces in laser technologies and biomedicine field which has been reported by Konorov et al. [15]. Another important application of PCF for sensing purpose is by inscribing a grating. A very detailed application of inscribing a grating in different types of MOF has been presented by Eggleton et al. [16]. The mode profile has been calculated using the beam propagation method (BPM). Experimentally inspecting the transmission spectra of gratings written in the core of the MOF's, provides a good knowledge of the optical properties of the higher order modes that are unique to the geometry of the fiber.

The grating inscribed in index guiding PCF for detecting the single stranded DNA molecule was reported by Burani and J. Laesgaard. [17]. A numerical method was demonstrated to compare and estimate the magnitude of the wavelength shift in the case of Bragg grating and the long period grating (LPG). It was reported that the technique was able to resolve wavelength of 0.1nm in the case of a Bragg grating and 10nm in the LPG case. It was also found that the PCF filled with water makes it easier for detection resulting in bigger wavelength shifts by a factor of approximately 1.5.

The label free detection by inscribing a long period grating has been first reported by Rindorf et al. They demonstrated water filled PCF to detect the thickness of a biomolecules layer such as DNA and proteins [18]. The device was able to measure the wavelength shift of poly-L-lysine and DNA layers, which determines their thickness as 4.79nm and 1.65nm respectively with a sensitivity of 10^{-4}.

Very recently, mechanically and electrically induced long period gratings (LPGs) in a photonic crystal fiber (PCF) filled with a high-index liquid crystal have been demonstrated by Noordegraaf et al. They have reported that tuning of resonance wavelengths of the PCF can be done by changing the temperature. In a particular set of experiments, they have shown linear tuning of -2.4 nm/°C over a broad temperature interval from 30°C to 80°C [19].

A very elegant use of PCFs for sensor applications is demonstrated by Myaing et al. The method demonstrated has improved the detection efficiency of two-photon fluorescence, in comparison to conventional single mode detection by double-clad fibers. The fiber used has an outer ring of air holes running around the core, effectively collecting the fluorescence emitted from the exited biomolecules [20]. Konorov et al. have reported two protocols for dual core cladding photonic-crystal fiber as a multifunctional optical sensor and sample collector [21].

Having discussed briefly some of the biosensor applications where PCF is being employed, in the following section we will look into biosensing application of PBF by non-selective filling technique. Filling a photonic bandgap fiber has been discussed in chapter 2 here is a quick recapitulation. The selective filling method leads to sealing of cladding holes while leaving the core open to be filled, as reported by several groups such as Kristian Nielsen et al. [10] and Vienne et al. [22]. In this method, the light is guided by total internal reflection instead of the bandgap effect. The second option is to simply fill all the holes of the HC-PBF with a sample would result in the transmission band supported by the fiber to be shifted depending on the refractive index of the sample [19].

3.3 Experimental Setup

A schematic of the experimental setup is shown in Figure 3-1.

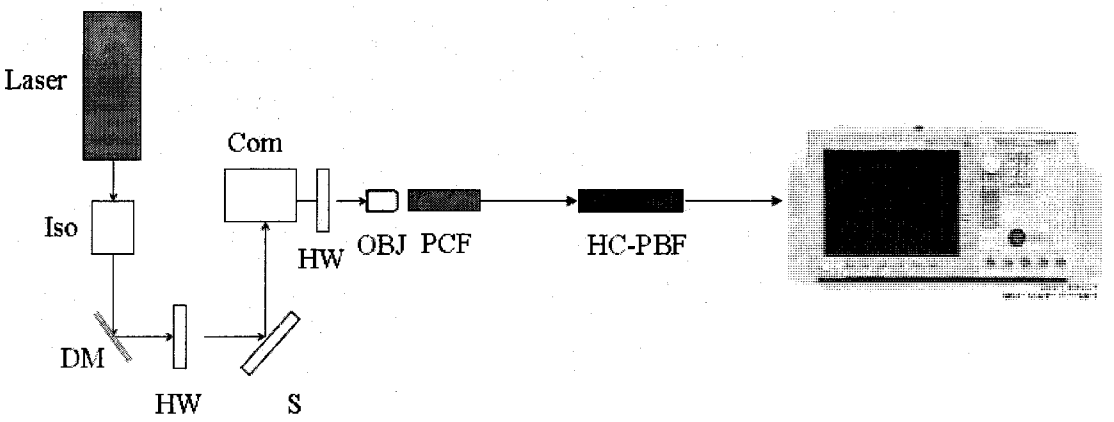

Figure 3-1 Schematic of the setup: PCF- Photonic Crystal Fiber with two zero dispersion wavelengths (ZDWs); Iso – Faraday Isolator; DM- Dichroic mirror; Com - Prism compressor; HW – Half wave plate; S – Beam Splitter; Obj – Objective; HC-PBF – Hollow core Photonic Bandgap Fiber HC 1060

In order to perform the experiment, we have used a supercontinuum light source as a broadband source. There are many ways to generate a supercontinuum. In our case, we coupled a Ti-sapphire laser (Tsunami by Spectra Physics) producing ~ 65fs pulses at 80MHz repetition rate into a 12.5cm long PCF (NL-1.4-775-945, Crystal Fibre A/S) [24]. The supercontinuum was then coupled to an endlessly single mode fiber which was in turn butt coupled to an HC-PBF (HC-1060-02, Crystal Fibre A/S). The output was monitored using an optical spectrum analyzer (OSA). The experimental setup picture with a far field pattern is shown in Figure 3-2.

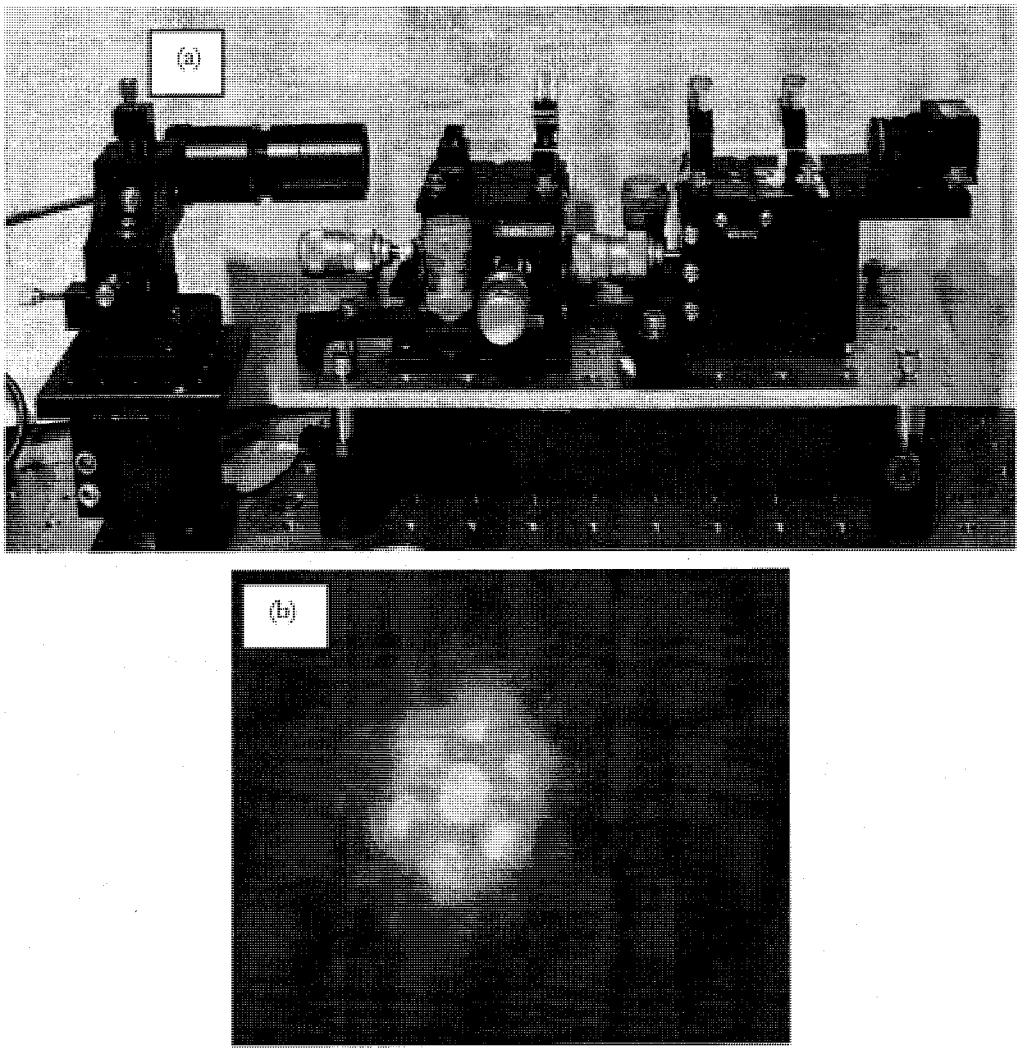

Figure 3-2 (a) Experimental setup of the fiber with a reservoir on a flexure stage.(b)Far field pattern from the HC-1060 fiber filled with heavy water.

The center wavelength of the HC-PBF is 1060nm with a NA of 0.12. The fiber has a core size of 9.7μm with a pitch of 2.75μm, and a mode field diameter of 6.5μm. In the experiment, a 10cm long piece of HC-PBF was mounted on a 5-axis flexure stage (Thorlabs). The fiber was filled using a reservoir at its end in order to ensure continuous supply of the sample. Light was coupled using a 6.3x, 0.20NA microscope objective with a coupling efficiency of 25%.

3.4 Results

The input spectrum obtained using continuum generation is a broadband spectrum with two peaks due to the two zero dispersion wavelengths of PCF used for coupling laser source. The broadband spectra one which is visible (550nm-750nm) and the other one being in the near infrared (NIR) region (950nm-1250nm) as shown in the Figure 3-3 (Black curve).

Experimentally, we started by coupling the continuum source to an empty fiber. As expected, the fiber guides the NIR wavelength band only (950-1250nm) as depicted in Figure 3-3 (red curve). When the same fiber is filled with heavy water, the transmitted wavelength band shifts to the visible wavelength band (550-750nm) (blue curve). We have used heavy water instead of MilliQ water to ensure that the observed spectrum is not due to the absorption in the NIR by water. By comparing the transmission spectrum of an empty fiber with that of a fiber filled with heavy water, it was determined that the refractive index of heavy water is 1.3282 which is consistent with the known refractive index of heavy water [25]. The calculation was done using the bandgap shift property principle as discussed in section 2.6.

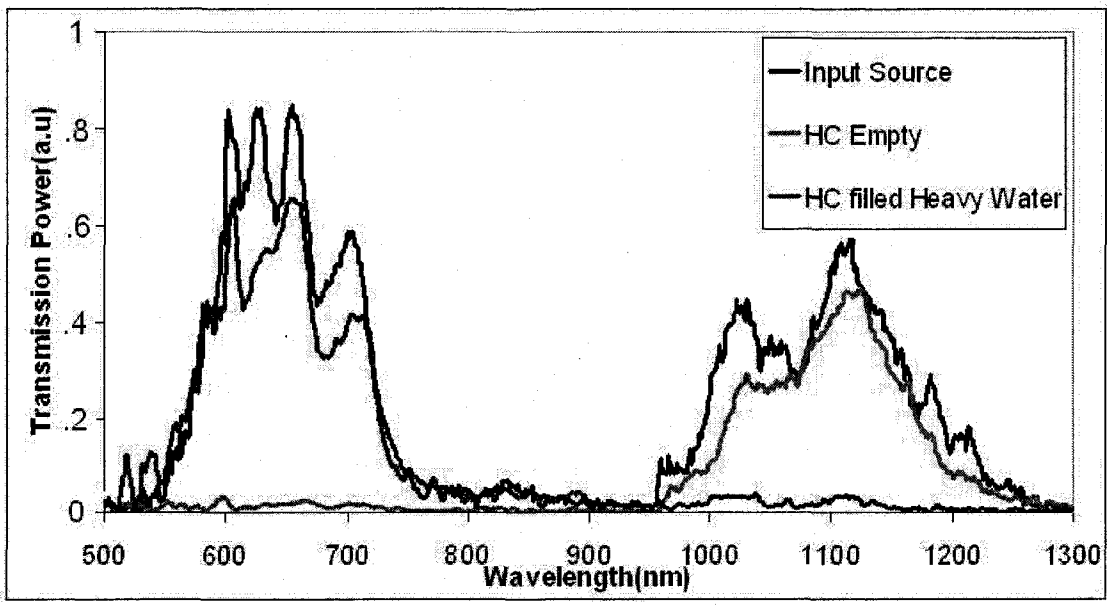

Figure 3-3 Output obtained from a. broadband source (black), b. HC-1060 when empty (red) c. HC-1060 when filled with heavy water (blue).

Although the bandgap shift property has been investigated by Antonopoulos et al. [14], our approach to use the same property as an effective type of biosensor has been presented. In order to verify that HC-PBF can be used as a sensor, we have filled the fiber with 10%, 25% and 50% ethanol. The different concentration of ethanol used will result in the transmission wavelength to be shifted due to the change in refractive index of the sample filled inside the fiber. The wavelength shift was monitored by an OSA. We have found that as the ethanol concentration is changed from 0 to 10%, the wavelength shift obtained is 24nm. Further, wavelengths shifts were observed as the ethanol concentrations were increased. The output spectra for each concentration are shown in Figure 3-4. By tracking the longer wavelength edge of the transmission band as a function of concentration/ refractive index, we plotted the change of refractive index as a function of change in wavelength as shown in Figure 3-5. In this figure, we have also plotted the expected relation based on Equation 2-2 (from Chapter 2). It should be noted that our choice of tracking the longer wavelength edge was only due to the limitation of the wavelength range of the input spectrum.

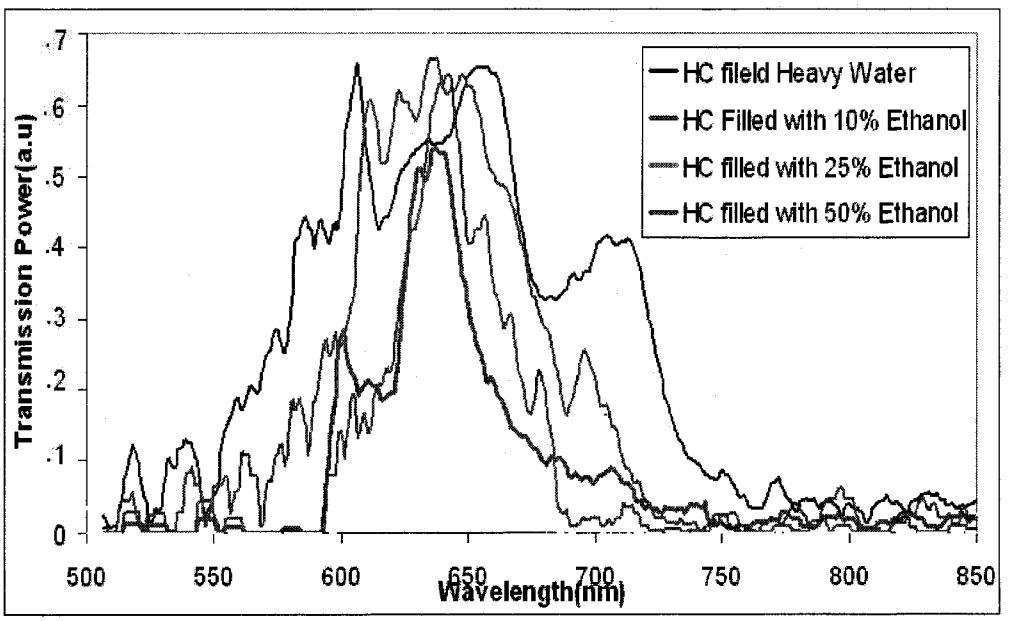

Figure 3-4 Experimental results of spectra obtained for 0%, 10%, 25%, 50% ethanol concentration.

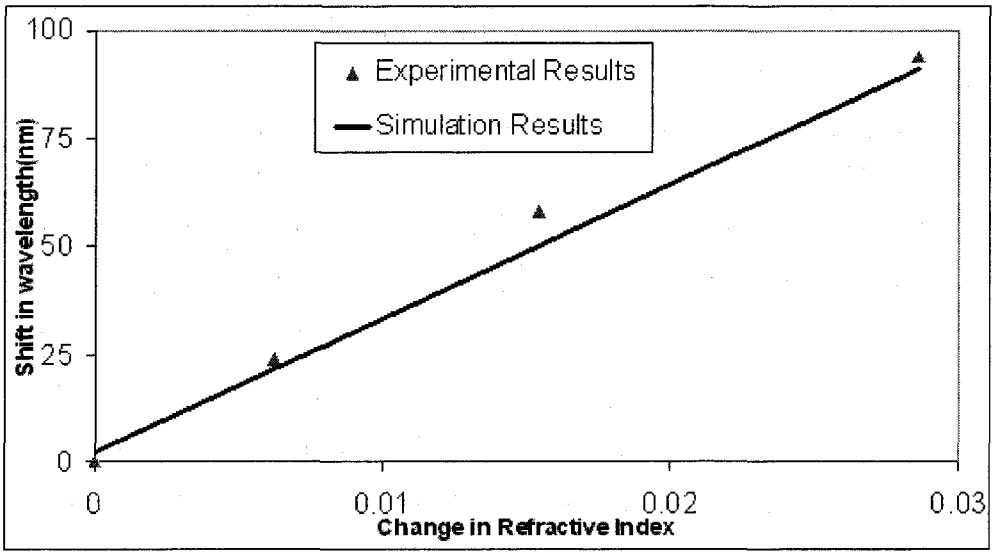

Figure 3-5 Change in the refractive index with wavelength shift at 0%, 10%, 25%, 50% concentration of ethanol

As shown in Figure 3-5, there is a good agreement between the measured and expected values. Moreover, it is seen that this technique can detect refractive index changes as low as 10^{-5} using an OSA with a 0.05nm resolution. In conclusion, we have demonstrated a simple, however effective technique for biosensing using a hollow core PBF.

Bibliography

1. M. A. van Eijkelenborg, M. C. J. Large, A. Argyros, J. Zagari, S. Manos, N. Issa, I. Bassett, S. Fleming, R. C. McPhedran, C. M. de Sterke, and N. A. . Nicorovici, "Microstructured polymer optical fibre," Optics Express 9, pp. 319 - 327 (2001).
2. F. M. Cox, A. Argyros, and M. C. J. Large, "Ultracompact biochemical sensor built with two-dimensional photonic crystal microcavity," Opt. Express 14, 4135 (2006)
3. T.M Monro, D.J. Richardson, P.J. Bennett, "Developing holey fibers for evanescent field devices," Electronics Letters, 35, pp.1188-1189 (1999).
4. Y. L. Hoo, W. Jin, H. L. Ho, D. N. Wang, and R. S. Windeler, "Evanescent-wave gas sensing using microstructure fiber," Optical Engineering, 41,pp.8-9 (2002).
5. J. B. Jensen, L. H. Pedersen, P. E. Hoiby, L. B. Nielsen, T. P. Hansen, J. R. Folkenberg, J. Riishede, D. Noordegraaf, K. Nielsen, A. Carlsen, and A. Bjarklev, "Photonic crystal fiber based evanescent-wave sensor for detection of biomolecules in aqueous solutions," Optics Letter 29, pp. 1974-1976 (2004).
6. J. Jensen, P. Hoiby, G. Emiliyanov, O. Bang, L. Pedersen, and A. Bjarklev, "Selective detection of antibodies in microstructured polymer optical fibers," Optics Express 13, pp. 5883-5889 (2005).
7. L. Rindorf, P. E. Hoiby, J. B. Jensen, L. H. Pedersen, O. Bang, and O. Geschke, "Towards Biochips Using Microstructured Optical Fiber Sensors," Analytical and Bioanalytical Chemistry, 385, pp. 1370-1375 (2006).
8. C. M. B. Cordeiro, M. A. R. Franco, G. Chesini, E. C. S. Barretto, R. Lwin, C. H. Brito Cruz, and M. C. J. Large, "Microstructured-core optical fibre for evanescent sensing applications," Optics. Express 14, pp, 13056-13066 (2006).
9. Y. Huang, Y. Xu, and A. Yariv, "Fabrication of functional microstructured optical fibers through a selective-filling technique," Applied Physics Letters 85, pp. 5182-5184 (2004).
10. K. Nielsen, D. Noordegraaf, T. Sørensen, A. Bjarklev and T. P Hansen "Selective filling of Photonic Crystal Fibres" Journal of Optics. A: Pure and Applied Optics, 7, pp.L13-L20 (2005).

11. L. Xiao, W. Jin, M. Demokan, H. Ho, Y. Hoo, and C. Zhao, "Fabrication of selective injection microstructured optical fibers with a conventional fusion splicer," Optics Express 13, pp. 9014-9022 (2005).
12. C. M. B. Cordeiro, E. M. dos Santos, C. H. Brito Cruz, C. J. de Matos, and D. S. Ferreiira, "Lateral access to the holes of photonic crystal fibers – selective filling and sensing applications," Optics Express 14, pp,8403-8412 (2006).
13. J. Sun, and C.C. Chan, X.Y. Dong "Refractive index measurement using a photonic crystal fiber" Optical Engineering, 46, pp. 014402 (2007)
14. G. Antonopoulos, F. Benabid, T. A. Birks, D. M. Bird, J. C. Knight and P. St. J. Russell "Experimental demonstration of the frequency shift of bandgaps in photonic crystal fibers due to refractive index scaling", Optics Express, 14,pp.3000-3006(2006)
15. S. O. Konorov, A. B. Fedotov, V. P. Mitrokhin, V. I. Beloglazov, N. B. Skibina, A. V. Shcherbakov, E. Wintner, M. Scalora, and A. M. Zheltikov, "Laser Ablation of Dental Tissues with Picosecond Pulses of 1.06-μm Radiation Transmitted through a Hollow-Core Photonic-Crystal Fiber," Applied Optics 43, pp. 2251-2256 (2004).
16. B. Eggleton, C. Kerbage, P. Westbrook, R. Windeler, and A. Hale, "Microstructured optical fiber devices," Optics Express 9, pp. 698-713 (2001).
17. N. Burani and J. Lægsgaard, "Perturbative modeling of Bragg-grating-based biosensors in photonic-crystal fibers," Journal of Optical Society of America B 22, pp. 2487-2493 (2005)
18. L. Rindorf, J. B. Jensen, M. Dufva, L. H. Pedersen, P. E. Høiby, and O. Bang, "Photonic crystal fiber long-period gratings for biochemical sensing," Optics Express 14, pp. 8224-8231 (2006)
19. D. Noordegraaf, L. Scolari, J. Lægsgaard, L. Rindorf, and T. T. Alkeskjold, "Electrically and mechanically induced long period gratings in liquid crystal photonic bandgap fibers," Optics Express 15, pp. 7901-7912 (2007)
20. M. T. Myaing, J. Y. Ye, T. B. Norris, T. Thomas, J. R. Baker, Jr., W. J. Wadsworth, G. Bouwmans, J. C. Knight, and P. S. J. Russell, "Enhanced two-photon biosensing with double-clad photonic crystal fibers," Optics Letters,28, pp. 1224-1226 (2003).

21. S. Konorov, A. Zheltikov, and M. Scalora, "Photonic-crystal fiber as a multifunctional optical sensor and sample collector," Optics Express 13, pp.3454-3459 (2005)
22. G. Vienne, M. Yan, T. Luo, T. K. Liang, P. Ho, and C. Lin, "Liquid core fibers based on hollow core microstructured fibers," in Proceedings of IEE conference on lasers and electrooptics/Pacific Rim (Institute of Electrical and Electronics Engineers, Tokyo) pp. 551-552 (2005).
23. T.A Birks, D.M Bird, T.D Hedley, J.M Pottage and P St J. Russell "Scaling laws and vector effects in bandgap-guiding fibers" Optics Express, 12, pp. 69-74 (2004).
24. K. Hilligsoe, T. Andersen, H. Paulsen, C.Nielsen, K. Molmer, S. Keiding, R. Kristiansen, K. Hansen and J. Larsen, "Supercontinuum generation in a photonic crystal fiber with two zero dispersion wavelengths", Optics Express 12, pp. 1045 - 1054 (2004)
25. Water structure and properties http://www.lsbu.ac.uk/water/data.html (accessed on March 20, 2008)

Chapter 4. Supercontinuum Generation in PCF for Biosensor Applications

This chapter demonstrates cladding mode assisted supercontinuum generation in a solid core photonic crystal fiber. Although the fiber is commonly considered as endlessly single mode, we show that coupling light into the cladding excites a much broader spectrum compared with the situation when only the fundamental mode is excited. Comparing experimental data with the results of the modal analysis and the simulations of the pulse propagation in the fiber, we conclude that the cladding mode has more favorable dispersion characteristics for the continuum generation. We discuss possible usage of the cladding mode assisted supercontinuum in biosensor applications.

4.1 Introduction

The chapter proposes the excitation of the cladding mode for supercontinuum generation in PCF. Section 4.2 covers a literature review of supercontinuum generation in bulk glass, optical fiber and PCF's. Section 4.3 discusses the experimental setup followed by Section 4.4, which covers PCFs dispersion characteristics. The results obtained by exciting cladding and core for supercontinuum generation is covered in the final section of the chapter. This work was done in collaboration with Dr. Yury Logvin, a research associate in our group. Dr. Logvin focused on carrying out the simulations while I focused on the experimental side.

4.2 Literature review

PCFs grabbed a lot of attention since their invention [1, 2], due to unique features such as dispersion properties [3], light guidance in air [4], endlessly single-mode guidance [5], higher birefringence [6], and enhanced nonlinear effects [7]. One of the prime application areas where PCF are actively used is supercontinuum generation [9, 10].

Supercontinuum generation occurs when temporally short high power pulses are coupled into a nonlinear medium, and the bandwidth of the pulses can experience a substantial spectral broadening. Alfano and Shapiro were the first to report supercontinuum generation in bulk glass [11]. The SC generation reported covered the whole visible spectrum from 400-700nm when bulk glass was excited with 5mJ, picosecond laser pulses at 570nm. Since then, various groups reported SC generation in many other nonlinear media [12]. SC generation in bulk medium is dominated by self phase modulation (SPM) and hence requires high power density. As the effective area in bulk is relatively large, the required power for SC generation is high.

In contrast, the use of optical fiber for SC generation requires minute power due to the wave confinement properties of the fiber and the resulting small effective area. The use of nanosecond lasers for supercontinuum generation in optical fiber was first reported by Lin and Stolen in 1976. SC generation was attributed to Stimulated Raman Scattering and

Self Phase Modulation (SPM) [13]. Later experiments revealed that cross phase modulation (XPM) and four wave mixing also plays an important role for SC generation. However, the restriction imposed by this fiber to operate at a near zero dispersion wavelength of 1300nm has led to the use of either tapered fibers [14] or Photonic Crystal Fibers (PCF) [2].

In PCF, SC is generated when the incident light is in the anomalous dispersion range or close to the zero-dispersion point [15]. Thus, PCFs with small mode areas and special dispersion properties can be used for SC generation. Although there are two classifications of PCF as discussed in Chapter 2, the index-guiding PCF is used in SC generation.

In 1998, Mogilevtsev et al. illustrated that in PCF, the zero dispersion wavelength can be shifted, and in 1999 Broderick et al. showed that the reduced effective area has resulted in enhanced non-linear effects [16, 17]. PCF for SC generation was first demonstrated by Ranka et al. They have demonstrated that launching pulses of 100-fs duration, 8-kW peak power into a fiber with a zero-GVD wavelength at 767nm has led to SC generation. The SC generation extends from 390nm to 1.6μm [18]. A full review of the progress made so far in SC generation using PCF has been done by Dudley et al. [15]. SC generation in PCF has many applications, such as time-resolved absorption and spectroscopy [19], DWDM optical telecommunications [20], optical frequency and meteorology [21, 22], and optical coherence tomography [23].

The presence of an array of holes in PCF makes it an interesting proposition for biosensing applications, due to their dual function as an analyte container as well as a photonic device supporting mode structure. This can allow light to interact with the analyte, thus providing a sensor with high sensitivity. In particular, there has been a growing interest in the evanescent-field spectroscopy where light is penetrates into the silica cladding of the PCF thereby interacting with the analyte present in the cladding channels [24-26].

Recently, a solid-core PCF has been used to demonstrate a novel platform for evanescent-field spectroscopy, where a Raman signal from the fiber core serves as a reference for

measuring the Raman scattering from the acetonitryl present in the cladding holes [27]. Although sensing using evanescent field is a popular approach, it suffers from a very low interaction between the light and the matter. Thus, the excitation of the cladding mode for SC generation in PCF's should extend the limits of this technique by allowing more efficient light penetration into the analyte material in the fiber holes and effectively use it for detection of analytes.

Supercontinuum generation in PCF so far reported is mainly due to the light propagation in the core mode, although the fiber's higher order modes can also be involved into spectrum broadening [28]. In this chapter, we investigate supercontinuum generation when light is coupled into the cladding mode of a PCF (ESM-12-01 from Thorlabs). Even though the fiber is generally considered as an endlessly single mode, we demonstrate that the cladding mode propagates over a certain distance, enabling the generation of the supercontinuum. We show that coupling light into the cladding mode excites a much broader spectrum compared with the situation when only a fundamental mode is excited. Comparing experimental data with the results of the modal analysis and the simulations of the pulse propagation in the fiber, we conclude that the cladding mode has more favorable dispersion characteristics for the continuum generation. We will discuss possible uses of the cladding mode assisted supercontinuum for biosensor applications.

4.3 Experimental setup:

The experimental setup used for supercontinuum generation as well as the cross-section of the "endlessly single mode" fibers (ESM-12-01 from Thorlabs) is shown in Fig. 3.1. The fiber was mounted on a 5-axis flexure stage (Thorlabs). Light pulses of 300fs at 1040nm from the IMRA μJewel laser have been coupled into PCF using 10x, 0.25 NA microscope objectives (Melles Griot).

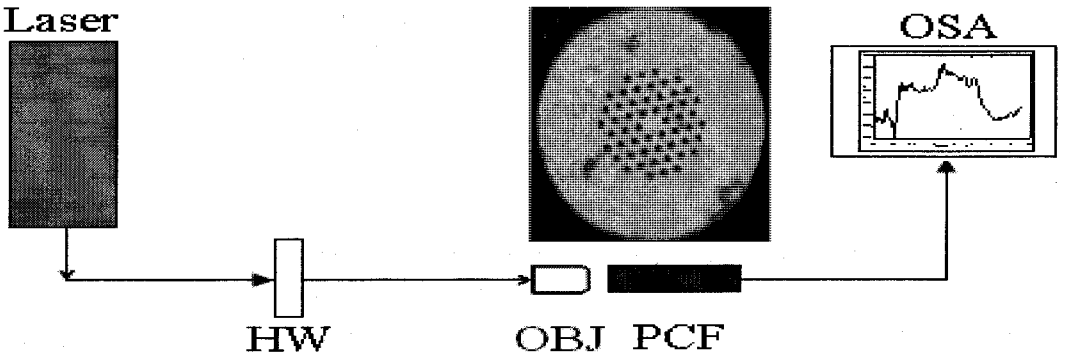

Figure 4-1 Schematic of SC generation: Laser: IMRA μJewel laser HW: Half wave plate OBJ: Microscope Objective lens PCF: ESM-12-01 Photonic Crystal Fiber OSA: Optical Spectrum Analyzer

The experiment has been performed with fibers of different length: 10, 21 and 60cm. It has been identified that the first few centimeters are responsible for supercontinuum formation. Consequently, the spectrum did not change as a function of length. Below, we present results for the case of the fiber length of 21cm.

The far field pattern of the signal transmitted through the PCF has been monitored so that the pattern shape has allowed the identification of the excited fiber mode. The spectrum of the transmitted light has been analyzed with an Ando AQ 6315 optical spectrum analyzer (OSA) with a resolution of 0.05nm.

4.4 Fiber Characteristics (Dispersion Characteristics)

There are two types of dispersion, namely material and waveguide dispersion. The material dispersion is defined as frequency-dependence of the refractive index of silica. The waveguide dispersion is defined as the difference in the refractive index between the core and cladding. In any optical fiber, the effect of dispersion on pulse propagation is typically accounted by expanding the propagation constant β into a power series around the carrier frequency ω_0 of the pulse as follows [32]:

$$\beta(\omega) = \sum_{m=1}^{\infty} \frac{\beta_m (\omega - \omega_0)^m}{m!} \tag{4-1}$$

where $\beta_m = \frac{d^m \beta}{d\beta^m} | \omega = \omega_0$

In the above equation, the coefficient β_1 is the group delay (GD) of the pulse, and its inverse β_1^{-1} is the group velocity (GV) of the pulse, which determines the propagation speed of the pulse envelope inside the fiber.

The coefficient β_2 is known as the group-velocity dispersion (GVD) parameter, denoting the different frequency components of the pulse propagating at different speeds. It is responsible for broadening a pulse during propagation along the fiber. Depending on its sign, the group-velocity dispersion in optical fibers can be divided as follows: normal when $\beta_2 > 0$ and anomalous when $\beta_2 < 0$. In the anomalous dispersion region, shorter wavelengths travel faster than longer wavelengths, while in normal dispersion it is vice-versa. The wavelength at which $\beta_2 = 0$ is referred to as the zero dispersion wavelength λ_{ZD}. For conventional optical fibers, the zero dispersion wavelength is $\lambda_{ZD} \approx 1.3 \mu m$. A common parameter used to describe the effects of dispersion in optical fibers is the parameter D defined as

$$D = -\left(\frac{2\pi c}{\lambda^2} \right) \beta_2 \tag{4-2}$$

where λ is the wavelength and c the speed of light in vacuum. D is often given in units of ps/(nm-km).

In the case of a photonic crystal fiber, the effective index of refraction of the cladding and of the core is determined by the pitch Λ and the relative air-hole diameter d/Λ of the structure. Therefore, varying the dimension's of the fiber permits tailoring the waveguide dispersion in a wide range. For comparison, the dispersion profile of a conventional single-mode telecommunication fiber (SMF) and different PCF design for values Λ and d/Λ are plotted in Fig. 4-2 [33]. The flexibility of dispersion tailoring in PCF is particularly important for efficient supercontinuum generation [33].

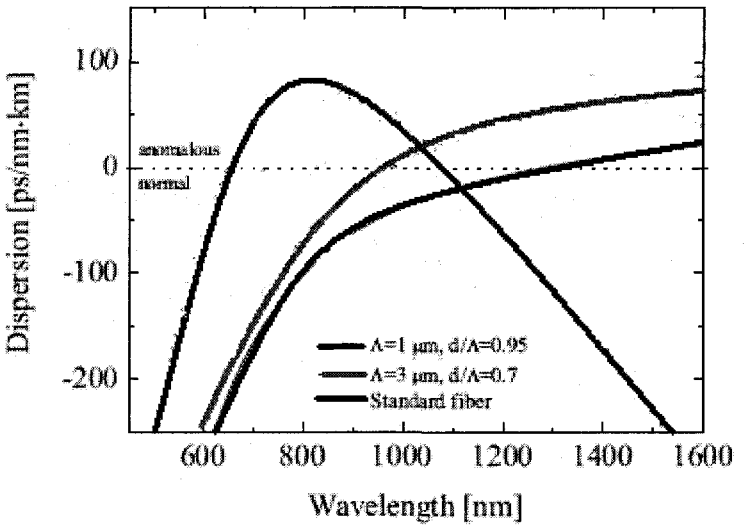

Figure 4-2 Dispersion profiles of SMF and PCF for different values of pitch Λ and air-hole diameter d/Λ [33]

The fiber used in our experiment belongs to a class of endlessly single-mode (ESM) photonic crystal fibers (PCF) which have been demonstrated in the earlier experiments [1, 4]. The ESM-PCF supports single-mode operation over a very wide wavelength range. The following studies, [e.g.29], however, have proved that such fibers support a family of leaky modes and the single-modeness should be considered as loss discrimination between the fundamental core mode and higher order cladding leaky modes. We found in our experiment that when the cladding mode is excited, it survives over a certain distance despite the power loss.

By using the finite-element based solver from COMSOL [30], we have calculated the modal structure of the ESM-12-01 fiber. Fig. 4-3 shows the main cladding mode together with its far field, where 6 spectral peaks correspond to a hexagonal symmetry of the fiber geometry.

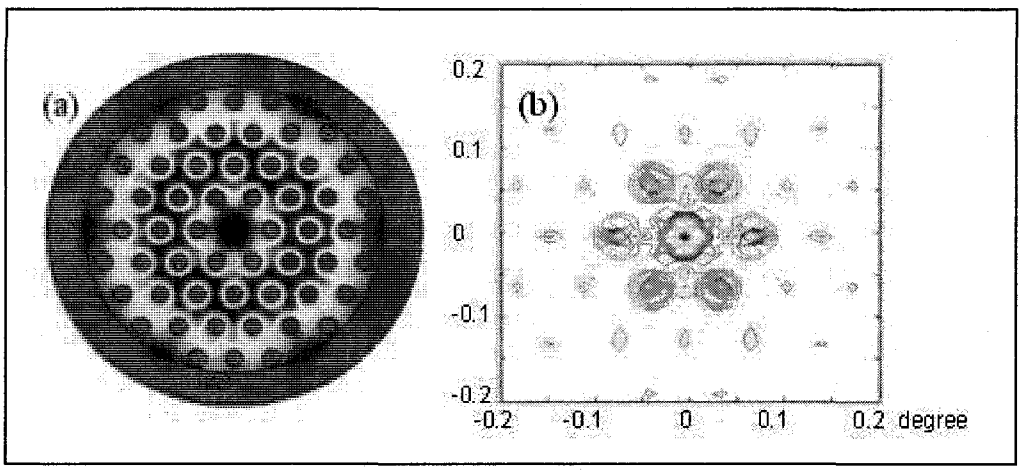

Figure 4-3 (a) Profile of the cladding mode and (b) corresponding far-field pattern indicating presence of higher order spatial harmonics.

The dispersion curves for the fundamental mode and cladding mode, shown in Figure 4.4, are obtained by substituting the values of the effective refractive indices of the fundamental core and cladding modes in Equation 4.2. It is observed that the curves follow each other with the difference lying in the zero dispersion point being shifted to shorter wavelengths for the cladding mode. The fundamental mode's zero dispersion wavelength is around 1.21μm while the cladding mode zero dispersion point shifts to 1.16μm. Clearly, when laser pulses at 1.04μm are launched into the cladding mode, more involved pulse dynamics should be expected as compared with the case of fundamental mode.

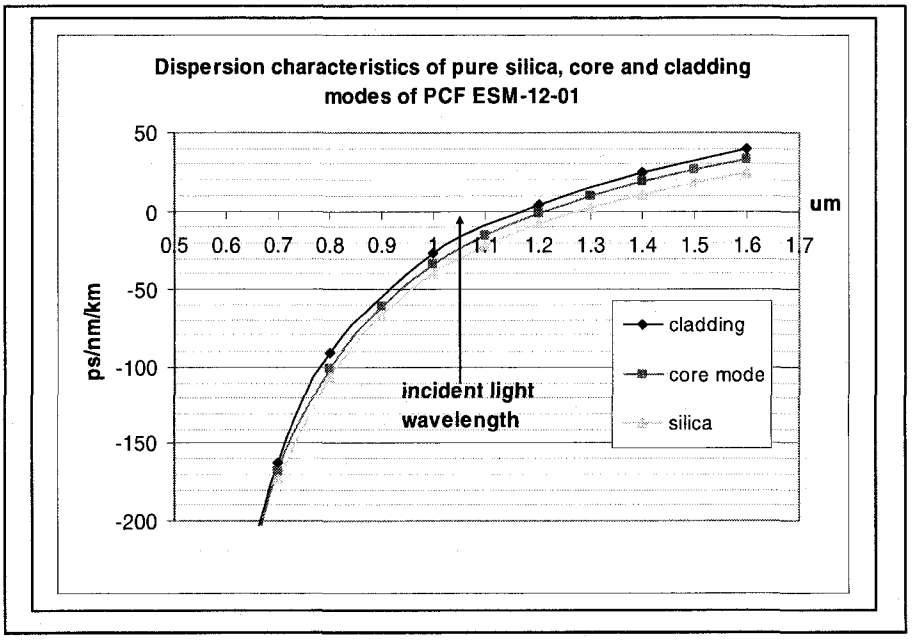

Figure 4-4 Dispersion characteristics of pure silica, core and cladding modes of ESM-12-01 PCF

4.5 Results

The different properties of supercontinuum generation are obtained by launching light from a μJewel [31] laser into the PCF as explained above. By changing alignment, and coupling into the core and the cladding mode, we observe different properties in the supercontinuum generation. Experimental results obtained are compared with the corresponding theoretical data based on the PCF modal analysis and the short pulse propagation described by the nonlinear Schrödinger equation.

The results thus obtained, can be attributed to the difference of the dispersion properties of the core and the cladding mode of the PCF as shown in Figure 4-3. This can be explained as the development of supercontinuum from μJewel laser with 300fs pulse, when launched into the cladding mode during propagation in the first 10cm of fiber (ESM-12-01 from Thorlabs Inc). It is seen that because the input wavelength is in the normal dispersion range, the self-phase modulation plays a major role in the first few centimeters of the propagating fiber. When the spectrum is wide enough to extend into the anomalous dispersion range (after 4cm), the soliton fission and the dispersive wave generation widens the spectrum into the blue side, down to 0.6μm [15].

The features of the supercontinuum spectrum have been reproduced in numerical simulations. The simulation spectrum shows (Figure 4-5(b)) the shoulder extending into the visible part of the spectrum, which is due to the cladding mode excitation, and the central plateau near the incident wavelength 1040nm is because of the core mode involvement. Therefore, the full spectrum can be explained as a superposition of the spectra from the core and the cladding modes.

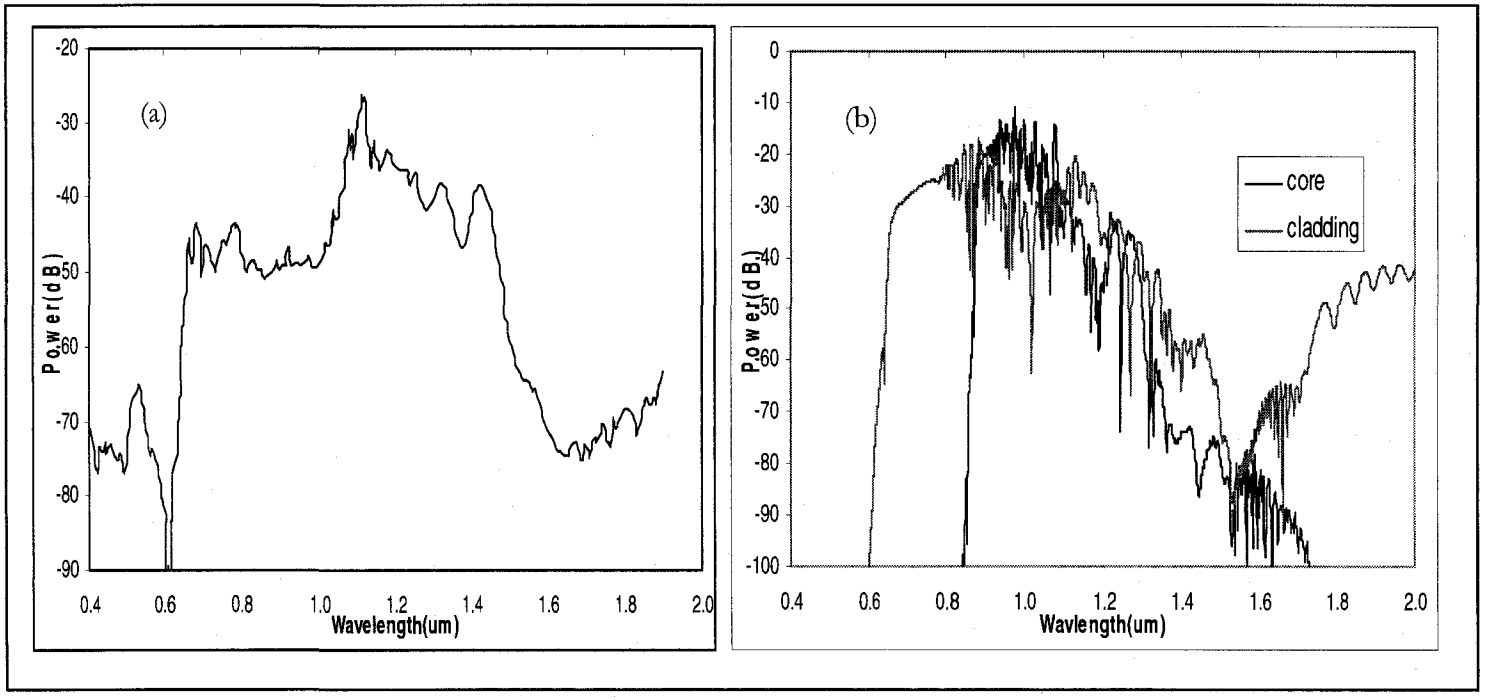

Figure 4-5 (a) Experimental Results of SC generation from ESM-12-01 fiber Figure (b) Simulation results of Core (blue) and Cladding (red) modes superimposed [40]

4.5.1 Effect of increasing the pump power

We have also studied the effect of increasing input power on the supercontinuum generation. In the experiment, the pump power has been increased from 10mW to 250mW. While increasing the input power, we have monitored the spectrum of the output signal through an OSA. We have found that, at low input power, the output spectrum does not differ from the spectrum of the incident pulse and appears as a narrow peak at 1040nm as seen from Fig. 4-6 (a). With the increase in incident power, from Fig. 4-6(b) to (c), the self-phase modulation starts playing its role for broadening into the Stokes direction, where the fiber dispersion becomes anomalous. Here, the conditions of soliton formations are satisfied. At higher power, corresponds to Fig. 4-6(d), the soliton fission in combination with the dispersive wave generation produces supercontinuum extending to the anti-Stokes direction down to 600nm [10].

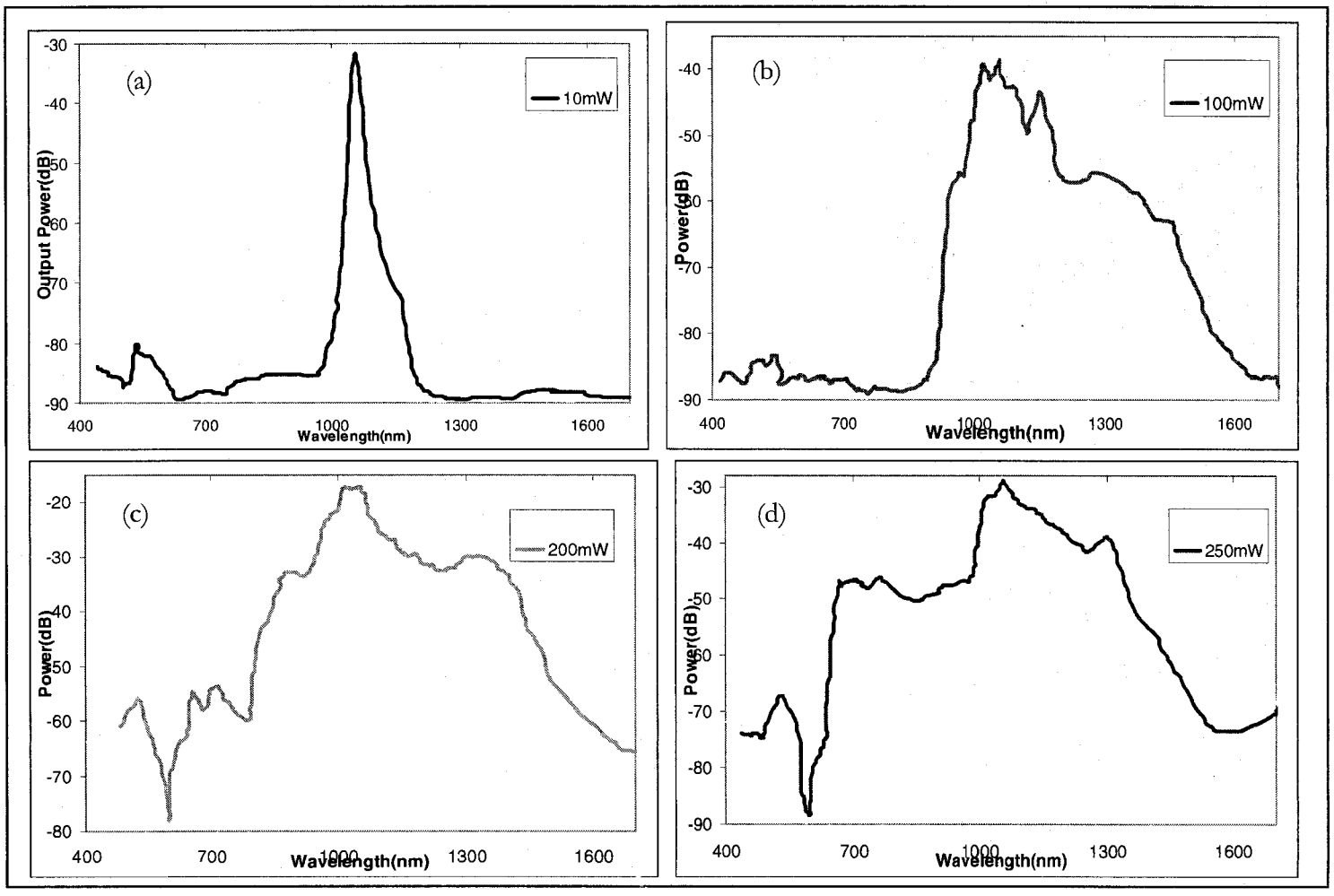

Figure 4-6 Experimental spectra of Supercontinuum generation in an ESM-PCF at different input power (a) 10mW (b) 100mW), (c) 200mW and (d) 250mW [40]

Far field patterns of the PCF with the excitation of the cladding mode along with the core mode are shown in Figure 4-7.

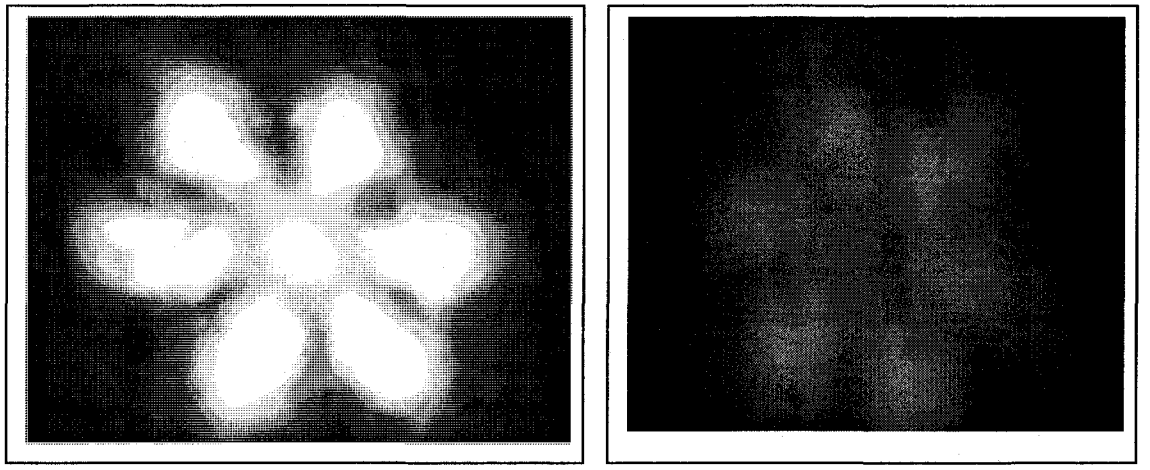

(a) (b)

Figure 4-7 (a)Far field pattern observed on a video screen through an IR camera Figure (b) Far Field pattern showing excitation of cladding mode for SC generation using Olympus camera

In conclusion, we have discussed wide supercontinuum generation in a solid-core photonic crystal fiber. While the fiber used is considered endlessly single mode, we show that this is only true when light propagates for sufficiently long propagation length. In contrast, when the fiber is short (tens of centimeters), the higher order cladding mode propagates and assists in the generation of a wide spectral supercontinuum. Results of the experimental studies are in good agreement with numerical simulations. The cladding mode efficiently penetrates into the fiber holes which can be used in PCF-based sensors relying on exploitation of the evanescent field. The strength of the cladding mode as well as spectroscopic characteristics of light transmitted through the PCF filled with analyte can be traced by analyzing details of the far field pattern of the transmitted signal.

Bibliography

1. P. St. J. Russell, "Photonic crystal fibers," Science 299, pp. 358-362 (2003).
2. J. C. Knight, T. Birks, P. S. J. Russell, and D. Atkin, "All-silica single-mode optical fiber with photonic crystal cladding", Optics Letters 21, pp. 1547-1549 (1996), Errata Optics Letters, 22, pp. 484-485 (1997).
3. J. C. Knight, J. Arriaga, T. A. Birks, A. Ortigosa-Blanch, W. J. Wadsworth, and P. St. J. Russell, "Anomalous dispersion in photonic crystal fiber", IEEE Photonics Technology Letters. 12, pp. 807-809 (2000).
4. R. F. Cregan, B. J. Mangan, J. C. Knight, T. A. Birks, P. S. J. Russell, P. J. Roberts, and D. C. Allan, "Single-mode photonic band gap guidance of light in air", Science 285, pp. 1537-1539 (1999).
5. T. A. Birks, J. C. Knight, and P. S. J. Russell, "Endlessly single-mode photonic crystal fiber", Optics Letters. 22, pp. 961-963 (1997).
6. A. Ortigosa-Blanch, J. C. Knight, W. J. Wadsworth, J. Arriaga, B. J. Mangan, T. A. Birks, and P. S. J. Russell, "Highly birefringent photonic crystal fibers", Optics Letters, 25, pp. 1325-1327 (2000).
7. J. K. Ranka, R. S. Windeler, and A. J. Stentz, "Efficient visible continuum generation in air-silica microstructure optical fibers with anomalous dispersion at 800 nm", Conference on Lasers and Electro-Optics CLEO '99, pp. CPD8/1-CPD8/2 (1999).
8. C. Peucheret, B. Zsigri, P. A. Andersen, K. S. Berg, A. Tersigni, P. Jeppesen, K. P. Hansen, and M. D. Nielsen, "40 Gbit/s transmission over photonic crystal fibre using mid-span spectral inversion in highly nonlinear photonic crystal fibre", Electronics Letters 39, pp. 919-921 (2003).
9. J. K. Ranka, R. S. Windeler, and A. J. Stentz, "Efficient visible continuum generation in air-silica microstructure optical fibers with anomalous dispersion at 800nm", Conference on Lasers and Electro-Optics CLEO '99, pp. CPD8/1-CPD8/2 (1999).

10. G. Genty, M. Lehtonen, H. Ludvigsen, J. Broeng, and M. Kaivola, "Spectral broadening of femtosecond pulses into continuum radiation in microstructured fibers", Optics Express 10, pp. 1083-1098 (2002).
11. R. R. Alfano, and S. L. Shapiro, "Emission in the region 4000 to 7000Å via four-photon coupling in glass,"\" Physical Review Letters 24, pp. 584–587 (1970).
12. R. G. Brewer, "Frequency shifts in self-focused light," Physical Review Letters 19, pp. 8–10 (1967).
13. C. Lin, and R. H. Stolen, "New nanosecond continuum for excited-state spectroscopy," Applied Physics Letters. 28, pp. 216–218 (1976).
14. T. A. Birks, W. J. Wadsworth, and P. St. J. Russell, "Supercontinuum generation in tapered fibers," Optics Letters 25, pp. 1415–1417 (2000).
15. J. M. Dudley, G. Genty, S. Coen, "Supercontinuum Generation in Photonic Crystal Fiber," Reviews of Modern Physics 78, pp. 1135 (2006).
16. D. Mogilevtsev, T. A. Birks, and P. S. J. Russell, "Group-velocity dispersion in photonic crystal fibers," Optics Letters 23, pp.1662-1664 (1998).
17. N. G. R. Broderick, T. M. Monro, P. J. Bennett, and D. J. Richardson, "Nonlinearity in holey optical fibers: measurement and future opportunities," Optics Letters 24, pp. 1395-1397 (1999).
18. J. K. Ranka, R. S. Windeler, and A. J. Stentz, "Visible continuum generation in air-silica microstructure optical fibers with anomalous dispersion at 800 nm," Optics Letters 25, pp. 25-27 (2000).
19. R.R Alfano, "The supercontinuum Laser Source" Spronger-Cerlag (1989)
20. H. Takara, T. Ohara, K. Mori, K. Sato, E. Yamada, Y. Inoue, T. Shibata, M. Abe, T. Morioka, and K-I. Sato "More than 1000 channel optical frequency chain generation from single supercontinuum source with 12.5 GHz channel spacing" Electronics Letters 7, 36, pp. 2089-2090 (2000).
21. D. J. Jones, S. A. Diddams, J. K. Ranka, A. Stentz, R. S. Windeler, J. L. Hall, and S. T. Cundiff, "Carrier envelope phase control of femtosecond mode-locked lasers and direct optical frequency synthesis," Science 288, pp. 635-639 (2000).

22. M. Bellini and T. W. Hänsch, "Phase-locked white-light continuum pulses: toward a universal optical frequency-comb synthesizer," Optics Letters 25, pp. 1049-1051 (2000).
23. I. Hartl, X. D. Li, C. Chudoba, R. K. Ghanta, T. H. Ko, J. G. Fujimoto, J. K. Ranka, and R. S. Windeler, "Ultrahigh-resolution optical coherence tomography using continuum generation in an air–silica microstructure optical fiber," Optics Letters 26, 608-610 (2001).
24. T.M Monro, D.J. Richardson, P.J. Bennett, "Developing holey fibers for evanescent field devices," Electronics Letters, 35, pp.1188-1189 (1999).
25. P. Russell, "Photonic Crystal Fiber", Science 299, pp. 358-362 (2004).
26. J. B. Jensen, L. H. Pedersen, P. E. Hoiby, L. B. Nielsen, T. P. Hansen, J. R. Folkenberg, J. Riishede, D. Noordegraaf, K. Nielsen, A. Carlsen, and A. Bjarklev, "Photonic crystal fiber based evanescent-wave sensor for detection of biomolecules in aqueous solutions," Optics Letters 29, pp. 1974-1976 (2004).
27. D. Pristinski and H. Du, "Solid-core photonic crystal fiber as a Raman spectroscopy platform with a silica core as an internal reference," Optics Letters 31, pp. 3246-3248 (2006).
28. Y. Vidne and M. Rosenbluh, "Spatial modes in a PCF fiber generated continuum," Optics Express 13, pp. 9721-9728 (2005).
29. T. P. White, R. C. McPhedran, C. M. de Sterke, L. C. Botten, and M. J. Steel, "Confinement losses in microstructured optical fibers," Optics Letters 26, pp. 1660-1662 (2001).
30. www.comsol.com (accessed on March 20, 2008)
31. www.imra.com (accessed on March 20, 2008)
32. G. P. Agrawal, "Nonlinear Fiber Optics", Academic Press (2003).
33. F. Brechet, J. Marcou, D. Pagnoux, and P. Roy, "Complete analysis of the characteristics of propagation into photonic crystal fibers by the finite element method", Optical Fiber Technology 6, pp. 181-191 (2000).
34. Y. Logvin, A. Khetani, H Anis, "Cladding mode assisted supercontinuum generation in solid core photonic crystal fiber for biosensor application", Photonics West 2008 (Paper 6875-22).

Chapter 5. Laser Flash Photolysis using Photonic Crystal Fibers

The Laser Flash Photolysis (LFP) technique provides one of the most effective methods for studying the reaction of transient species such as radicals, excited states or ions, in chemical and biological systems. Photonic crystal fiber as a sample container as well as a photonic device supporting mode structure offers new opportunities for carrying out laser flash photolysis experiments with ultra small samples. The experiments performed resulted in bringing down the sample volume to 10^{-10} l with signal improvements of at least an order of magnitude

5.1 Introduction

The chapter proposes a novel approach in carrying laser flash photolysis using a photonic crystal fiber. In Section 5.2, we introduce laser flash photolysis as well as summarize the history and principle behind it. In this section, we focus on conventional laser flash photolysis scheme and the interpretation of the data recorded. Finally in Section 5.3, we present the laser flash photolysis using PCF and PBF for recording transients in samples like xanthone and benzoin. It should be noted that this work was done in collaboration with Dr. Tito Scaiano and Dr. Marie Laferriere in the Chemistry department at the University of Ottawa. Our work focused on selection and simulation of fiber, setting up the experimental setup and optimizing the setup while they focused on choosing chemicals under test and analyzing the data. Dr. Scaiano is a leader in laser flash photolysis and this collaboration enabled us to attempt using PCF in flash photolysis for the first time.

5.2 Introduction to Laser Flash Photolysis

New fundamental discoveries in natural science have led to the introduction of new revolutionary research methods. Optical spectroscopy is one of the many new methods which has emerged and has helped in many applications through the study of absorption and emission of light by matter. One of the many fields where optical spectroscopy is applied is in the study of photochemical reactions. Photochemical reactions are very important for understanding atmospheric chemistry like the production of ozone in the stratosphere [1], the decomposition of chlorofluorocarbons in the stratosphere [2], and the oxidation of sulfur species with photo-chemically generated hydroxyl radicals in the troposphere [3]. Other areas where this is applied are: aqueous environmental chemistry and synthetic chemistry.

The absorption of light by molecules produces electronic excited states. Electronically excited molecules can be very reactive. In Figure 5-1 the different absorption phenomena are shown [4].The absorption commonly occurs when an electron moves from the lowest vibrational state of an occupied molecular orbital into a higher vibrational state of an unoccupied electronic state. The other absorption phenomena such as the creation of

singlet-triplet and triplet-triplet states are also possible for chemical compounds but it is strongly dependent on the spin of electrons in the molecules. Fluorescence is an emission process which occurs from a singlet excited state while phosphorescence is another process which takes place from a triplet excited state.

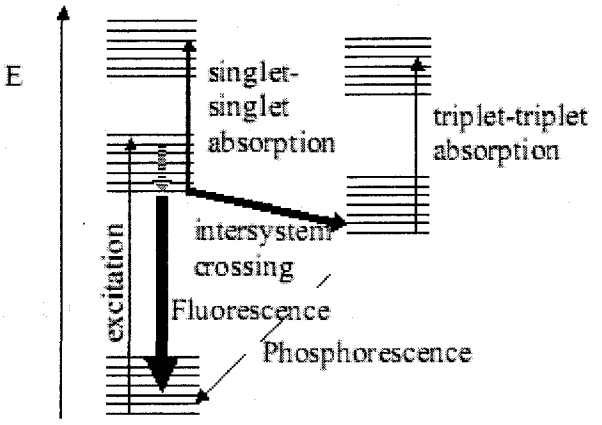

Figure 5-1 Typical electronic energy diagram [4]

Usually photochemical reactions involving triplet absorption produce electronically excited molecules which are very reactive. As a consequence they are often very rapid and short lived, which requires fast reaction techniques. In general, two approaches are followed to study short lived intermediates. In the first method the experimental conditions are adjusted to lengthen the intermediate lifetime, so that the detection becomes possible with standard spectroscopic techniques (such as cryogenic technique or bimolecular techniques). Although this approach yields excellent spectroscopic and structural data, it cannot provide any information about the reactivity of the sample under conditions.

The second approach is to allow reactions to proceed under normal laboratory conditions with fast detection techniques, thereby monitoring the reactive intermediates. This approach also requires a fast generating laser pulse to excite the sample under study and is used in numerous techniques such as magnetic and optical spectroscopy. In optical spectroscopy, one of the directions of improvement was aimed at time resolution which can be achieved through a technique popularly known as Laser Flash Photolysis (LFP) [5].

5.2.1 Brief History

In 1967, the Nobel Prize was shared by Eigen, Norrish, and Porter for the development of the flash photolysis method, "a powerful tool for the study of the various states of molecules and transfer of energy between them" [6]. In the flash photolysis method, the excitation is done using a flash lamp for reactive intermediate to study millisecond transients. It was clear that in order to study sub-micro and nano second transients, a better system needed to be employed. With the invention of laser in the early 1960s, it was evident that the laser flash photolysis would yield better time resolution. Lindqvist in 1966 was the first one to demonstrate Laser Flash Photolysis, detecting the triplet state of acridine using a short pulse from nitrogen laser (337μm). Over the past few decades, research in the field of LFP has been fuelled by many groups [7].

5.2.2 Basic Principle

The fundamental idea of laser flash photolysis is to disturb the system under study, by using a short light flash and monitor the absorption properties of the system through photo-reactions. The excitation laser increases the energy of the system, thereby triggering a chain of spontaneous reactions. In other words, the excitation beam causes some reactions in the samples which will result in attenuation, amplification or refraction of the transmitted beam. By monitoring the change in the transmitted beam, the type of reactions taking place in the samples can be detected.

5.2.3 Reaction Mechanism [8]

For example, a molecule M is in equilibrium with the solvent molecule under normal conditions, which means that the electronic subsystem is in its lowest energetic state (i.e. ground state). Light acts as a trigger to initiate a series of reactions. In the first step the absorption of energy (E) of a photon takes place by the compound, which can be shown as:

$$E = h\upsilon \tag{5-1}$$

where h is Planck's constant and υ is the frequency of the light. As a result of absorbing the photon, the molecule (M) gains energy and is promoted to an excited state (M*). This step can be represented as:

$$M + h\upsilon \rightarrow M^* \tag{5-2}$$

where M* is a new chemical species that is highly reactive.

After absorbing the photon, excited molecule M* can either lose its extra energy and decay back to M through a singlet or triplet absorption of the monitoring beam, or it can proceed to form stable products (M* $\rightarrow$products) by mean of charge transfer [8].

5.2.4 Laser Flash Photolysis

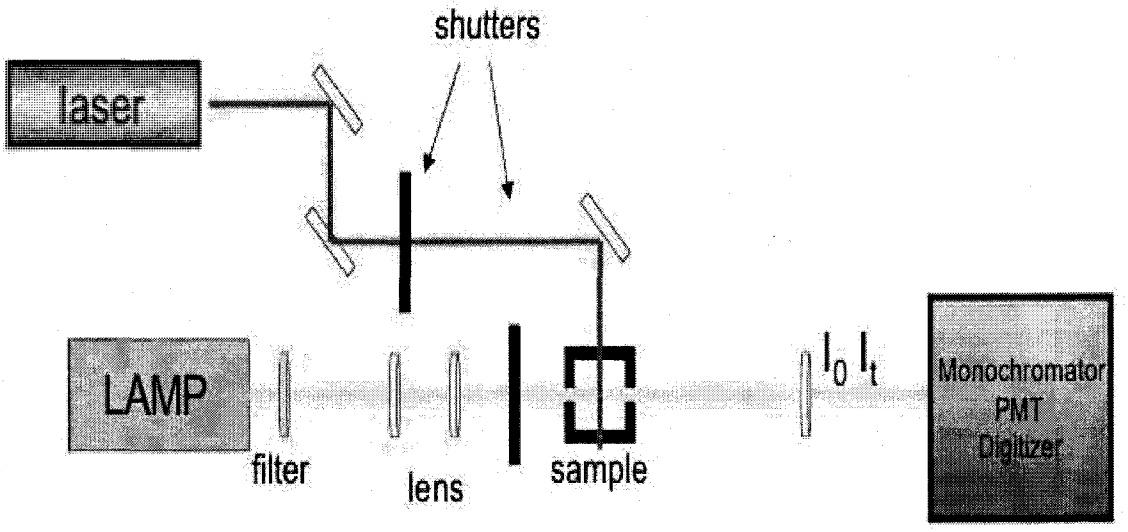

Figure 5-2 Laser Flash Photolysis schematic setup [9]

A general scheme of laser flash photolysis is shown in Figure 5-2. The scheme is similar to the simple absorption spectrophotometer in which the absorption is measured by determining the light intensities of the monitoring beam (lamp) before and after the sample passes through it. The difference in laser flash photolysis lies in the pulse excitation of laser source and detecting the system. The aim of LFP is to measure through the

spectrophotometer the temporal change in the light intensities but not the light intensities itself.

The purpose of the pulse excitation laser is to generate a transient or excited state in a sample. The change in absorption in the sample is monitored with a continuous monitoring source. The function of the monochromator is to pass a monitoring beam (lamp) and reject the excitation laser. The mechanism of the LFP is that the laser pulse causes changes in absorption of the sample leading to change in the intensity of the monitoring beam. The theory involved and the signal obtained in LFP is mentioned in Appendix A.

5.2.5 LFP absorption spectra

A schematic of the conventional laser flash photolysis performed at Scaiano's photochemistry lab at the University of Ottawa is shown in Figure 5-2. Different excitation wavelengths are provided by multiple lasers: 266, 355 and 532nm by two Surelite Nd-YAG lasers, 308 nm by an EX 530 Lumonics laser, and 157, 193 and 248nm by a GSI-Lumonics excimer laser. All the results reported in this thesis have been performed using a 308nm laser as the excitation source. The monitoring beam usually is a 150W Xe pulsed lamp [11].

The monitoring lamp is focused with the help of lenses onto the sample. The laser beam is directed at 90^0 on the sample where it is concentrated. A monochromator and a photo multiplier tube (PMT) are positioned after the sample. The system is connected to an oscilloscope, a line synchronizer, and a computer. The sequence that leads to data acquisition is coordinated with a line synchronizer [9]. The sequence is as follows: the lamp shutter is first opened and a first channel records the monitoring lamp intensity. The photo multiplier (PMT) voltage decreases when the lamp is pulsed. The laser shutter opens and the laser is fired, the laser beam reaches an optical fiber that sends a signal to the digitizer to start acquiring data points in a second channel. The laser beam reaches the sample where a transient is formed and the laser shutter is subsequently closed. The monitoring beam shutter is finally closed. The signal from the monitoring beam acts as a

baseline and is subtracted from the signal. The changes in PMT voltage are representative of the changes in absorption of the sample during and after laser irradiation [9].

5.3 Laser Flash Photolysis using Photonic Crystal Fibers

During the past 40 years, LFP has evolved with dramatic improvements in time resolution, computer control, and the availability of a wide range of pulsed lasers, offering great flexibility in excitation wavelength, pulse energy, and pulse duration. However, sample size have remained in the 0.1 to 10ml range for static samples, and significantly larger when flow systems are required. Usually the sample container is a cuvette as shown in the Figure 5-3 below for holding the sample.

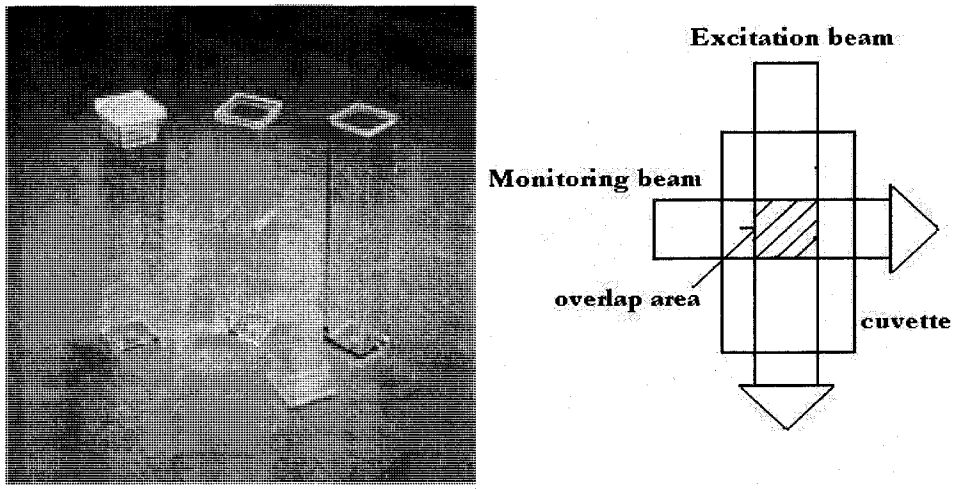

Figure 5-3 Cuvette as a sample holder [12] and T-scheme for performing LFP for liquid samples where the excitation beam and monitor are perpendicular

On the left of Figure 5-3 is the schematic of a typical T-scheme, where the excitation beam is at a right angle and crossing the monitoring beam. Usually the active area is very small which leads to low signal. In the past decade, the development of photonic crystal fiber has been used for applications related to absorbance and fluorescence [13]. However, laser flash photolysis was never attempted using PCF.

5.3.1 Experimental Setup

The types of photonic crystal fibers used are an endlessly single mode PCF (ESM-12-01), and hollow core PCFs (HC-1060-02) which were purchased from Thorlabs Inc. [15] and manufactured by Crystal Fiber A/S [16]. Typically, an 8-10cm long piece of the PCF was mounted on a 5-axis flexure stage [15]. Light from a He-Ne laser at 633nm, was coupled into this PCF using a 10x, 0.07 NA microscope objectives [16] with a coupling efficiency of ~ 80%. The experiments are carried out by having a reservoir attached to the end of the fiber for continuous supply of sample inside the channels of the PCF (as discussed in Chapter 2). The experimental setup is shown in Figure 5-4.

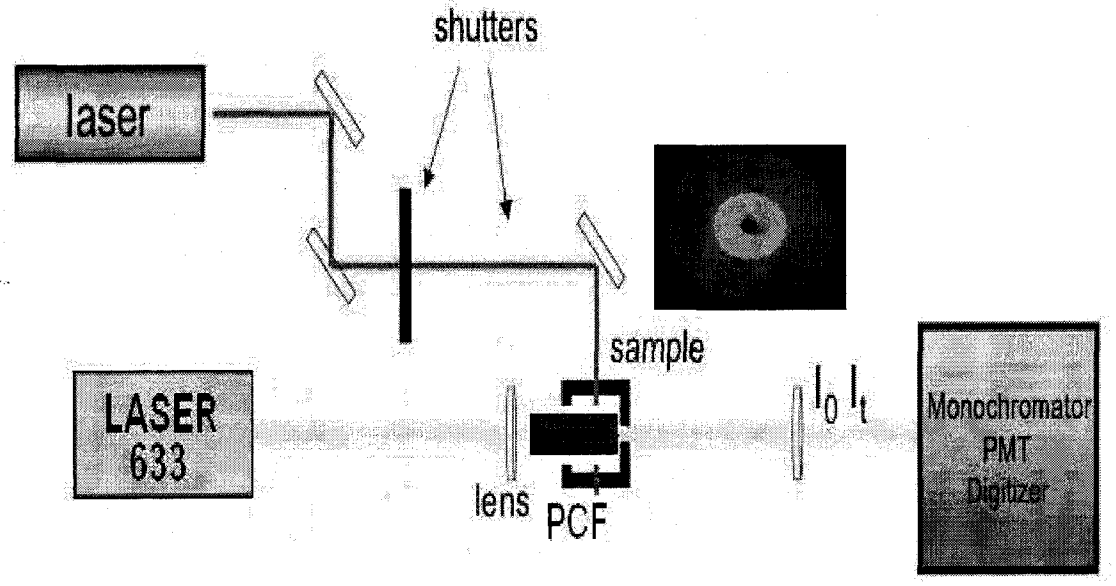

Figure 5-4 Schematic of the laser flash photolysis setup.

The setup shown has an excitation laser perpendicular to the fiber axis; the fibers light guiding property will direct the monitoring beam through the sample into the detection system. The monitoring beam which was coupled into the fiber was from a He/Ne laser at 633nm. Figure 5-5 shows the fiber mounted on a flexure stage and Figure 5-6 shows the far-field pattern obtained after coupling the light into the fiber.

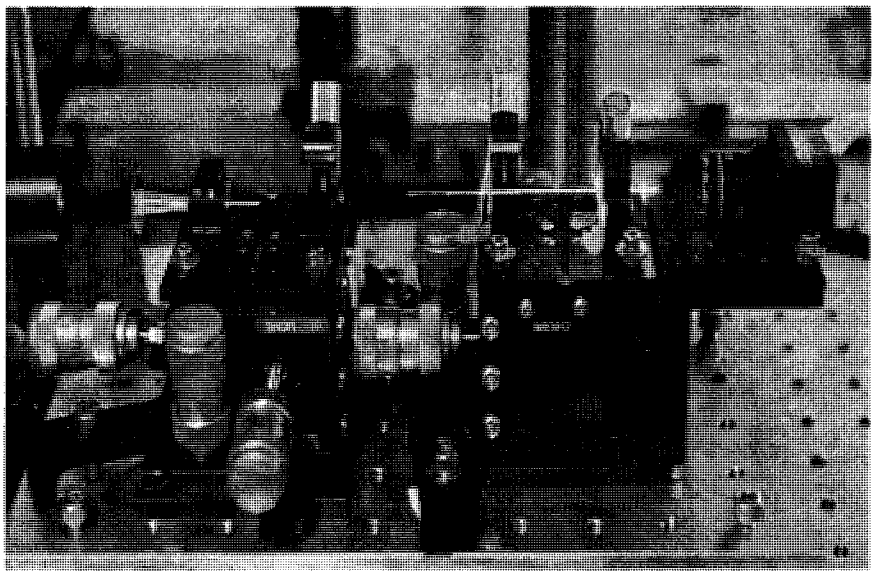

Figure 5-5 Experimental setup for launching light into the fiber for laser flash photolysis setup

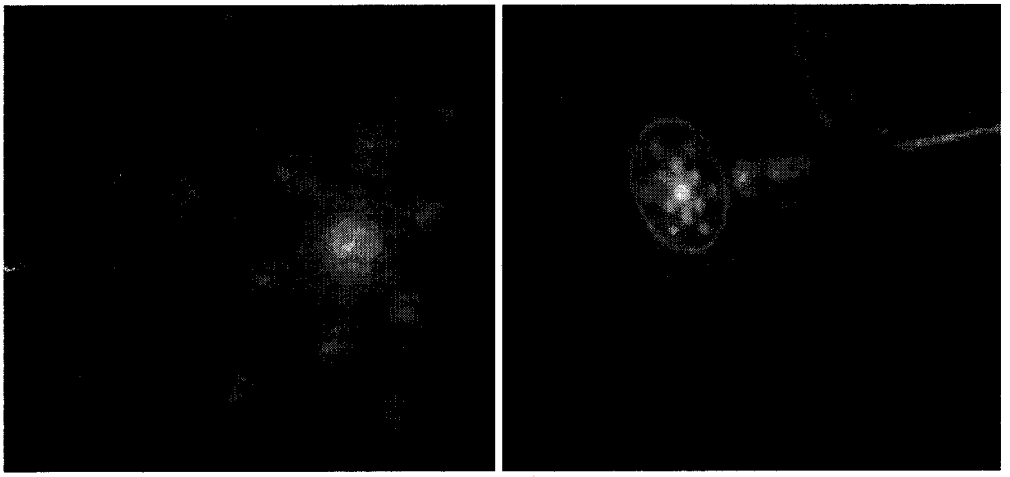

Figure 5-6 Far Field pattern of a filled fiber.

5.3.2 Experimental Results

Selection of the chemical systems was based on the sample which would give transient in the spectral range of 600nm. The chemicals used to perform LFP are: Acetonitryl (ACN) Omnisolv was purchased from EM Science and toluene chromasolv, xanthone 97% and methyl viologen dichloride hydrate 98% (MV) were purchased from Sigma-Aldrich, and Irgacure® 2959 (2-Hydroxy-1-[4-(2-hydroxy-ethoxy)-phenyl]-2-methyl-propan-1-one) from Ciba. Milli-Q water was used to prepare the methyl viologen (MV) (0.008gm in 10ml of solution) and 2.5mM I-2959 solutions.

All the solutions prepared have a common property that they generate transient intermediates with a strong absorbance in the 600nm region, and their presence could be probed with the 633nm He/Ne laser source, which we had successfully coupled with the fibers used in this work. Some early tests had shown that we could record time-resolved fluorescence from methylene blue, coumarin 6 and coumarin 110 originating from the fibers, thus giving us hope that laser flash photolysis could be performed with the fibers. The following section describes reaction and results while measuring transient states of xanthone in acetonitryl, xanthone in toluene and benzoin in water.

5.3.3 Reaction mechanism in xanthone

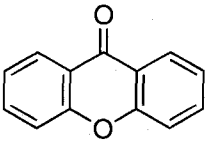

Xanthone

Figure 5-7 Xanthone

Figure 5-7 shows the structure of the xanthone molecule. The xanthone molecule in solvents (acetonitryl, toluene) gets into an excited state with the excitation laser pulses thereby triggering a series of reactions by an oxygen molecule which has a lone pair of electron ($2p_x$) state. The excitation results in a singlet state. This state absorbs the 600nm wavelength range. Thus, the monitoring laser source at 633nm would cause a triplet excited state, which decays with time. The decay in time is recorded by the detector system [18].

5.3.3.1 Results of LFP from ESM-PCF filled with xanthone and toluene

In the first experiment we have used an endlessly single mode PCF for performing laser flash photolysis. The fiber was filled with xanthone and toluene. A good coupling efficiency was obtained by coupling He-Ne 633nm and the sample in the fiber was excited with the 308nm laser. The results were really encouraging as we were able to detect triplet absorbance decay of xanthone which can be seen from Figure 5-8.

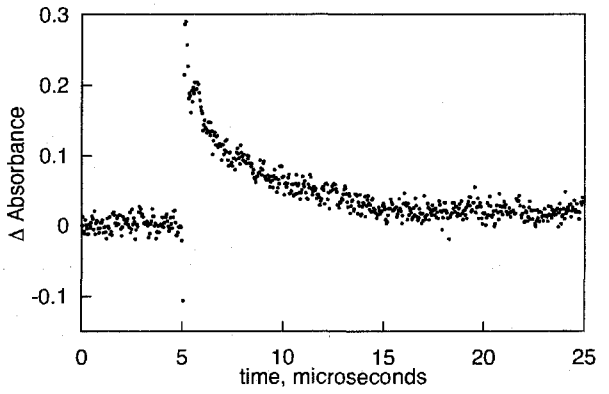

Figure 5-8 Decay of triplet absorbance of xanthone in toluene with 633 nm excitation inside the channels of an ESM fiber. One negative point (fluorescence) was cropped to facilitate viewing of the triplet decay.

The signal detection was possible as a small amount of light penetrates into the cladding channels, thus leading to a signal through the evanescent field method. While the results of Figure 5-8 were quite encouraging, it quickly became evident that this method was not an effective way, as the signal obtained was very weak due to very low mode field overlap between the light and the solution occupying the channels. It was also found that this method was not very useful for acetonitryl and water which have refractive indices less than silica. The reason was that the light penetrating into cladding channels was not sufficient enough to get a strong signal, which has led us to move to hollow core photonic bandgap fiber where the sample is present in the core where most of the light is confined.

5.3.3.2 Results of LFP from HC-PBF filled with xanthone and acetonitryl

The other approach being employed is using hollow core photonic bandgap fibers. We used a HC-1060-02, a photonic bandgap fiber with a 9.7μm core size and 2.75μsm diameter of cladding holes. The non-selective filling technique was used to perform laser flash photolysis, so that a better overlap between the EM field and the sample could be obtained as all the channels of the fiber are filled. A number of experiments with liquids of refractive index below that of silica, specifically acetonitryl and water were carried out in fiber HC-1060, under these conditions couple well at 633 nm as discussed in Chapter 2. A trace for xanthone in acetonitryl is shown in Figure 5-9.

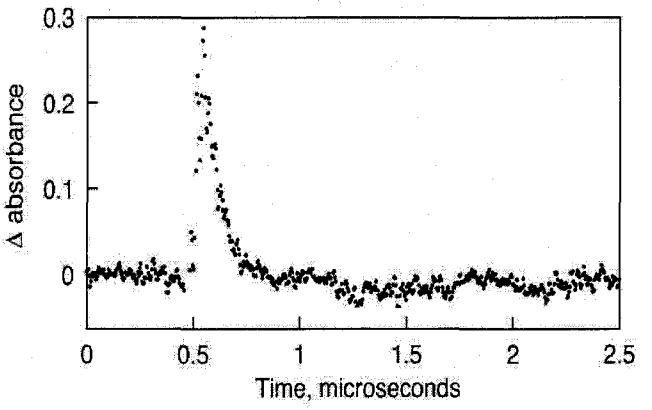

Figure 5-9 Decay of triplet absorbance of xanthone in acetonitryl inside the channels of HC-1060 PCF obtained with the 633nm laser monitoring.

5.3.3.3 Results of LFP from HC-PBF filled with xanthone and toluene

Experiments were also carried out in toluene as solvent, having a refractive index higher than that of silica. As shown earlier, in these cases the light is guided at all wavelengths by total internal reflection. This technique provided an easy approach for the measurements of transient lifetimes. The material used was xanthone and an experimental result obtained is shown in Figure 5-10 [21].

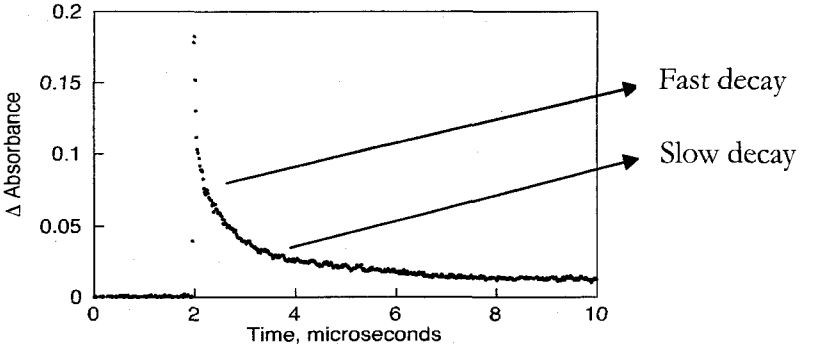

Figure 5-10 Decay of triplet xanthone in toluene inside the channels of a HC-1060 PCF following 308 nm excitation and monitored at 633nm.

The decay of Figure 5-10 reveals a very fast component with a lifetime of about 30ns, characteristic of xanthone in toluene, along with a much longer component following a complex decay and with an initial half life time around 2μs [22].

5.3.3.4 Reaction mechanism for benzoin in presence of methylviologen

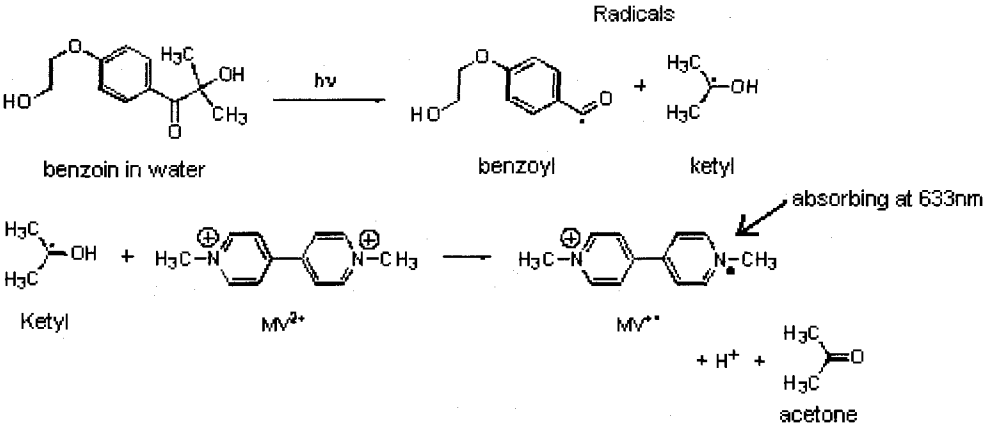

Figure 5-11 Mechanism of Benzoin in presence of Methyl Viologen

In this set of experiments, we used a water soluble benzoin (Irgacure-2959) in the presence of methyl viologen (MV^{2+}). Benzoin in the presence of excitation light will split into two radicals: benzoin and ketyl. The ketyl radical is very reactive and in presence of methyl viologen, undergoes an electron transfer. This results in radical cation ($MV^{+\bullet}$), that is expected to give its strongly absorbing radical cation ($MV^{+\bullet}$) with a maximum at 603nm, but strongly absorbing at 633nm. This scheme is shown in Figure 5-11.

5.3.3.5 Results of LFP from HC-PBF filled with benzoin in presence of methylviologen

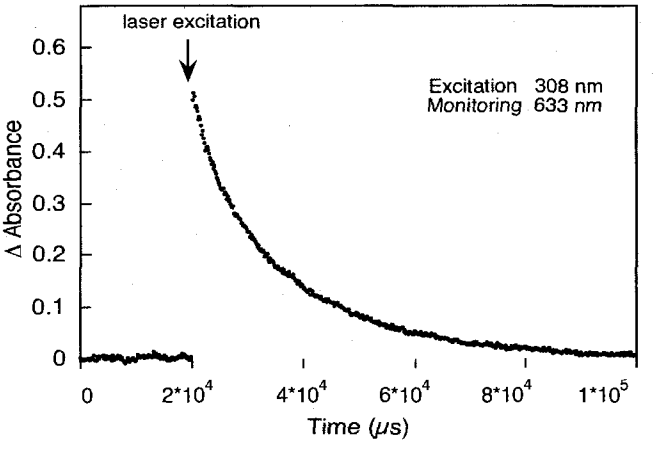

Figure 5-12 Decay of the $MV^{+\bullet}$ cation following its generation according to Figure 5-11.

The experiments gave a remarkable signal with a lifetime of about 17ms (Figure 5-12). The decay reflects a combination of reaction with traces of oxygen as well as the RC component of the oscillator in the detection system. The methyl viologen radical cation $MV^{+\bullet}$ is known to react with oxygen (Figure 5-13) regenerating the starting material, i.e., MV^{2+} [19, 20].

Figure 5-13 Scheme of methyl viologen cation reacting with oxygen

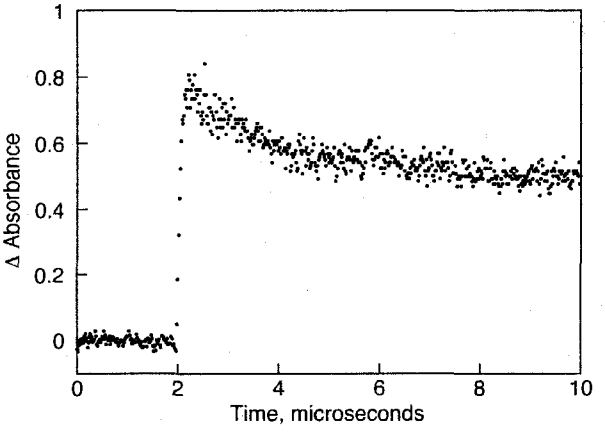

Figure 5-14 The system of Scheme 1 excited at 308nm under oxygen with a HeNe laser (633nm) coupled to an ESM HC-1060 fiber.

The oxygen initially dissolved in the solution provides a sacrificial mechanism for regenerating methyl viologen. Thus, decay lifetimes for $MV^{+\bullet}$ change get longer as the experiment proceeds. The high signal obtained, corresponding to 80-90% of the monitoring light being absorbed is a clear indication of the excellent coupling between the He/Ne laser and the PBF fiber. The phenomenal results obtained due to the sample consumption reduction and long interaction length makes PBF one of the useful techniques for performing laser flash photolysis experiment.

Bibliography

1. W.D McGrath, R.G.W Norrish, "The Flash Photolysis of Ozone" Proceedings of the Royal Society of London. Series A, Mathematical and Physical Sciences,242, pp. 265-276 (1957)
2. J.E. Lovelock, K.J. Maggs, R.J. Wade "Halogenated hydrocarbons in and over Atlantic," Nature 241, 194-196(1973).
3. G. S. Tyndall, A. R. Ravishankara "Atmospheric oxidation of reduced sulfur species" International Journal of Chemical Kinetics 23, pp, 483 – 527(1991).
4. "Laser Flash Photolysis", www.colby.edu/chemistry/PChem/lab/LFP.pdf lab manual (accessed March 20, 2008)
5. J. C. Scaiano "Nanosecond Laser Flash Photolysis: A Tool for Physical Organic Chemistry" Reactive Intermediate Chemistry, John Wiley & Sons, Inc. (2004).
6. G. Porter, ''Flash Photolysis and Primary Processes in the Excited State," Fast Reactions and Primary Processes in Chemical Kinetics, Proc. 5th Nobel Symposium, S. Claesson, Ed., Almqvist and Wiksell, Stockholm, pp. 141–161 (1967).
7. J. C Scaiano, "Early History of Laser Flash Photolysis", Accounts of Chemical. Research 16, pp. 234 (1983).
8. Alison M. Gurney "Flash photolysis of caged compounds", Microelectrode techniques, The Plymouth workshop handbook (1994).
9. M. Laferriere, "Cinetique de la photo deposition d'alcenes sur le silicium", M.Sc., University of Ottawa (Canada), (2002).
10. N.V. Tkachenko "Optical spectroscopy: Methods and Instrumentation" Elsevier Science 2006).
11. A. Berinstain, "Development of laser techniques for applications in biomolecules and cellular systems" , Ph.D., University of Ottawa (Canada), (1997)
12. http://www.perf-sci.com/d_cuvettes/cuvette-3.jpg (accessed March 20, 2008)
13. P. St. J. Russell, "Photonic crystal fibers," Science 299, pp. 358-362 (2003).

14. J. Jensen, P. Hoiby, G. Emiliyanov, O. Bang, L. Pedersen, and A. Bjarklev, "Selective detection of antibodies in microstructured polymer optical fibers," Optics Express 13, pp. 5883-5889 (2005)
15. http://www.thorlabs.com/ (accessed on March 20, 2008)
16. http://www.crystal-fibre.com/ (accessed on March 20, 2008)
17. http://www.mellesgriot.com/ (accessed on March 20, 2008)
18. J. C. Scaiano "Solvent effects in the photochemistry of xanthone" Journal of American Chemical Society, 102, pp 7747–7753 (1980).
19. K.L. McGilvray, M.R. Decan, D. Wang, and J.C Scaiano, "Facile Photochemical Synthesis of Unprotected Aqueous Gold Nanoparticles" Journal of American Chemical Society, 128, pp. 15980 - 15981 (2006).
20. L.K Patterson, R.D Small Jr, J.C Scaiano, "Reaction of Paraquat Radical Cations with Oxygen. A Pulse Radiolysis and Laser Photolysis Study," Radiation Research 72, pp, 218 (1977).
21. C. Coenjarts, J.C. Scaiano, "Reaction Pathways Involved in the Quenching of the Photoactivated Aromatic Ketones Xanthone and 1-Azaxanthone by Polyalkylbenzenes," Journal of American Chemical Society, 122, pp. 3635 (2000).
22. F. Wilkinson, C. J. Willsher, H. L. Casal, Linda J. Johnston, and J. C. Scaiano "Intrazeolite Photochemistry. IV. Studies of Carbonyl Photochemistry on the Hydrophobic Zeolite Silicalite Using Time-Resolved Diffuse Reflectance Techniques", Canadian Journal Chemistry 64, 539 (1986).
23. Altaf Khetani, Marie Laferrière, Hanan Anis and J.C. Scaiano "Laser flash photolysis with subnanoliter samples. Photonic crystal fibers as ultra small smart test tubes", submitted Journal of Material Science (2008).

Chapter 6. Photonic Bandgap Fiber as a Raman Biosensor

The chapter demonstrated a new method for using a non-selectively filled hollow-core photonic crystal fiber (HC-PCF) as a sensitive Raman spectroscopy platform suitable for biosensing applications. A 1550 HC-PCF was completely filled with ethanol (core and cladding holes). Using a relatively short 9.5cm length of HC-PCF, a Raman signal enhancement factor of 40 over a bulk solution of ethanol was observed under the same excitation conditions. The small sample volume utilized and longer interaction length provides the potential for compact, sensitive, and low-power Raman sensing of biological materials.

6.1 Introduction

This chapter proposes a novel approach for measuring spontaneous Raman signal enhancement using PBF. In section 6.2, an introduction to Raman spectroscopy is given. Raman Effect, theory, instrumentation and literature review has also been covered in the same section. Section 6.3 discusses the novel method proposed for enhancing Raman signal using a PBF. The approach was carried out at University of Ottawa along with my colleagues Majid Naji and Dr. Neil Lagali (from Dr. Rejean Munger's lab). My contribution focused on the PCF. This included filling the PCF, performing the simulation, setting up the experiment and recording the data.

Section 6.4, demonstrates for the first time characterizing quantum dots by selectively filling a HC-PBF. This was done in collaborations with Juan Irizar, a Master's student at Dr. Amr Helmy's lab at University of Toronto. My contribution was to help in the selection of fiber, performing the selective filling approach and setting up the initial experimental setup.

6.2 Introduction to Raman Spectroscopy

Optical techniques have played an important role in instrumentation and sensor applications especially in non-contact measurements. It is very well established that the detection and identification of bacteria, protein, and pathogens as infectious agents in people, environment and food samples is very important and has been the prime focus of interest. In recent years, the advancement in optical technologies has surged in the field of sensors [1]. Most optical based sensors are spectroscopic techniques involving fluorescence or absorbance. Although these techniques are very popular and effective they require, for instance in fluorescence, labeling of the molecule, which can lead to alterations in target-receptor interactions caused by conformational changes [2]. This has led to considerable effort for investigating other alternatives.

Raman spectroscopy is a compelling technique. It provides an optical fingerprint of chemicals and biomolecules corresponding to the vibrational frequencies of molecular bonds. Therefore, this label-free optical sensing technique has the ability to quantify molecules attached to the sensing surface, which should improve the well known problem of non-specific binding in all solid surface sensing systems. Additionally, it is desirable to have small, rapid assays that use small sample volumes and are capable of detecting several compounds of species in parallel. This is significant because, in many cases, sample collection is limited and sample processing also requires time. All of these factors point toward being able to detect multiple agents in parallel using small sample volumes.

6.2.1 Raman Effect

Raman Spectroscopy is based on a light scattering phenomenon known as the "Raman Effect" discovered by Sir C.V Raman and K.S Krishnan in 1928. In 1930, Raman was awarded with a Nobel Prize for this spectacular discovery [3]. The Raman Effect can be explained as follows: when a monochromatic light is incident on an atom or molecule, a fraction of light is scattered and another is absorbed. Most of the scattered light is elastically scattered known as Rayleigh scattering, which has the same wavelength and frequency as the incident light. However, a small fraction (1ppm) of photons is scattered at a different frequency, usually lower than the incident light. The amount of energy corresponding to the shift in wavelength is due to the vibrational and rotational energy level of the molecules of the sample. The spectrum caused due to shift in frequency is known as the Raman Spectrum and the phenomenon is called the Raman Effect. The Raman spectra usually contain many sharp peaks corresponding to the specific molecular vibrational frequencies and thus give a clear signature of the presence of specific molecules in the sample. The Raman spectra can, therefore, be used to discriminate between several chemical species in materials for qualitative and quantitative analysis [4].

6.2.2 Theory

When the energy of the incident photon is unaltered after collision with a molecule, the scattered photon has the same frequency as the incident photon. This is Rayleigh or elastic

scattering. Quantum mechanically, Raman scattering is a result of an energy transition of the scattering molecule to a virtually excited state and its return to a higher (or lower) vibrational (or rotational) state, with the emission of a photon. The virtual state is not a stationary energy state of a molecule in the quantum-mechanical sense; rather it is just a distortion of the electron distribution of a covalent bond [2]. Since the energy can be transferred from the photon to the molecule (or from the molecule to the photon), the scattered photon can have less (or more) energy than the incident photon, in which case the process is referred to as Raman Stokes (anti- Stokes) scattering. Figure 6-1 shows Raman and Rayleigh scattering processes involving virtual states [2, 4].

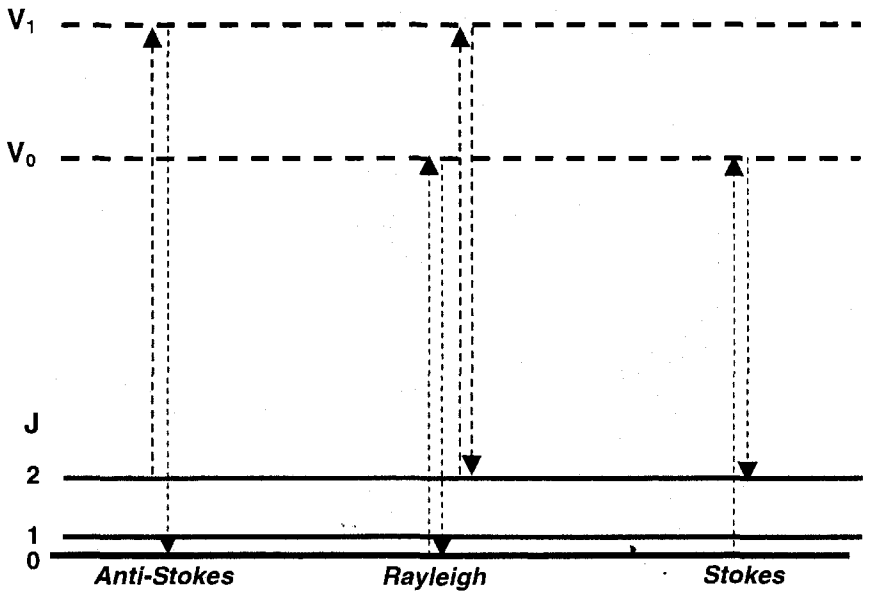

Figure 6-1 Electronics states [4]

The intensities of Rayleigh scattered light and Raman scattered light for the same samples are proportional to the number of molecules being illuminated. Rotational Raman bands result from transitions between rotational energy levels within a single vibrational energy level (pure rotational bands), or between different vibrational energy levels (rotation-vibration bands). The Raman scattering model was quantum-mechanically modified and was first used by Placzek [7] to derive an expression for Raman scattering intensity.

6.2.3 Instrumentation

The first commercial Raman instrument was introduced in 1953 and the development of lasers in 1960 allowed superior performance and ease of use [5]. A simple Raman instrument normally has a laser in a visible or near-infrared region with a dispersion/Fast Fourier transform (FFT) spectrometer for analyzing the spectrum. A diffraction grating is used to disperse the Raman scattered beam into multiple beams corresponding to specific frequencies, which are subsequently focused on an array of detectors, such as a high sensitivity charge coupled device (CCD). The spectrometer has to be equipped with a notch or edge filter to reject the elastically scattered photons (Rayleigh photons), which have the same energy as the laser photons. This would produce an intense background signal which covers the Raman signals.

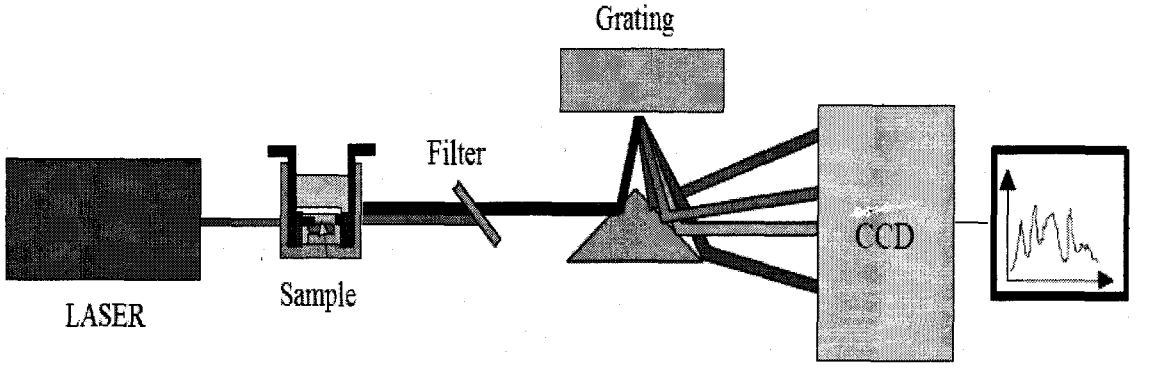

Figure 6-2 Instrument for Raman Spectroscopy [4]

Besides spontaneous Raman spectroscopy as discussed above, there are other types of Raman spectroscopy such as stimulated Raman spectroscopy, surface enhanced Raman spectroscopy (SERS), and Coherent anti-stokes Raman spectroscopy (CARS). In the following section we will look into a brief review where PCF is used for Raman sensors.

6.2.4 Literature review

During the last couple of decades, Raman spectroscopy— a powerful analytical technique—has been used for studying biological samples. Raman micro-spectroscopy can

provide useful biochemical information regarding live cells, which can be related to the interaction with toxic agents or drugs, disease, cell death and differentiation [6-9].

Because of its unique properties, PCF has many applications. Raman Spectroscopy is one area where PCF has been used and in the past 5 years it has received tremendous attention for biosensor applications due to its simplicity and its ability to offer a label free detection of biomolecules at a single molecular level.

In 1997, Altkom et al. did a complete analysis of liquid core fiber. In their experiment they were initially able to fabricate a capillary made up of Teflon AF 2400 and were able to detect the low refractive index liquids such as water, ethanol, acetonitryl, and methanol. The guiding principle was total internal reflection and the system was lossy [10].

D. Pristinski and H. Du have reported solid core photonic crystal fiber (PCF) as a promising platform for evanescent-field Raman spectroscopy of low-volume analytes [11]. In the experiment it was shown that, with different fiber length, the Raman spectrum of acetonitryl was obtained by subtracting the silica background. The disadvantage with this method is that the Raman spectrum is very weak, which is detected through an evanescent field that is about 5% of the total field propagated inside the fiber.

Benabid et al. have used stimulated Raman scattering in an approximately 1-meter-long hollow-core photonic crystal fiber, filled with hydrogen gas under pressure [12]. The HC-PCF core was formed by 7 missing channels while the cladding structure was arranged in a Kagomé lattice, so that a very broad transmission band (400-1700nm) was obtained. Yiuo et al demonstrated hollow core photonic crystal fiber for stimulated Raman scattering by filling it with low refractive index. The fiber was filled with ethanol and they studied the dependence of Stokes line on the input power [13].

Other techniques, such as surface enhanced Raman spectroscopy, will be reviewed in this section. Zhang et al, have selectively filled PCF with Silver nanoparticles. They reported the detection of analytes such as rhodamine 6G, human insulin, and tryptophan. In the experiment, the selective filling technique is applied so that the core of the fiber is filled with the analyte. The fiber is excited with a 785nm that is launched through one end of the

fiber and the same end is then used to collect the Raman spectrum. Silver nanoparticles of size 40-60nm were prepared by citrate reducing agents, which were mixed with the above mentioned analytes to detect a sample concentration of 10^{-4}-10^{-5}[14].

Very recently, Cox et al. have reported improvements on surface enhanced resonant Raman scattering in MOF with Kagome lattice cladding for rhodamine 6G detection. The Fiber used is 3 ring HC-PCF with Kagome lattice fabricated from polymer, which guides the wavelengths from 480-840nm when filled with water. They have reported that resonance Raman signal in R6G is enhanced by silver nanoparticles. The paper reports the detection of 10^{-6} M Rhodamine concentration [15].

In the following section we discuss our Raman work using a hollow core PBF. In this experiment we have demonstrated for the first time the enhancement of a spontaneous Raman signal by non-selectively filling HC-PBF [18].

6.3 Enhancement of Raman signal by non-selective filling HC-PBF

Use of this method of Raman spectroscopy is particularly well-suited for biological sensing applications where low-power laser radiation is needed to maintain sample integrity, or where only small sample volumes are available. In terms of measuring Raman signal enhancement using the non-selective filling approach, we considered ethanol as a solvent. The first step was to find the fiber which would guide 785nm when filled with ethanol. Applying the theory discussed in Chapter 2 and analyzing different fibers it was found that HC-1550 would be the fiber which would guide 785nm when filled with ethanol.

The experimental setup is shown in Figure 6-3. A single mode 100mW, 14 pin butterfly pin lasers was purchased from Innovative photonic solutions (I0785SB0100B) and was coupled into a hollow core PBF fiber. The laser beam was directed through a silver coated mirror and then passed through a 785 nm Iridian band pass filter. Coupling into the fiber was achieved by using a 40 x Newport microscope objective lens with NA. =0.65.

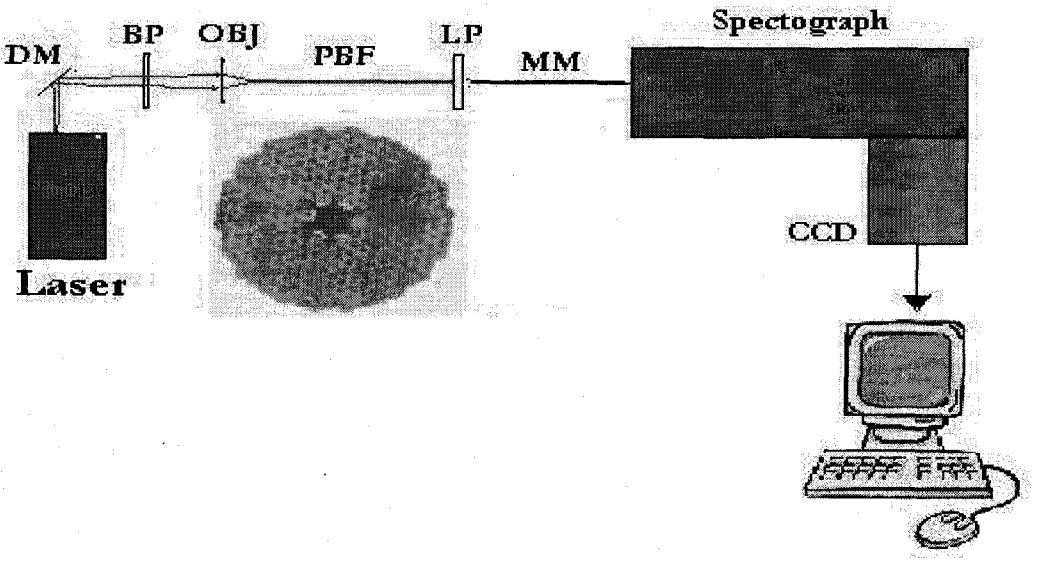

Figure 6-3 Schematic of the Raman Enhancement setup. Laser: 100mW butterfly laser at 785nm DM: Dichroic Mirror BP: Band pass filter OBJ: Microscope objective lens PBF: Hollow Core Photonic Bandgap fibers LP: Low pass filter MM: Multimode Fiber [18]

The fiber was filled with ethanol; light was coupled into the fiber with a coupling efficiency of about 25%. Figure 6-4 shows the mode pattern from the laser which is mainly fundamental mode (left) and some higher order mode (right).

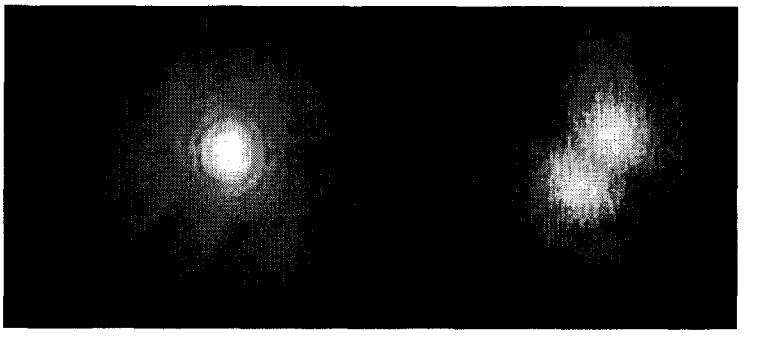

Figure 6-4 Laser beam consisted of mostly fundamental and partially second mode [18]

The output obtained from hollow core PBF was passed through a long pass filter (Iridian 785nm) and collected through a multimode fiber bundle, which in turn was coupled into a Kaiser f/18 Spectrograph, which had a TE-cooled Andor CCD camera. The data processing was done through a computer.

We found that coupling laser light into an ethanol filled PCF was sensitive, and spurious higher order coupling modes had to be avoided, as they caused a tremendous reduction in the Raman generated signal. Therefore, the near field laser beam pattern out of the PCF was checked to ensure that the output beam came from the core and not the fiber cladding or jacket (Figure 6.5).

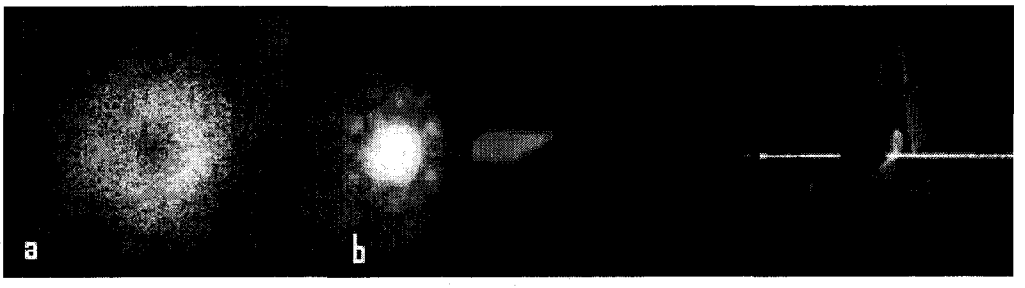

Figure 6-5 The near field laser beam pattern out of PCF, a) when light came from cladding and jacket c) when it came from core, true coupling [18]

Another effect observed was a change in coupling of the filled fiber over time, originating at the input side of the fiber. Over a few hours, coupling usually became weaker or was lost completely. The exact reason for this is unclear, however, we hypothesize that local heating of the fiber tip may have displaced or deformed the fiber over time.

Simulation was done as mentioned earlier in chapter 2 using commercial software, COMSOL Multiphysics version 3.1, to check guidance at 785nm as well as to see whether the Raman shift at 890nm is supported. This result predicts the guidance of Raman-shifted light in a range up to 1500cm^{-1}, which is sufficient for spontaneous Raman spectroscopic fingerprinting of a wide range of materials that can be seen in Figure 6-6.

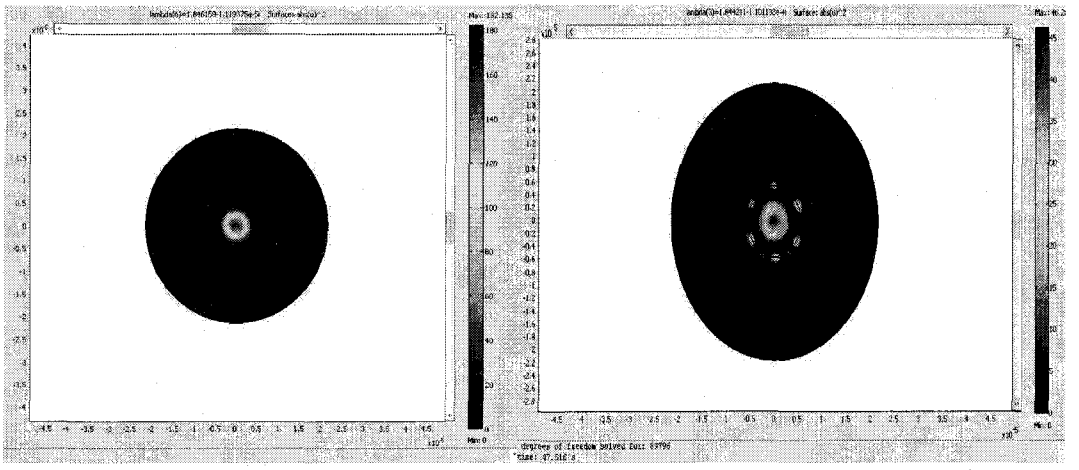

Figure 6-6 Simulation Results mode field intensity in HC-1550-02 PCF filled with ethanol at 785nm (left) and 890nm (right).

6.3.1 Measuring the Raman Spectra

Light at the output of the non-selectively filled PCF was passed through a long-pass filter to reduce the excitation light, and then directly coupled to a collecting fiber bundle, consisting of 30 - 100μm multimode fibers arranged in a circular pattern at the collection end and stacked in a linear fashion at the output end (Fiber Optic Systems Inc.). The setup with long-pass filter and then coupling to the fiber bundle proved cumbersome, so it was decided to exclude the long-pass filter and instead record the silica Raman background noise generated in the fiber bundle by the excitation light, and subtracted from each recorded ethanol spectrum (Figure 6.7).

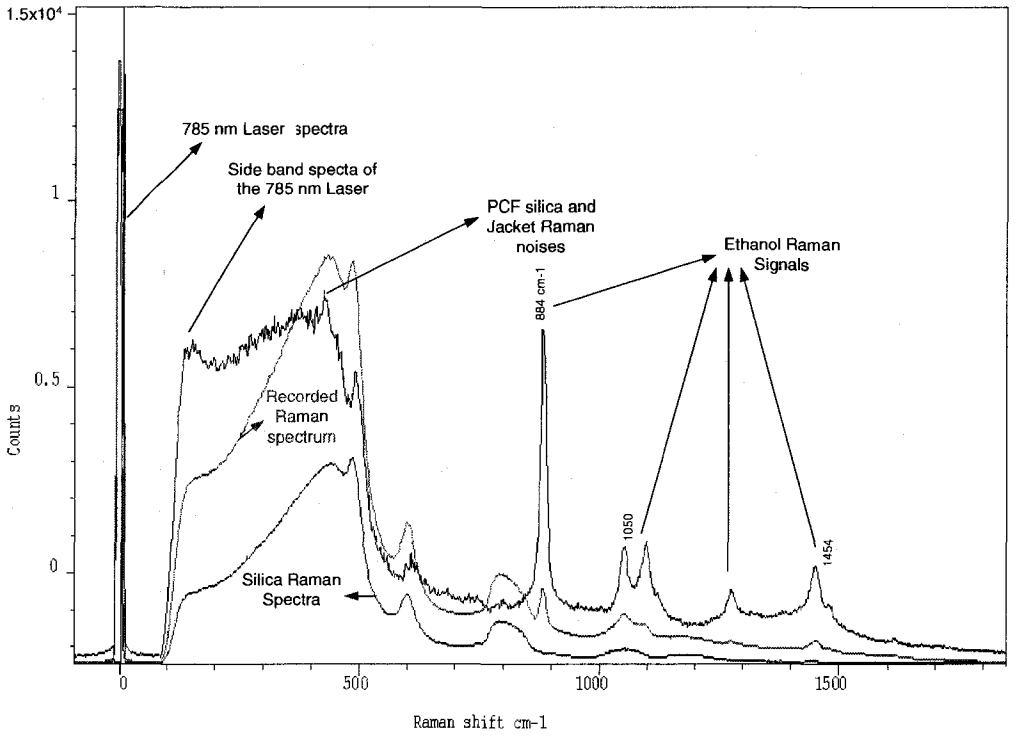

Figure 6-7 The silica (SiO2) Raman spectra of the collecting fiber bundle (blue spectra) was subtracted from the recorded Raman spectrum of the ethanol-filled PCF with collecting fiber bundle (red spectrum), to give the pure ethanol Raman spectrum (black spectrum). [18]

Because of the 785 nm laser side band and spectra generated by the PCF cladding and jacket, the acquired spectra were not completely clean. Note that the black spectrum does not have the same Raman signal count scale, but is expanded for clarity.

6.3.2 Experimental Results

To derive a Raman signal enhancement factor from the non-selectively filled PCF, the ethanol spectra from 3, 5, 7, and 9.5 cm of filled PCF were acquired and compared with the Raman spectrum from a 1cm path-length ethanol-filled quartz cuvette (Figure 6-8). Using the 885 cm^{-1} ethanol peak from each spectrum, ratios of peak heights were used to determine the enhancement at each PCF length.

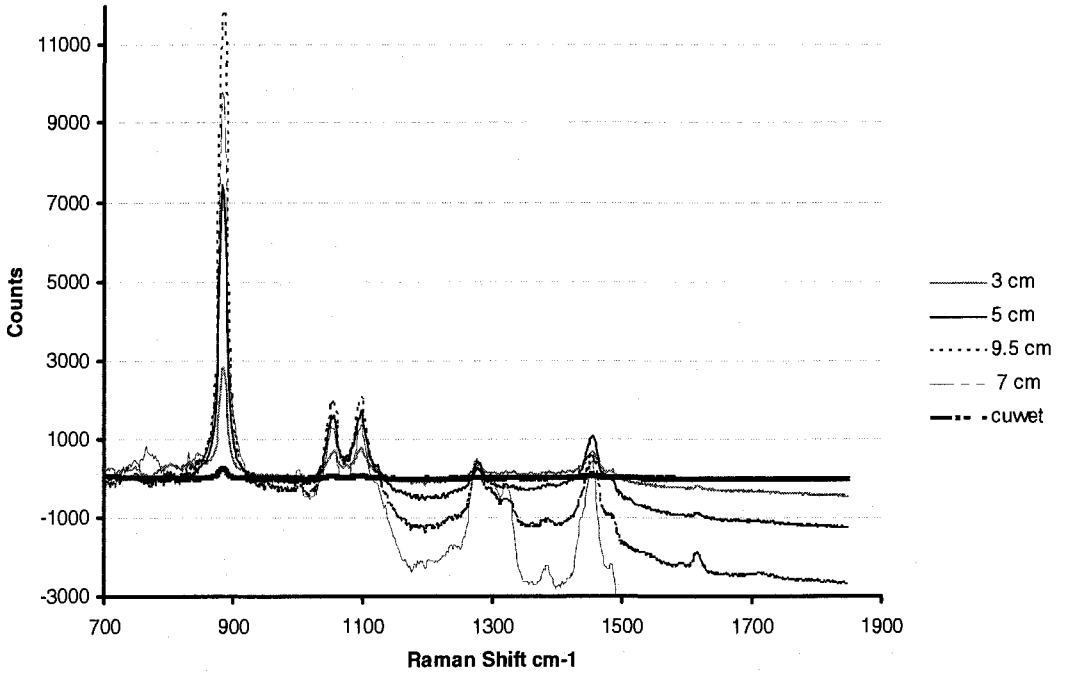

Figure 6-8 The background-subtracted Raman spectra of ethanol from 3, 5, 7 and 9.5 cm lengths of non-selectively filled PCF, and a 1cm path length quartz cuvette [18]

Because of the PCF guiding loss increase by increasing Raman shift of spectrum, the spectrum lines with higher Raman shift attenuated more, this attenuation is proportional to the fiber length. Therefore, this non-uniformity of PCF attenuation as a function of Raman shift and PCF length can be easily seen.

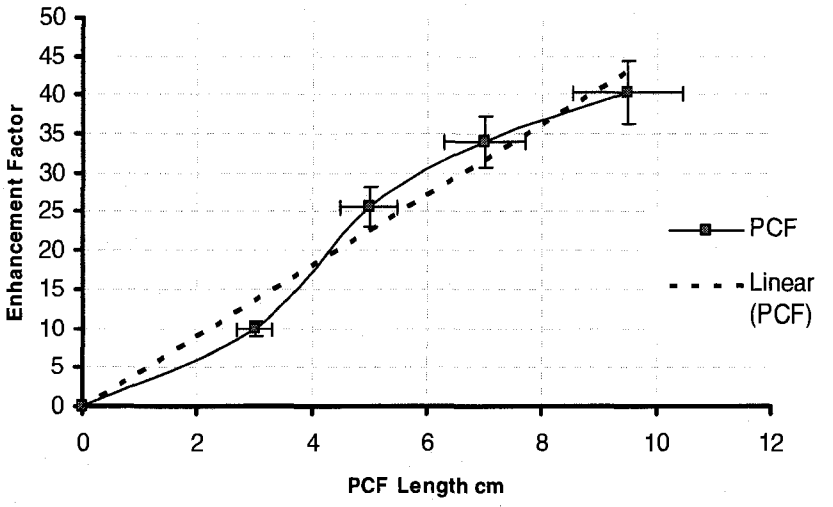

Figure 6-9 Relative enhancement factor for different PCF length compare to the 1cm path length quartz Cuvette .The bar lines are 10% error bars. [18]

Figure 6-9 shows the enhancement factor measurements in the non-selective ethanol filled PCF as a function of PCF length. The enhancement observed in PCF of length 9.5cm is 40 times in comparison to the conventional cuvette technique. In theory, for spontaneous Raman spectrum we expect a linear relation, by ignoring the fiber loss for short fiber lengths between the interaction length and the Raman enhancement factor (Black dashed line in Figure 6-9). Therefore, a good correlation between the theory and our measurements were observed.

Thus, we have seen a novel Raman spectroscopy platform by filling HC-PCF non-selectively. The simplicity of this method, having reasonable Raman signal enhancement combined with the high degree of overlap of the propagating mode with the analyte and small sample volumes required, makes it a promising candidate for sensitive and low-power identification of biological specimens.

6.4 Characterization of Nanoparticles using Hollow Core Photonic Bandgap Fibers

The nanometer scale (1-100nm) lies between the bulk solid and isolated atoms or molecules, which are unique in length scale due to the fact that most of its physical and chemical properties are changed, compared to its bulk material. For example, bulk gold has golden color which is in complete contrast with its ruby-red color of gold nanoparticles in colloidal solutions. Small nanocrystals like semiconductor and metal quantum dots, exhibit discrete energy level structure due to strong quantum confining effect. [19, 21]

In the past decade, semiconductor nanoparticles have attracted enormous attention as novel optical, electrical, and magnetic material. zinc oxide being a group II-IV compound semiconductor, has been widely used in many applications such as transparent conductive films, varistors, solar cell windows, bulk acoustic wave devices, lasers, and diodes [19]. Currently, there are a number of important areas being investigated in the case of colloidal nanoparticles including synthesis of various structures, properties, and applications. A number of techniques, such as photoluminescence and absorption have been employed to characterize these systems in terms of their composition, structure, optical properties, and their size distribution [20].

Raman spectroscopy is a very useful technique that has not been fully exploited in the study of colloidal nanoparticles. The advantage of using Raman spectroscopy is that it is an optically non-invasive technique. The following section covers studying ZnO nanoparticles capped with PAA (Poly Acrylic Acid) solvated in distilled water.

6.4.1 Experiment

HC-19-532 is a hollow core photonic bandgap fiber manufactured by Crystal Fibre Inc. It has been used to perform the experiment. The fiber has a core size of 9.5μm with a pitch of 1.5μm. The fiber has been selectively filled, as mentioned in Chapter 2, using a fusion splicer. Simulations have been performed using COMSOL and shows lowest order mode guidance at 532nm.

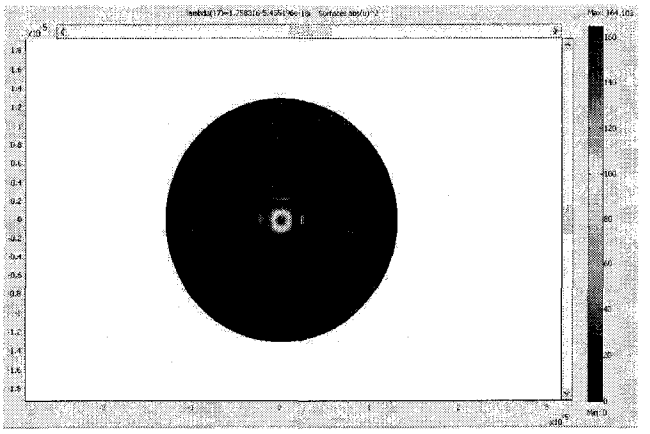

Figure 6-10 Simulation results of HC-532 fiber selectively core filled with water

In order to study ZnO nanoparticles, water soluble ZnO was prepared by the base hydrolysis of zinc nitrate in the presence of PAA in water. The Raman characterization of the sample is done on JY Horiba LabRAM micro-Raman system. The system features an external 532nm frequency-doubled diode pumped by an Nd: YAG laser with a maximum output power of 25mW. Light is coupled into the core of the fiber through a 10x objective with a numerical aperture of 0.22. The back scattered radiation is collected through the same objective as it is refocused and passed through a confocal aperture. The spectrometer incorporates a 1200g/mm grating, providing a resolution of 2.4cm-1/pixel, and a monochromator length of 300mm. A 16 bit Peltier cooled 1024x256 pixels CCD is used to record the spectra.

6.4.2 Results

Raman spectra of ZnO nanoparticles were investigated in three different ways: cuvette, dried on a microscope slide, and selectively filled HC-PCF core. Figure 6-11 shows the Raman signal measured. The water mode at 1640cm-1 is only visible with the PCF setup. Similarly, the modes between 500cm-1 to 1500cm-1 corresponding to different vibrations bands of the ZnO are only visible with the fiber setup. Finally, although much more feeble than the rest, the ZnO second order Raman mode at 318cm-1 was consistently observed for the liquid sample confined within the PCF.

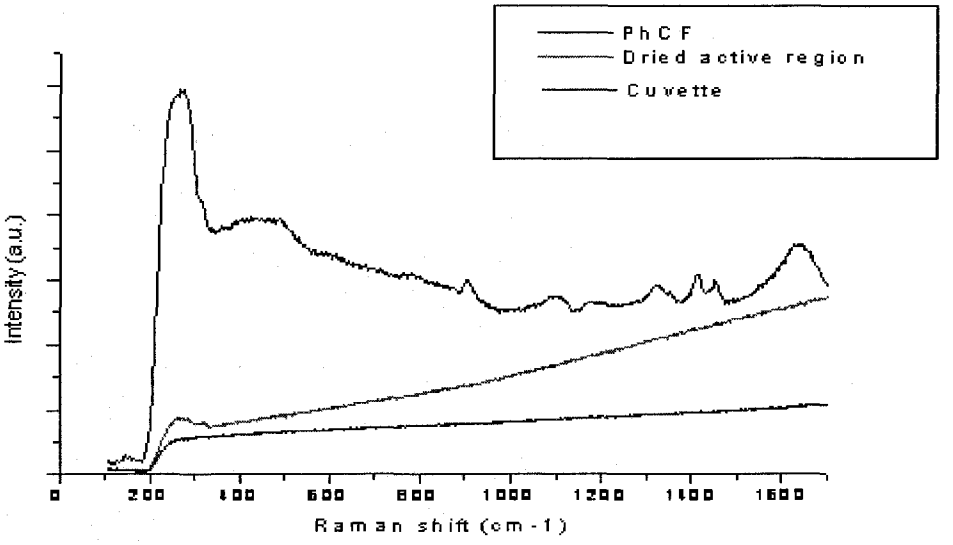

Figure 6-11 The Raman spectra of ZnO nanoparticles obtained from PhCF (Photonic Crystal Fiber), dried on a microscope slide and in cuvette. [21]

By selectively filling the core of the fiber, enhancements of up to two orders of magnitude were obtained, allowing the detection of modes that never before had been detected with the low input powers used in these experiments. .

The Raman enhancement obtained through a photonic crystal fiber has several advantages compared to other Raman enhancement techniques. The sample remains uncontaminated unlike surface enhanced Raman spectroscopy (SERS), vibrational modes are uniquely accessible and there is no influence of electronic states unlike Resonant Raman spectroscopy. It may be employed as parts of an in line process to asses the quality of the nanoparticles, as well as their stage of growth. Additionally, this technique may be extended to the exploration of substances with an arbitrary index of refraction.

In conclusion, Raman spectroscopy was used to analyze the ZnO nanoparticles in solution. Given their low concentrations accounting for less than 1% by weight of the total mass of the system, photonic crystal fibers were demonstrated as an optimal platform for enhancing the Raman signals to study nanoparticles properties in liquid for the first time.

Bibliography

1. P. Bishnu Pal "Fundamentals of Fiber Optic in Telecommunications and Sensor Systems," New Age International, (1992).
2. V.S Tiwari, "Optical fiber laser Raman sensor for monitoring hydrocarbons," M.S., Mississippi State University, (2005)
3. S. Krishnan and R. K. Shankar "Raman Effect: History of the Discovery" Journal of Raman Spectroscopy, 10, pp.1-8 (1981).
4. Ioan Notingher, "Raman Spectroscopy Cell-based Biosensors," Sensors, 7, pp. 1343-1358 (2007).
5. R.L McCreery, M. F Lesichmann and P.Hendra, "Fiber Optic Probe for remote Raman Spectroscopy," Analytical Chemistry, 55, pp. 146 (1983).
6. A.J Mahadevan. R.K Richards "Raman Spectroscopy for the detection of cancers and precancers," Journal of Biomedical Optics, 1, pp. 31-70 (1996).
7. H.U Gremlich, B. Yan, "Infrared and Raman Spectroscopy of Biological Materials," Marcel Dekker Inc. (2001).
8. G.J Thomas Jr., "Raman Spectroscopy of Protein and Nucleic Acid Assemblies," Annual review of biophysics and biomolecular structure 28, pp. 1-27 (1999).
9. I. Notingher, L.L Hench, "Raman microspectroscopy: a non-invasive tool for studies of individual living cells in vitro," Expert Review of Medical Devices 3, 215-234 (2006)
10. R. Altkorn, I. Koev, R.P. Van-Duyne, M. Litorja. "Low-loss liquid-core optical fiber for low-refractive index liquids: fabrication, characterization, and application in Raman spectroscopy," Applied Optics 36, pp. 8992 (1997)
11. D. Pristinski and H. Du, "Solid-core photonic crystal fiber as a Raman spectroscopy platform with a silica core as an internal reference," Optics Letters 31, 3246-3248 (2006).
12. F. Benabid, J.C. Knight, G. Antonopoulos, P.S.J. Russell. "Stimulated Raman Scattering in Hydrogen-Filled Hollow-Core Photonic Crystal Fiber," Science, 298, pp. 399 (2002).

13. S. Yiou, P. Delaye, A. Rouvie, J. Chinaud, R. Frey, G. Roosen, P. Viale, S. Février, P. Roy, J. -L. Auguste, and J. -M. Blondy, "Stimulated Raman scattering in an ethanol core microstructured optical fiber," Optics Express 13, 4786-4791 (2005).
14. Y. Zhang, C. Shi, C. Gu, L. Seballos, and J. Z. Zhang, "Liquid core photonic crystal fiber sensor based on surface enhanced Raman scattering," Applied Physics Letters 90, pp. 193504 (2007).
15. F. M. Cox, A. Argyros, M. C. J. Large, and S. Kalluri, "Surface enhanced Raman scattering in a hollow core microstructured optical fiber," Optics Express 15, pp. 13675-13681 (2007).
16. A. Hassani, and M. Skorobogatiy, "Design of the microstructured optical fiber-based surface plasmon resonance sensors with enhanced microfluidics," Optics Express, 14 pp. 11616 (2006).
17. A. Hassani and M. Skorobogatiy, "Design criteria for microstructured-optical-fiber-based surface-plasmon-resonance sensors," Journal of Optical Society of America. B 24, pp. 1423-1429 (2007).
18. M. Naji, A. Khetani, N. Lagali, R. Munger, H. Anis, "A novel method of using hollow-core photonic crystal fiber as a Raman biosensor" Photonics West 2008 (Paper 6865-13)
19. L. Shen, N. Bao, K. Yanagisawa, K. Domen, A. Gupta, C.A. Grimes "Direct synthesis of ZnO nanoparticles by a solution-free mechanochemical reaction," Nanotechnology 17 pp. 117-5123 (2006).
20. J. Irizar, J. Dinglasan, J.B. Goh, A. Khetani, H. Anis, D. Anderson, C. Goh, A. S. Helmy "Ultra sensitive Raman Spectroscopy of Nanoparticles using Photonic Crystal Fibers" accepted Journal of Selected Topics in Quantum Electronics
21. J. Rongchao "Nobel metal nanocrystals: synthesis, optical properties and biological application" PhD thesis, Northwestern University.
22. J. Motz, M. Fitzmaurice, A. Miller, S. Gandhi, A. Haka, L. Galindo, R. R Dasari, J. Kramer, and M. Feld, "In Vivo Raman Spectral Pathology of Human Atherosclerosis and Vulnerable plaque", Journal of Biomedical Optics 11 pp. 021003 (2006).

Chapter 7. Summary and Future Work

This chapter gives summary of the entire chapters covered followed by future direction to carry out research in the field of photonic crystal fiber as Biosensor

7.1 Summary

The primary objective of this thesis was to find different biosensing techniques in which Photonic Crystal Fibers can be used primarily for enhancing the signal, thereby providing a label-free, non-invasive, unique and novel type of techniques to be implemented. For instance, it was the first time that the non-selective filling technique was applied to enhance a Raman signal. Furthermore, the laser flash photolysis was one of the earliest attempts to implement PCF for monitoring intermediate states in chemical reactions. Here is a summary of the work done in this thesis.

7.1.1 PCF filling techniques

- In chapter 1, the techniques covered were selective filling and non-selective filling to fill a hollow core PBF. In the case of the selective filling technique, the approaches followed were overhead pressure and fusion splicer for capping cladding channels so that the core could be filled with the desired liquid. In order to detect a sample, other techniques like Raman must be applied. The other technique discussed was the non-selective filling where the cladding as well as the core channels was filled with liquid. An important and challenging step was to find the fiber meant for guiding source wavelength filled with a particular liquid. In order to find this, a formula derived by Antonopoulos et al. was used to determine the wavelength supported by a filled fiber depending upon the source wavelength and refractive index of the sample [1]. Thus, this technique is very simple to implement, and hence, was extensively used in the thesis for most of the applications.

7.1.2 Non-Selective technique for biosensor application

For most of the applications discussed in the thesis, filling the fiber was done through a non-selective filling approach. A special reservoir was made in order to avoid evaporation of the liquid inside the channels of PCF.

- The principal application of hollow core PBF discussed in chapter 3 was to use the bandgap shift property of the fiber by non-selectively filling it with different liquids and monitoring the wavelength shift. The method reported is very simple, as the fiber used was a very short piece which could detect 10^{-5} change in the refractive index of the sample.

- The photonic crystal fiber for laser flash photolysis was covered in chapter 5. Laser flash photolysis is a very popular technique for chemical and biological samples to monitor the transient state occurring during a reaction. Most of the experimental results reported here were obtained by filling the hollow core PBF non-selectively. The results were quite encouraging as the signals achieved with this technique exceeded at least an order of magnitude (in intensity) compared to those in conventional techniques. Moreover, the sample used to perform LFP using PCF was of the order of 10^{-4} □l, thereby proving its feasibility.

- The thesis also covers a novel method to measure a Raman signal. The method, discussed in chapter 6, followed a non-selective filling technique for measuring Raman enhancement with a fiber of different length. We were able to obtain a Raman signal by using a fiber piece of 9cm, an enhancement of at least 40 times in comparison to a conventional cuvette technique. It must be noted that the Raman signal enhancement obtained was proportional to the length of the fiber.

7.1.3 Excitation of cladding mode for SC generation for Biosensor application

- In chapter 4 we have demonstrated supercontinuum generation by exciting the cladding and core modes. The possible application could be for biosensing purposes because of the strong interaction between light and the sample present in the cladding channels. In the method, we have used a solid core "endlessly single mode" fiber which supports a single mode operation for a specific range of wavelength. By exciting the fiber with a laser very close to its zero dispersion wavelength and by misaligning, one can excite higher order leaky modes. The

strength of the cladding mode as well as the spectroscopic characteristics of the light transmitted through the PCF filled with analytes could lead us to trace analytes by analyzing details of the far field patterns.

7.2 Future Work:

Here we present an outlook on further work which can be carried out by employing PCF.

7.2.1 Non-Selective technique for biosensor application

Since the first demonstration of PCF, the field has generated much interest among researchers around the world. The non-selective filling technique was reported by groups such as Antonopoulos et al, Cox et al. [1, 2] but the technique has not been published much in the literature.

- Bandgap shift property demonstrated for measuring refractive index was used for ethanol and water, but it can be further extended to measure any liquid by employing a very wide SC generation source covering a very wide band. Moreover, the very small wavelength band covered by hollow core fiber can be overcome by using a different kind of fiber geometry known as the Kagome lattice. [2] The Kagome lattice fiber is supposed to cover a transmission span of 900nm. The other application which needs to be looked further is for glucose monitoring as this technique would provide a simple and effective way for monitoring changes in glucose levels. Furthermore, various fiber geometry designs would also help in obtaining a very highly sensitive sensor.

- The application of PCF for performing LFP discussed had a limitation due to the monitoring wavelength (633nm) which resulted in choosing a sample which absorbs in the range 600-630nm. Moreover, the fiber used had a narrow wavelength band which limits the potential for LFP application. The future direction to carry out the experiments is by using wide band SC generation as a monitoring source which can be coupled very easily into the fiber. The limitation of PBF can be overcome by using a Kagome lattice PCF which supports a very wide band

transmission wavelength. To study very short lifetimes in the range of pico- and femto-seconds, a different approach known as pump-probe technique is followed. Application of PCF for pump-probe spectroscopy will lead to the study of a very wide range of chemical and biological samples.

- The enhancement of spontaneous Raman signal for ethanol filled with PCF has been discussed in chapter 5. The enhancement of a Raman signal measurements for material like heparin could lead PCF for studying further biomolecules. The other forms of Raman spectroscopy's in which non-selectively filling PCF can be put into practice are surface enhanced Raman spectroscopy and stimulated Raman spectroscopy.

- In addition to the future work mentioned above, inscribing gratings inside the channels of PBF could be used as a strain sensor. PBF filled with different liquids could also lead for dispersion management in nonlinear applications.

7.2.2 Excitation of cladding mode for SC generation for Biosensor application

- Though the excitation of cladding mode is in initial stages, it has the potential to be used as an effective type of biosensor because of the strong penetration of the supercontinuum generated light in the channels of the PCF. This technique needs requires more investigation to be carried out to find the fiber geometries which not only excites cladding mode but also has a strong penetrating evanescent field. The excitation of the cladding modes can be used with other techniques for measuring absorption, fluorescence, Raman spectroscopy.

Bibliography

1. G. Antonopoulos, F. Benabid, T. A. Birks, D. M. Bird, J. C. Knight and P. St. J. Russell, "Experimental demonstration of the frequency shift of bandgaps in photonic crystal fibers due to refractive index scaling," Optics Express 14, pp. 3000-3006 (2006).
2. F. Benabid, J. C. Knight, G. Antonopoulos, and P. St. J. Russell "Stimulated Raman scattering in hydrogen-filled hollow-core photonic crystal fiber," Science, 298, pp.399–402 (2002).
3. Y. Zhang, C. Shi, C. Gu, L. Seballos, and J. Z. Zhang, "Liquid core photonic crystal fiber sensor based on surface enhanced Raman scattering," Applied Physics Letters 90, pp. 193504 (2007).
4. F. M. Cox, A. Argyros, and M. C. J. Large, "Liquid-filled hollow core microstructured polymer optical fiber," Optics Express 14, pp. 4135-4140 (2006).

Appendix-A

A-1 Theory [1]

The theory behind the laser flash photolysis is discussed in this sub-section. Let us consider a beam propagating in x-direction in a medium.

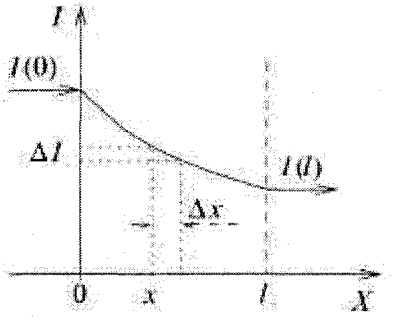

Figure A-1 Light absorption in a medium

We start by assuming that at a point x the light intensity is $I(x)$. In a layer of thickness Δx, the light interacts with the medium and at a point $x+\Delta x$; the light intensity is changed by ΔI which results in $I(x+\Delta x) = I(x) + \Delta I(x, \Delta x)$. As $\Delta x \to 0$, the ratio $\frac{\Delta I(x,\Delta x)}{\Delta x}$ is proportional to the light intensity, which can be written as

$$\lim \frac{\Delta I(x, \Delta x)}{\Delta x} = -\alpha I(x) \text{ Or } \frac{dI(x)}{dx} = -\alpha I(x) \qquad \text{(A-1)}$$

where α is the proportionality coefficient determining efficiency of the light absorption. The minus sign on the right side of the equation is due to the fact that the light is absorbed by the medium, i.e., the function $I(x)$ is decreasing with increasing x, and, thus, it has a negative slope.

[1] Nikolai V. Tkachenko "Optical spectroscopy: Methods and Instrumentation" Elsevier Science (2006).

Rearranging and solving the equation (A-1) through partial differential equation results in $\ln(I(x)) = -\alpha x + C$ where C is a constant and can be found using initial condition at $x = 0$, $I(0) = I_0$ which is an incident light. Finally the above equation can be written as

$$I(x) = I_0 \exp(-\alpha x) \tag{A-2}$$

This equation is known as Lambert Law. In the equation α is called absorption coefficient and its units are m^{-1} or cm^{-1}.

This equation is usually expressed in power of 10 rather than exponential which transforms the above equation to be

$$I(x) = kI_0 10^{(-\alpha x)} = kI_0 10^{(-A)} \tag{A-3}$$

where k is a constant, A is absorbance or optical density.

For simple absorption spectroscopic technique the equation (A-3) is used for calculation of absorption in a sample, but for Laser Flash Photolysis technique temporal change in sample absorbance $A(t)$ caused by excitation pulses used for calculating absorbance. As absorbance cannot be measure directly, the monitored light is required represented by light intensity $I(t)$ is the parameter to be recorded. The light intensities before and after the sample can be written as

$$I_{out}(t,\lambda) = I_{in}(\lambda)10^{-A(t,\lambda)} \tag{A-4}$$

where $I_{out}(t,\lambda)$, $I_{in}(\lambda)$ are the monitoring light intensities after and before the sample respectively.

It is convenient to present absorbance into two parts, expressed as

$$A(t,\lambda) = A_0(\lambda) + \Delta A(t,\lambda) \tag{A-5}$$

where $A_0(\lambda)$ is the sample absorbance before the excitation and $\Delta A(t,\lambda)$ is known as the differential absorbance which occurs due to excitation of the sample and photoreactions.

Therefore the above equation (A-5) can be written as

$$I_{out}(t,\lambda) = I_{in}(\lambda)10^{-A_0(\lambda)-\Delta A(t,\lambda)}$$

$$= I_{in}(\lambda)10^{-A_0(\lambda)}10^{-\Delta A(t,\lambda)}$$

$$= I_0(\lambda)10^{-\Delta A(t,\lambda)} \qquad \text{(A-6)}$$

where $I_0(\lambda) = I_{in}(\lambda)10^{-A_0(\lambda)}$ is the monitoring light intensity after the sample at some time before excitation. The absorbance change is given as

$$\Delta A(t,\lambda) = -\log_{10}\frac{I_{out}(t,\lambda)}{I_0(\lambda)}$$

Or

$$\Delta A(t,\lambda) = -\log_{10}\left(1+\frac{\Delta I(t,\lambda)}{I_0(\lambda)}\right) \qquad \text{(A-7)}$$

where $\Delta I(t,\lambda) = I_0(\lambda) - I_{out}(t,\lambda)$

The equation (A-7) implies that in order to obtain the differential absorbance the relative change in the monitoring light intensity must be measured but not the absolute value of the intensity. Since the detecting signal detected by photo detector is proportional to the light intensities, equation (A-7) can be replaced with a corresponding detector signal. Below is a signal typically recorded in LFP in which signal A_t being the absorbance at time t, A_{pk} being the maximum transient optical density and A^{∞} being the absorbance of the products.

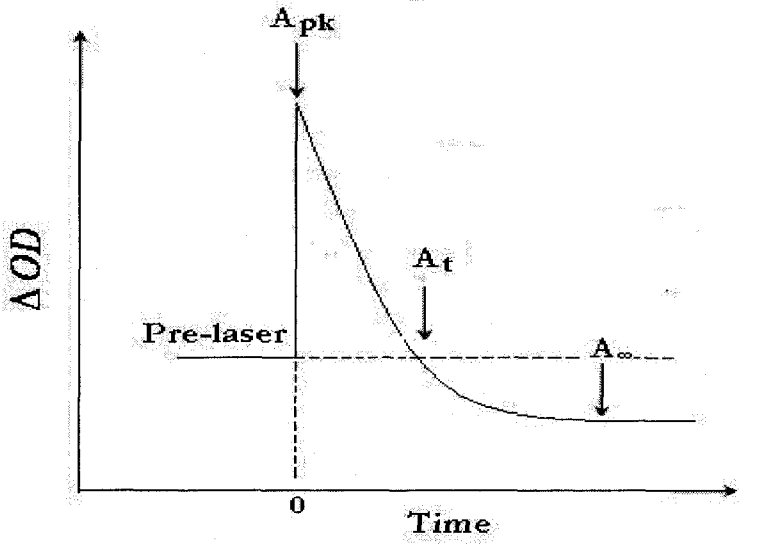

Figure A-2 Signal recorded during a LFP

In order to obtain relation between time constant and absorbance we use two relations, one is between concentration and time constant (Rate law) and the other between absorbance and concentration (Beer Law).

Let the final concentration be c and initial concentration of the sample is c_0. The rate law gives a dependence of reactant concentration c, with time t given by equation (A-8)

$$c = c_0 e^{-kt} \quad \text{Or} \quad \ln(c/c_0) = -kt \tag{A-8}$$

According to Beer's Law, the absorbance is given as

$$A = c\varepsilon l \tag{A-9}$$

where ε molar absorption coefficient, l being the length of the light interacting with a sample.

From the signal shown in Figure A-2 we can determine absorption at initial concentration c_0 which has a value $A_{pk} - A_\infty$ and, at final concentration c as $A_t - A_\infty$. Thus, the Beers law can be written as

$$A_{pk} - A_\infty = c_0 \varepsilon l \tag{A-10}$$

$$A_t - A_\infty = c \varepsilon l \tag{A-11}$$

Taking the ratio of equations (A-10) and (A-11) and replacing that in A-8 we find the relation between absorbance and rate constant which is as follows:

$$\ln\left(\frac{(A_t - A_\infty)}{(A_{pk} - A_\infty)}\right) == -k_{\exp}\, t \tag{A-12}$$

This gives the relation between absorbance and rate constant for laser flash photolysis analysis.